Development of Surface Electromyogram Operated Exoskeleton for Lower Limb

A Thesis

submitted for the award of the degree of

Doctor of Philosophy

in

Electrical and Instrumentation Engineering Department

Submitted by

Anurag Sohane
(Reg no: 901404004)

Under the Guidance of

Dr. Ravinder Agarwal
Professor

Thapar Institute of Engineering and Technology, Patiala,
Punjab - 147004, India
October 2021

Certificate

I hereby certify that the work, which is being presented in the thesis, entitled "**Development of Surface Electromyogram Operated Exoskeleton for Lower Limb**", in partial fulfilment of the requirements for the award of the degree of Doctor of Philosophy and submitted to the institution, is an authentic record of my work carried out under the supervision of Dr. Ravinder Agarwal. I have cited the reference about the text(s)/figure(s)/table(s) from where they have been taken. The matter presented in this thesis has not been submitted either in part or full to any other University/Institute for the award of any other degree. The matter presented in this thesis has not been submitted either in-part or full to any other University/Institute for the award of any other degree.

(Anurag Sohane)
Reg No. 901404004

This is to certify that the above statements made by the candidate are correct and true to the best of my knowledge.

Verified by:

(Dr. Ravinder Agarwal)
Professor and Supervisor
EIED, TIET, Patiala, India

Dedicated to my parents Sh. Ashok Kumar Sohane and Smt. Suman Sohane; to my wife Neha Sohane and my son Ketan Sohane.

Acknowledgements

I thought this day would never arrive. Now that it has, my heart overflows with gratitude for those who have been with me throughout the ordeal. I want to express my deep gratitude to Dr. Ravinder Agarwal, my research supervisors, for their patient guidance, enthusiastic encouragement, and useful critiques of this research work. His guidance helped me in all the time of research since beginning at TIET.

I would like to thank Prof. Prakash Gopalan, Director, TIET, Patiala, for providing facilities for current research work. I am also highly thankful to Prof. R. S. Kaler, Head, EIED and URB members of my doctoral research committee for providing valuable suggestions throughout this research work. I am sincerely thankful to my venerable faculty of the Electrical and Instrumentation Engineering Department for their invaluable suggestions and caring concern at every stage during the entire stretch of studies.

Sincere thanks to Dr. Prashant Singh Rana, Dr. Vishal Srivastav and Dr. AM Gaur for their continuous support. They also generously gave their time to offer insightful comments towards improving my work. I truly appreciate my colleagues, including those from other disciplines, for enriching me by sharing their experiences. I am thankful to the graduate and post-graduate students at TIET. My life would have been very dull without their fun interactions. The office staff has always been available and ready for assistance of any kind.

My heartiest thanks are due to Dr. Amod Kumar, Acting Director CSIR-CSIO and Dr Sanjeev Kumar Verdi, Sr. Scientist, CSIR-CSIO, Chandigarh for the help rendered to me besides taking personal pains to see the completion of my research.

Last but not least, I wish to thank my parent and my sister for always having my back. Irrespective of what they were dealing with on an individual level, they were always available for a conversation. I owe a lot to my parents, who encouraged and helped me at every stage of my personal and academic life, and longed to see this achievement come true. Interacting with my son has always allowed me to drop all baggage and enjoy the moment.

(Anurag Sohane)

Abstract

Surface electromyography (sEMG) is a technique used in human-machine interface, rehabilitation, and exoskeleton control. In recent years, cost reductions and increased availability of essential technology have made sEMG a more realistic alternative for the development of the exoskeleton. sEMG based exoskeletons can identify the user's intentions and enable cooperative interaction, but sEMG base control strategy in assistive devices is currently unclear since each individual's muscles and joint forces are unique. This may eventually increase the time and cost of developing a real-time design exoskeleton. Biomechanical simulation tools and artificial intelligence are being used to save time and cost to improve the design.

This thesis presents a human biomechanics analysis for knee joints in AMS, interfacing of design exoskeleton with human musculoskeletal, Artificial Intelligence (AI) techniques for prediction and classification. These are brought together to set a new baseline for optimizing the real-time development of sEMG based exoskeleton. The thesis work includes the design of a 3D lower limb exoskeleton in SolidWorks CAD software. The sEMG signals were obtained from lower limb muscles and converted into muscle force using the Hill muscle model. In addition, a statistical comparison of experimentally generated muscle forces with human musculoskeletal muscle forces was performed in AMS. ANOVA t-test was conducted on validation datasets.

A new approach for predicting muscle force was developed using a Machine Learning (ML) approach called a force simulator. These models were trained and tested using dataset 500 human musculoskeletal generate using python tools in AMS, where human musculoskeletal utilized to perform squatting movement during inverse dynamic analysis. To predict knee muscle force, four different ML models were trained and tested on datasets. The random forest-based ML model outperforms the other models: Neural Network, Generalized Linear Model, Decision Tree in terms of mean square error (MSE), coefficient of determination (R2), and Correlation (r) for the musculoskeletal datasets. The MSE of predicted vs actual muscle forces obtained from the random forest model for Biceps Femoris, Rectus Femoris, Vastus Medialis, Vastus Lateralis was $19.92, 9.06, 5.97, 5.46$, and Correlation was $0.94, 0.92, 0.92, 0.94$, and R^2 was $0.88, 0.84, 0.84,$ 0.89 for the test datasets, respectively.

Particle Swarm Optimization-Long Short Term Memory (PSO-LSTM) was used to classify three different movements (Flexion, Extension, Ramp Walking) based on sEMG signal and predict the results of sEMG signal and knee angle. After that, random

LSTM was used to validate the results to explore the effectiveness of PSO-LSTM. Four knee muscles sEMG signals, namely biceps femoris (BF), vastus medialis (VM), rectus femoris (RF) and semitendinosus (ST), and knee angle, were used as model inputs. RMSE, r, and R^2 were taken as evaluation parameters to identify the model's robustness for predicting SEMS signal and knee angle. The average RMSE value for an extension, flexion and ramp walking for both PSO-LSTM and random LSTM model was $(80\%, 10.16\%), (133.33\%, 30.96\%)$ and $(116.66\%, 19.48\%)$, respectively. The average 'r' value for an extension, flexion, ramp walking for both PSO-LSTM and random LSTM model was more by $(4.65\%, 4.04\%), (6.60\%, 3.03\%)$ and $(3.57\%, 7.07\%)$, respectively. The average R^2 value of sEMG for an extension, flexion, ramp walking for both PSO-LSTM and random LSTM model was higher by $(5.88\%, 4.08\%), (5.05\%, 4.04\%)$ and $(5.33\%, 8.16\%)$, respectively. The PSO-LSTM model was used to classify three different movements (Flexion, Extension, Ramp Walking) with an accuracy of 98.58%. It was observed that the proposed PSOLSTM model shows better capability than the random LSTM model for both inputs (sEMG signals, knee joint angle).

The prototype of the knee was developed in the laboratory and operated through sEMG signal for three activities (Flexion, Extension, Ramp Walking) to actuate the linear actuator. The PSO-LSTM model helped was used to validate the results of three different activities.

Keywords: Musculoskeletal model, Knee, Squatting, Lower limb, Machine Learning, Optimization, LSTM

Table of Contents

List of Figures

List of Tables

List of Abbreviations

AE	Auto Encoder
AMS	AnyBody Modelling Software
ARI	Autoregressive Integrated
BF	Biceps Femoris
CAD	Computer Aided Design
DBN	Deep Neural Network
DWPT	Discrete Wavelet Packet Transform
GMED	Gluteus Medius
LSTM	Long Short Term Memory
MLPs	Multilayer Perceptron
MSE	Mean Square Error
PSO	Particle Swarn Optimization
RF	Rectus Femoris
RMSE	Root Mean Square Error
RNN	Recurrent Neural Network
sEMG	Suface Electromyography
STEM	Semitendinosus
VL	Vatus Lateralis
VM	Vastus Medialis
WNN	Wavelet Neural Network

Chapter 1

Introduction

Exoskeletons are electromechanical devices worn by human beings to increase their physical performance. An exoskeleton is an external structure that supports and protects an animal's body, in contrast to the internal skeleton, for example, a human. The most emerging application field is now focusing on industrialized countries because the ratio of people older than 65 years reached 17.5 over the whole population in the European Union in 2011 and is estimated to reach 29.5% in 2060. Similarly, in the USA, the over-65 population percentage was 13.3% in 2011 , with an expected increase to 21% in 2040 [1,2]. Furthermore, due to low birth rates and the highest life expectancy in these countries, the trend of ageing is accelerating. Therefore, it takes considerable attention from social and ethical points of view to provide aid for older adults in their everyday lives, especially concerning mobility and self-reliance. In this era, where technology is becoming more human-friendly, more innovative and safer, the development of self-standing lower limb orthoses or exoskeletons for physical assistance represents one of the most addressed mobility assistance options.

There are three types of robotic exoskeletons, each divided into two categories (single joint and multiple joints): augmentation exoskeleton, assistive exoskeleton, and rehabilitation exoskeleton. Augmentation exoskeletons increase strength and enhance human endurance. A rehabilitation exoskeleton is used to regain strength and abilities through training. Finally, the assistive exoskeleton amplifies the strength and endurance of healthy users to perform heavy load carrying work. These are all mechanically compatible with human anatomies. Researchers use various control strategies to assist users, as shown in Figure 1.2. The most advanced exoskeletons are BLEEX [3], HAL [4], and MIT exoskeletons [4], *etc,* used to provide additional power for walking, as shown in Figure 1.1.

Estimating human motion intentions demonstrate good potential for human-robot interaction such as exoskeleton robot control. It's a safer and more advantageous method for man-machine interaction. The continuous motion of joints aims to establish a mapping relationship between sEMG signals and a continuous variable such as joint angle, joint speed, or joint torque. Such motion estimation plays a vital role in compliance control for robotic joints. At present, the main estimation methods for continuous joint motion intentions include the biomechanical model method and the regression model method.

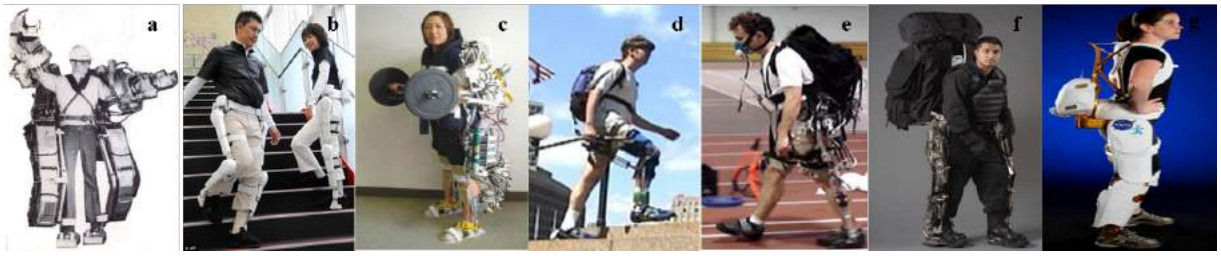

Figure 1.1: (a) Hardiman, (b) Hybrid Assistive Leg (HAL), (c) Nurse-Assisting Exoskeleton, (d) Robo knee, (e) MIT Exoskeleton, (f) BLEEX Exoskeleton, (g) X1: A Robotic Exoskeleton

The relationship between sEMG signals and muscle force has had a long history since 1952. The biomechanical model method estimates the EMG-Force relationship using the Hill muscle model, which bridges the gap between the sEMG and the muscle force [5, 6]. The advantage of the biomechanical model method is that it can explain human muscle force. However, the model's parameters are complicated, and it necessitates a thorough understanding of human muscle. In addition to the biomechanical model-based method, regression-based machine learning and deep learning algorithms have also been used for EMG-based force/torque estimation [7]. These muscle force/torque estimation algorithms are nearly identical to continuous limb joint angle, joint speed, and joint torque estimation algorithms [7–9]. It can be selected for angle and sEMG signal prediction of various body positions, such as the wrist, hand, upper limb, and lower limb [6, 8, 10, 11]. Therefore, the regression model method for the recognition of continuous joint motion intentions has undergone rapid development. There are various approaches for joint motion intentions, like wavelet neural network (WNN) [10], multilayer perceptrons (MLPs) [12–14], state-space model [15, 16], and machine learning approaches [17–19], and deep learning approach [20, 20–26], optimization technique [27, 28]. The performance of these models was measure using mean square error (MSE), root mean square error (RMSE), coefficient of determination (R2), and correlation coefficient (r).

Classification is used to predict specific postures of the human body based on sEMG signals or images. Different supervised classification algorithms based on machine learning and deep learning were trained and tested to predict better accuracy [29–33]. Previous classification models used include descrete wavelet packet transform (DWPT) [10], convolution neural network (CNN) [21, 24, 32, 34], recurrent neural network (RNN) [22, 25], and long short term memory (LSTM) [21, 35, 36]. Unsupervised deep neural networks, such as auto-encoder (AE) [37] and deep belief network (DBN) for movement classification [38, 39], have been used in addition to the supervised learning approach. The above techniques apply a single type of deep learning method for hand gesture prediction. For

a classification task, mixed network structures have also been used, such as multi-stream networks [35, 40–42].

Developing an efficient exoskeleton in real-time is challenging as each individual's muscles and joint forces are unique. The aim was to analyze and evaluate the design of the lower limb exoskeleton during full squatting movement in a simulated environment in order to address issues concerning the development of a functional exoskeleton for individuals.

1.1 Lower Limb Exoskeleton

Starting from the early research in the 1960s [4], especially in the last two decades, "Hardiman" full-body exoskeletons [43] or, in other terms, known as an active orthosis were significantly developed by General Electric in cooperation with Cornell University to augment wearer strength. Berkeley lower body, the first load-bearing exoskeleton that includes seven degrees of freedom (BLEEX) [3]. Developments of exoskeleton systems have grown in recent decades for multi-joint and single joint of humans, respectively. The exoskeleton is used in many applications to improve the military, industry, and nursing quality of life.

According to the Wearable Robotics Association Standards and Education Committee [44, 45], exoskeleton devices do not lift more weight, but they can improve lifting tasks, reduce the user's muscle activities, and reduce the risk of a work-related injury while performing physical activities like dynamic lifting, static holding, and load support [46–49]. In February 2015, the USA government food and drug administration (FDA) had classified exoskeletons as class II devices [50,51]. Despite this, the FDA has identified some technical design drawbacks and technical challenges in current exoskeleton applications, such as instability, fall and related injuries, battery failure, electrical interference, device failure and unintended movement, user error, change in blood pressure, skin effects and soft injuries, lightweight, energy consumption, exoskeleton design aspects, and prices that vary between $100,000 to $30,000.

Exoskeleton robotics developments is still a challenge with many technological issues. More sensors and actuation used in the exoskeleton device will lead to more operating complexity. Therefore, one of the challenges and motivations in exoskeleton developments is to make them cheaper and affordable.

3D design frame is essential in the real-time development of the exoskeleton. Some aspects are necessary for exoskeleton design: lightweight, comfortable design, robust structure,

user's compatibility, and safety [52]. The exoskeleton frame design has an important effect on the overall performance of the exoskeleton. According to Young and Ferris [53], most exoskeleton designs used rigid metal frames to support human limbs and links between joints. Thermoplastic and carbon composite use has increased exoskeleton frames to create a light, solid and effective frame. Aluminium, titanium and carbon steel are other materials commonly used in exoskeleton frames [54]. Soft exoskeletons are a new approach to exoskeleton design that were developed [55]. Exoskeletons made from soft materials provides ultra-lightweight, *i.e.*, suitable to reduce complexity and manufacture cost [55–57].

After that, actuators are used for physical torque to support the exoskeleton device's weight, inertia, size, and user load during locomotion [53]. Torque-mass ratio, range of motion, velocity and controllability are essential in selecting exoskeleton actuators [52]. Various actuators are used in robotic applications such as hydraulic, pneumatic, electrical and electroactive polymers. A review of actuator technologies for wearable robotics show that electrical actuators are highly used amongst orthoses robotics due to high specific power and ease to control [3, 53, 58]. However, hydraulic actuators are standard in performance exoskeletons such as military, industry, and load augmentation applications due to the high power to mass ratio [3, 52, 59].

Exoskeletons currently on the market use a variety of sensor types to collect biomechanical data, depending on their application and control strategy [60–63]. The tibia and femur bones connect at the knee joint.The knee joint is the most restrained of all body joints, with strong muscles and ligaments protecting it from damaging movements. It is the most important and durable joint in the human limbs because it is responsible for walking and standing as well as supporting body weight. The main movements of the knee joint occur in the sagittal plane; however, when the knee is in the flex position, small rotations are possible.

1.2 Human Biomechanics

The lower extremity exoskeleton provides support for the hip, knee, and ankle joints. The lower limb exoskeleton's mechanical structure should follow human lower limb biomechanics characteristics such as type of motion, range of motion (ROM), degree of freedoms (DoF), and force. Lower extremity exoskeletons can be designed to support single or multiple joints in the human lower limb.

Exoskeleton devices for a single lower limb joint were divided into the hip, knee, and ankle systems [50]. Multi-joint exoskeletons are classified as trunk–hip–knee–ankle–foot

(THKAF), hip–knee–ankle–foot (HKAF), trunk–hip–knee (THK), hip–knee (HK), or knee–ankle–foot (KAF) orthoses and exoskeletons. According to Winter [64], the function of these joints is different: while walking in the swing stage, the knee joint is almost damping free, whereas, in the stance phase, it is almost locked. The hip and ankle joints are primarily used for swing control and ground actuation during the stance stage. The hip, knee and ankle are the lower limb segments linking together. However, it has identified that lower limb joints have a more important role than other joints for implementing the movement.

The hip joint is the body's second most weight support joint after the knee. It allows the body to carry out stable locomotion even in a straight line due to its spherical shape allowing three degrees of freedom (DoF). The hip joint can move in three different ranges of motions:

(a) **Flexion-extension**: In the limbs, flexion decreases the angle between the bending of the joint, while extension increases the angle and straightens the joint.

(b) **Abduction-adduction**: Abduction moves the limb laterally away from the body's midline, while adduction is the opposing movement that brings the limb toward the body or across the midline.

(c) **Medial-lateral rotation**: Medial rotation is a rotational movement towards the midline. It is sometimes referred to as internal rotation. Lateral rotation is a rotating movement away from the midline. It is in the opposite direction of the lateral rotation.

The knee joint connects the tibia and femur bones. The knee joint is the most restrained of all the joints in the body, with strong muscles and ligaments protecting it from damaging movements. It is the most important and durable joint in the human limbs, as it is essential for walking and standing and supporting body weight. The main movements of the knee joint occur in the sagittal plane; however, small rotations are possible when the knee is flexed. These motions are:

(a) **Flexion-extension**: flexion is the motion when the leg is approaching the thigh while in the same plane; the range of motion is up to 160 degrees depending on the hip movement condition. An extension is an opposite movement with a range of motion from 0-10 degrees.

(b) **Medial-lateral rotation**: medialis an internal rotation and happens at the end of the extension stage, which takes the knee to the locked position to maintain stability with a range of motion of 10 to 15 degrees. Medial is external rotation

and happens at the beginning of the flexion stage with a range of motion of 30 to 50 degrees based on knee flexion level.

The ankle and foot together have 26 bones, 30 joints, and 100 muscles supporting them. The foot and ankle play a critical role in lower limb stability while walking. The foot acts as a shock absorber, transferring force from the lower limbs to the ground and as a solid pedal to apply force while walking on uneven surfaces. The ankle joint can move in two directions in the transverse plane: dorsal flexion and plantar flexion. Dorsal flexion is a movement in which the ankle rotates the foot up to 20 degrees towards the inner surface of the leg. On the other hand, plantar flexion occurs when the heel is lifted off the ground, and the toe is flat on the floor with a range of motion of 40 to 50 degrees.

1.3 Control Strategy

Several designs were developed over the last few decades to aid in rehabilitation and augmentation of the lower extremity. It is essential to ensure a smooth control strategy to improve the exoskeleton device's effectiveness, accuracy, and comfort based on the user's intentions. Here, nine control strategies are discussed for the single and multi-joint exoskeleton, as shown in Figure 1.2.

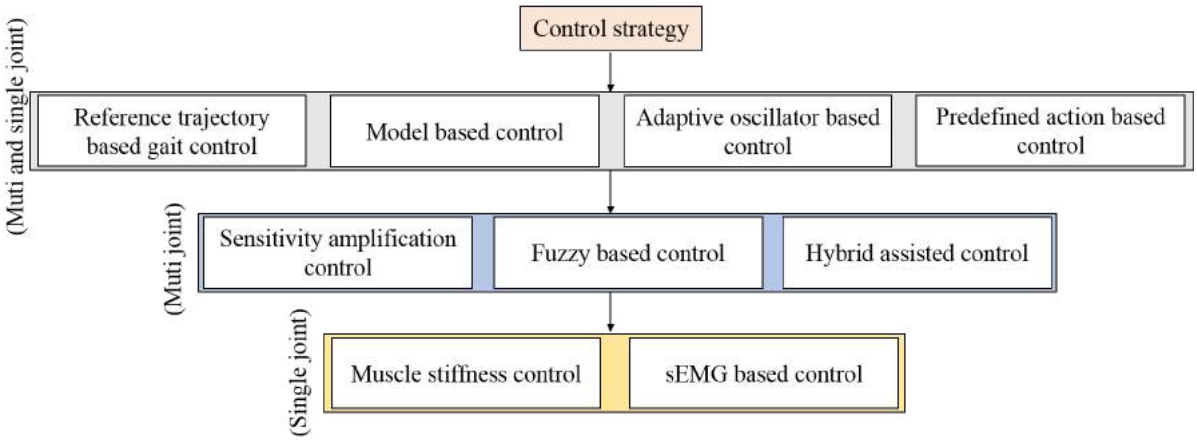

Figure 1.2: Control strategies for designing lower limb exoskeleton with various joint

(a) **Sensitivity amplification control** is more applied to THKAF exoskeletons to augment the wearer's load-carrying ability.

(b) **Reference trajectory based gait control** is easier to implement but forces the user to walk in a reference gait which maybe not natural because the desired joint trajectory is pre-recorded from a healthy person.

(c) **Model based control** is popular in various applications, but it needs accurate

modelling of the coupled human/exoskeleton dynamic system. Under a model-based control structure, the desired robotic action is computed based on a human–exoskeleton model, usually considering gravity compensation, zero moment point (ZMP) balance criterion.

(d) **Adaptive oscillator based control** follows the user's intended movements that are relying on the periodicity of the gait pattern and periodic locomotion-related signals features (*i.e.* phase, frequency, amplitude, offset) in walking or cyclic rehabilitation exercises.

(e) **Predefined action based control** is used to regulate the controller's action. Distinguish from the predefined trajectory control . This assistive strategy controls the device to act synchronously with expected gait events.

(f) **Hybrid assistive control** is used two or more control methods together to make effective control.

(g) **Muscle stiffness control** effectively interacts with their environment, and humans must adjust the stiffness of their limbs. This is accomplished via the co-contraction of antagonistic muscle groups. Humans use neural control and the mechanical constraints of the body to adjust this stiffness as the body performs various tasks.

(h) **sEMG based control** utilizes a microcontroller or computer to input electromyography (EMG) signals from sensors and activates the corresponding joint actuator.

(i) **Fuzzy based control** It isn't easy to structure an accurate dynamic model. A fuzzy control could be considered to handle a physical system . However, a fuzzy controller requires many variables to be tuned manually according to the specific motion tasks and individuals.

There are three major types of multi-joint and single-joint lower-limb exoskeleton systems. Assistive exoskeletons help individuals who cannot perform daily activities, who are usually unable because of a stroke, spinal cord injury, or muscle weakness. Rehabilitation exoskeletons are used to regain strength and abilities through training. Augmentation exoskeletons amplify the strength and endurance of healthy users to perform the heavy load carrying work.

1.3.1 Preprocessing of sEMG signals and Artificial Intelligence

The preprocessing stage is required to remove unwanted interference from the recorded signals. When sEMG signals are recorded, noise is often captured from inherent noise in the electronic components, power line interference, motion artifacts, and the inherent

instability of signals, especially biological signals. Significant electrical interference has affected the sEMG signal, making it unreliable in analysis and quantification. Interference with sEMG signals must be removed when the quality of the signal is important, as shown in Figure 1.6. Depending on the quantity of fatty tissue and the muscle type, the frequency range of sEMG signals is 0 Hz to 250 Hz.

Computational techniques based on Artificial Intelligence (AI), such as machine learning or deep learning, are useful in the robotics field for rehabilitation. Machine learning employs a set of algorithms to analyse and interpret data, learn from it, and make the best decisions possible based on the learning, as shown in Figure 1.3. On the other hand, deep learning divides the algorithms into multiple layers to form an artificial neural

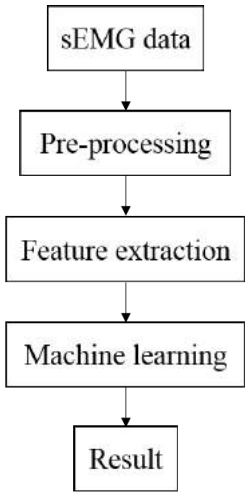

Figure 1.3: Machine Learning Flowchart for sEMG signal

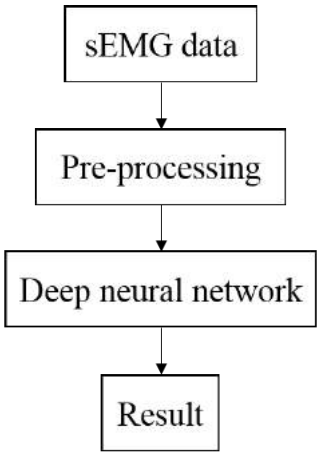

Figure 1.4: Deep Learning flowchart for sEMG signal

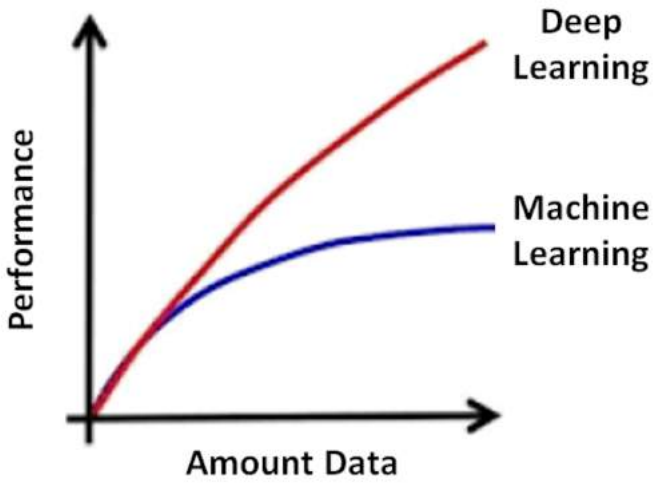

Figure 1.5: Comparison graph of machine learning and deep learning

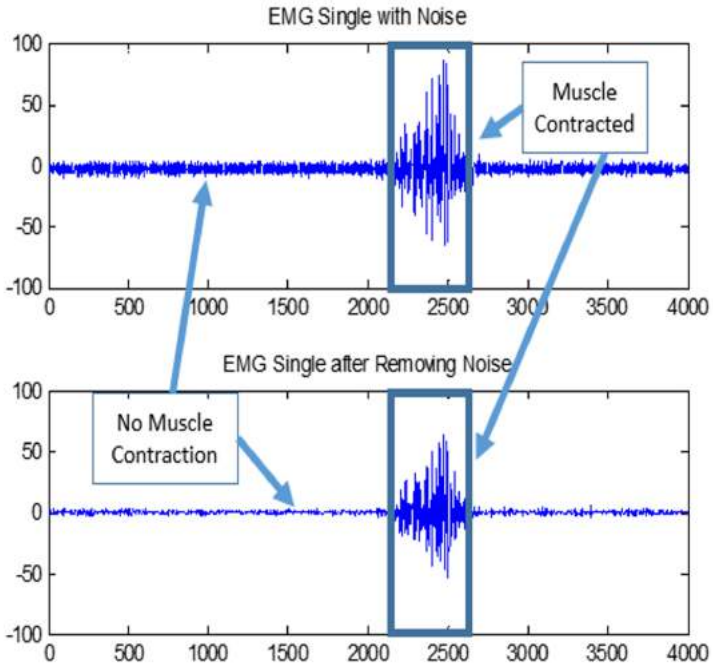

Figure 1.6: sEMG signal with and without noise

network, as shown in Figure 1.4. This neural network is capable of learning from data and making intelligent decisions on its own so it is computationally faster than machine learning techniques, as shown in Figure 1.5. Many sEMG signal tasks such as movement classification, joint angle prediction, and force/torque estimation were addressed using deep learning machine learning methods. Deep learning and machine learning play an important role in the development of an efficient sEMG-based exoskeleton prototype in this thesis.

1.4 Objectives and Outline of Chapters

This research aims to design and develop an exoskeleton to assist in daily life activities. The following objectives defined to meet this research:

(a) To select appropriate linkage models for load-bearing lower limb exoskeleton from various existing designs

(b) Adapt different sensors, electric actuator and sEMG signal enabled the actuating system to promote the applicability

(c) Incorporating force simulator for the develop sEMG operated to improve its functionality

(d) Test the design for Flexion and Extension movement of the lower limb for ramp

climbing

To achieve the objectives of the research work Solidwork, ANYBODY Modelling Software, MATLAB, Nexus-10 MKII, TM4C123GH6PM tool, many Ic's, linear actuator and knee exoskeleton were used.

The subject matter is covered under the next five chapters, besides Chapter 1.

Chapter 2: This chapter deals with the literature survey of human knee biomechanics, followed by sEMG signal preprocessing and muscle force estimation, prediction and classification of knee joint angle and sEMG signal, and finally, a description of control strategies for the single and multi-joint exoskeleton.

Chapter 3: This chapter begins with 3 D design of the lower limb exoskeleton and AnyBody Modeling Software (AMS). The performance of 3 D designed exoskeleton was evaluated by placing various loads on both the shoulders of the human musculoskeletal in AMS. Hill muscle model was used to muscle force estimation from sEMG signals. ANOVA t-Test was used to validate results. The developed model helped understand the load effects on different muscles and provided useful information for constructing an individual's optimized exoskeleton.

Chapter 4: Different simulation tools and conventional algorithms were used in dynamic motion to determine the knee muscle forces of humans. Cost-efficient and efficient Machine Learning (ML) models were developed to predict knee muscle force for clinical interventions on certain input parameters such as height, mass, and angle. Four ML models were trained and tested to predict the force of the knee muscle: Neural Network, Generalized Linear Model and Decision Tree, random forests.

Chapter 5: This chapter begins with the prediction of sEMG signal and knee joint angle, followed by movement classification using PSO-LSTM.To validate the performance of the Particle Swarm Optimization - Long Short Term Memory (PSO- LSTM) model, it was compared to a random LSTM model. PSO-LSTM outperforms the other models in terms of RMSE, r and R^2. The developed lower limb knee exoskeleton prototype and its control sequence are described in this chapter.

Chapter 6: This chapter concludes and evaluates the outcomes of the study in achieving the research objectives. Future work suggestions to extend and improve the system potentials also included.

Chapter 2

Literature Survey

This chapter begins with a study of human biomechanics of the knee followed by preprocessing of sEMG signals for estimation of force, knee joint angle and movement classification using machine learning and deep learning approach, and finally a description of control strategy for the design of lower limb exoskeleton.

2.1 Human Biomechanics of the Knee

Mariem *et al*. [65] provide an overview of the current biomechanical knowledge on normal and injured knee joints. The biomechanical parameters including angle, moment, power, and stiffness from various researchers in different daily motions for a better assessment of the knee joint function were reviewed and compared. The main functions of the knee joint include supporting the body weight (BW), absorbing the shock of heel strikes, and assisting lower limbs swing.

Robert *et al*. [66] described human biomechanics and motor coordination while climbing stairs at different angles (24°, 30°, and 42°). To compute joint moments and powers, an inverse dynamics approach was used. The inclination had a small but significant influence on joint angles and moments. As a result, it suggests that subjects switch between a level walking and a stair walking gait pattern at a specific inclination angle or angular range.

Law *et al*. [67] examine the effects of body mass and sex on the joint biomechanics of the lower extremity during stair ascent and descent. Joint mechanical loading presented by a joint moment of force and peak joint angles at the hip, knee, and ankle during stair climbing were recorded and analyzed using a motion analysis system with ten cameras and four force plates.

Tung *et al*. [68] described the history and methodology of human movement biomechanics, as well as the theoretical and experimental methods for the study of human movement, were discussed by. It was suggested that further study of the biomechanics of human movement and its clinical applications will benefit from the integration of existing

engineering techniques.

2.2 SEMG signals preprocessing and estimation of force

Roberto *et al*. [69] present a review of techniques for estimating, interpreting, and comprehending time variations in the surface electromyographic (EMG) signal during sustained voluntary or electrically elicited contractions. Amplitude variables, spectral variables, and muscle fibre conduction velocity were all affected by these variations.

Phinyomark *et al*. [70] present cutting-edge EMG signal processing and classification techniques that address these dynamic factors and practical considerations.Hands-busy conditions and cross-user classification models that present additional challenges for gesture recognition tasks were also investigated.

Isreal *et al*. [71] provided a detailed analysis of the data acquisition system for EMG signals from myoelectric interfaces. Monitoring of muscular activation for rehabilitation, muscle activation plans, and identification of possible pathologies, exoskeletons, electric wheelchairs, prosthetics control, myoelectric bracelets, handwriting recognition, and silent speech recognition were all examined.

Buchanan *et al*. [72] proposed a dynamic forward model based on the Hill muscle model to control the movements of an sEMG-based prosthetic hand to assist disabled patients. **Ao *et al***. [73] proposed a control method based on a combination of the Hill muscle model and a linear scale model to achieve assistance via an ankle exoskeleton. **Yokoyam *et al***. [74] used MLP with multiple hidden layers and electrodes on the back of the hand to predict handgrip forces.

Yang *et al*. [75] develop a system that maps the force of a 3-DOF wrist motion to the cursor's position on the screen. A deep CNN was imposed for the 3-DOF wrist force regression task, with raw EMG data as input. A system was designed to recognise the magnitude and direction of the various forces acting on a designed facility by a hand at the same time.

Chen *et al*. [76] estimate the force of the multi-DOF finger continuously with HD-EMG data as the input and compare the performance of the CNN and CNN plus RNN with classical methods. This study found that CNN combined with the LSTM achieves the best performance.

Yu *et al*. [77] used a five-layer stacked auto-encoder (SAE) based deep neural network

to continuously estimate wrist torque. The SAE was used to reduce data dimension, and the fully connected layers were used to calculate torque.

2.3 Prediction and Classification of Knee Joint Angle and sEMG signal

Liu *et al*. [78] used a nonlinear autoregressive model to extract the mapping relationship between sEMG signals and upper limb joint motion, allowing them to accurately decode multi-joint motion intentions for human upper limbs]. **Tang *et al***. [79] used a back propagation neural network (BPNN) to learn the mapping relationship between sEMG signals and elbow angles.

Ding *et al*. [15] used a high-order polynomial to develop a stable model for accurately predicting the multi-joint motions of human upper limbs based on sEMG signals. **Kawase *et al***. [80] proposed a novel biomechanical upper limb model based on sEMG to estimate multiple joint angles for a human upper limb.

Bao *et al*. [81] estimate wrist movement using an EMG spectrum image. Several machine learning-based methods are compared to CNN, and the results show that the CNN-based method was superior. **Ren *et al***. [82] predict both arms' upper limb joint angles using the multi-stream LSTM (MS-LSTM) model.

Ameri *et al*. [83] use the Fitts' law test and a regression CNN to decode wrist movements. It demonstrates that deep neural networks outperform the feature extraction method when it comes to representation. **Xia *et al***. [84] estimate the angle of the shoulder and elbow using the CNN sequentially combined with the RNN. **Xunju Ma *et al***. [85] described the continuous estimation of knee joint angle based on surface electromyography using an LSTM to improve the exoskeleton's performance.

Huang *et al*. [26] use EMG and IMU data to predict knee joint angle during walking. Deep neural networks are built using a fully connected RNN with the relu activation function. When compared to the LSTM or GRU, the method had a lower computational cost.

Gautam *et al*. [21] propose a CNN-LSTM combination model to classify lower limb movement and estimate knee joint angle at the same time. The parameters learned during angle estimation were transferred to movement classification using transfer learning.

Chenfei Ma *et al*. [86] used the SCA-LSTM deep learning approach to estimate continuous upper limb joint angle from sEMG signals. Eleven participants' sEMG signals

corresponding to seven classes of shoulder-elbow joint angle movements were recorded simultaneously. Afterwards, SCA-LSTM models were trained and tested using the pre-processed data for continuous estimation of arm movements.

Feng Zhang *et al*. [87] described the continuous joint angle estimate for human legs using the BP neural network as based on the sEMG. The model inputs are time series sEMG, the outputs being hips, knees and ankles joint angles. There were simultaneously seven channels of SEMG from the leg muscle and three joint angles. The results indicate that this method was performing well with the sEMG signal joint angle estimation.

Ardestani *et al*. [10] described human lower extremity joint moment prediction using a wavelet neural network approach. Based on the mutual information technique, a total of ten inputs were determined to be the most informative for the WNN, including eight electromyography (EMG) signals and two ground reaction force (GRF) components.

Feiyun Xiao *et al*. [17] described continuous joint angle estimation from electromyography using multiple time-delayed features and random forests. Extract hidden information from sEMG and generalise an estimation model was done in order to estimate continuous human motion from surface electromyography (sEMG).

Duan *et al*. [88] used the discrete wavelet transform and a wavelet neural network algorithm to recognise six gestures with only three sEMG sensors accurately. **Naik *et al***. [89] proposed an sEMG-based control method based on ICA and Icasso clustering, with the goal of identifying 11 amputee poses with the fewest number of EMG sensors.

Ghulam Rasool *et al*. [90] described Surface myoelectric signal classification using the autoregressive-generalized autoregressive conditional heteroscedastic (AR-GARCH) model and used this model parameters as a feature set for signal classification.

Geng *et al*. [91] used high-density sEMG sensors to acquire sEMG images and deep convolutional neural networks to accurately recognise eight gestures. **Islam *et al***. [92] proposed a feature classification indicator based on the SVM algorithm that uses directional map histograms for high-density EMG images and achieved the accurate classification of 8 gestures.

Atzori *et al*. [93] evaluate the performance of a simple CNN on Ninapro DB1, DB2, and DB3 EMG data, which contains approximately 50 hand gestures collected from 67 healthy subjects and 11 amputees. The accuracy of CNN was superior to that of traditional methods on average. **Olsson *et al***. [33] present a CNN-based multi-labelled classification using HD-EMG as the input. Complex movements are expressed using multilabel methods as a sum of multiple simpler movements. The state of the hand was

modelled using 16 different movements.

Nasri *et al*. [94] propose a GRU-based scheme for processing EMG segments using the sliding window method, and the accuracy for six gestures performed by 35 subjects was 77.85 %. **Simão *et al***. [95] process the single frame sEMG with several deep learning methods, such as RNN, LSTM, and GRU, to extract temporal information inside the EMG.

Samadani *et al*. [96] compare a step-wise learning rate and several optimization methods, including the bidirectional recurrent layer and attention mechanism. Better accuracy achieved was achieved for 18 gestures with the Ninapro DB2 using bidirectional LSTM (Bi-LSTM).

Alfaro-Ponce *et al*. [97] compare the performance of the time-delay neural network (TDNN), differential neural network (DifNN), and complex-valued neural network (CVNN) for two different physiological signals, including EMG and foot pressure of the gait for Parkinson disease (PD) patients, and the accuracy of all three networks was greater than 95 %.

In addition to the CNN and RNN mentioned earlier, which belong to the supervised learning approach, unsupervised deep neural networks, such as auto-encoder and deep belief networks, were also used for movement classification. The AE-based schemes can be classified into two types according to the input format: hand-crafted feature-based methods and raw data-based methods.

Rehman *et al*. [98] apply stacked sparse auto-encoders (SSAE) to multiday EMG recordings to improve the performance. The results of the SSAE was better than linear discriminant analysis (LDA) for both intact and disabled subjects with four time-domain features.

DBN usually takes hand-crafted features as the input. **Shim *et al***. [99] propose the split and Merge DBN, which chooses the genetic algorithm to augment the performance of the DBN; the precision outperforms classical DBN by 12.06 %. **Zhang *et al***. [100] recognized normal and aggressive EMG signals, and each contained ten actions using DBN with time-domain feature sets. The best accuracy reached was 90.66 $\pm$ 1.47 %. Additionally, **Sun *et al***. [101] proposed a novel method using a generative flow model (GFM), an unsupervised learning method similar to the DBN that converts sEMG data into various features and applies the features for sEMG classification using a softmax classifier.

The above techniques apply a single type of deep learning method for hand gesture

prediction. There are mixed network structures, such as multi-stream networks, chosen for this task.

Ding *et al*. [102] handled the hand gesture classification task using a parallel multiple-scale convolutional neural network. **Wei *et al***. [40] decomposed EMG into multiple streams, and a CNN with multiple sub-streams was used for gesture classification. Mixed architectures that are connected were widely used for EMG-based gesture classification. **Cao *et al***. [103] proposed a dual-flow network that uses the CNN and LSTM individually to extract the EMG features simultaneously; then, the features are given into fully connected layers for classification.

Wu *et al*. [35] propose a system based on CNN and LSTM with the attention mechanism for hand gesture classification with CWT of EMG as the input. **Xie *et al***. [104] combine CNN with LSTM into a unified structure, and an accuracy of 98.14 % was achieved. **Tong *et al***. [105] combine three layers of CNN with three layers of RNN for hand gesture classification.

Tsinganos *et al*. [106] outperform state-of-the-art performance by 5 % on Ninapro DB1 with a temporal convolutional network (TCN). However, this technique chooses complete EMG data instead of the envelopes under 300 ms as the input. **Zanghieri *et al***. [107] developed a TCN-based network named TEMPONet, which runs on an embedded system. The performance reaches 49.6 % on a Ninapro DB6, which outperforms the current state-of-the-art method by 7.8 %.

Shen *et al*. [32] proposed a scheme using a CNN and a stacking ensemble learning algorithm with three types of inputs, including EMG data, DFT of EMG data, and discrete wavelet packet transform (DWPT) of EMG data. The CNN works as a low-level classifier, and the results are optimized by an ensemble learning-based secondary classifier.

Chen *et al*. [108] propose a novel technique with typical CNN networks whose output layer was replaced by machine learning methods, including SVM, LDA, and K-nearest neighbour (KNN). All three methods outperform the traditional feature-based method. This shows that features obtained by CNN are efficient for human intention recognition. EMG can be used for robot hand control for amputees.

Shao *et al*. [109] present a scheme for twelve upper limbs' motion recognition with single-channel EMG. The spectrum acquired by the FFT was first decomposed by the singular value decomposition (SVD) method and then processed by wavelet deep belief networks (WDBN).

2.4 Control Strategy for Single and Multi-Joint Exoskeletons

Pratt *et al*. [110] designed to assist the wearer during stairs ascent and squatting with heavy loads. **model-based control strategy** aims to relieve the quadriceps muscle of the **knee joint** while performing one-legged deep squatting with a 60-kg backpack.

Gams *et al*. [111] was a **knee augmentation exoskeleton** intended for the wearer's squatting movement. This device follows a **model-based control strategy**. Seven healthy young subjects performed five-minute squatting exercises in a randomized order. Their oxygen consumption, minute ventilation, heart rate, blood oxygenation, and muscle EMG were monitored during these tests.

Lai *et al*. [112] was developed to help the elderly and patients to achieve a more regular walking pattern. Its strategy based on **predefined gait trajectory control**. The desired knee angle was computed based on the hip joint angle through a polynomial interpolation of clinical gait data during the swing phase. Available results from one subject walking on a treadmill wearing the **powered knee orthosis (PKO)** confirmed the feasibility of this control strategy.

Kim *et al*. [113] An assistive **muscle stiffness control strategy** tested on this **knee orthosis**. Two pneumatic artificial muscles simulate the functions of the rectus and biceps femoris muscles. The muscle stiffness force sensor (MSFS) was used to quantify the pressure changes. Twenty participants performed sit-to-stand and squat movements. The experimental results showed that lower limb muscular activities were reduced during sit-to-stand and squatting motions under assistance.

Karavas *et al*. [114] consists of two cuffs for the thigh and shank and a rotational actuation system. This **knee exoskeleton** aims to empower the user's knee by augmenting the robotic joint stiffness. A healthy subject's standing up trials proved the effectiveness of this knee exoskeleton with its assistive strategy.

Alexander *et al*. [115] used for stand-to-sit and sit-to-stand tasks. The **knee extension assist device (KEA)** provides assistance from a spring and a pneumatic actuator by using a **predefined action-based control strategy** on the gait pattern. Two healthy male adults were recruited to test the device. Participants performed stand-to-sit and sit-to-stand motions in both deactivated and activated conditions. A seven-camera motion analysis system was used to capture the motions, and surface electrodes recorded the EMG activities. Results demonstrated that both subjects could stand up and sit down in a slower but more controlled manner.

Fleischer *et al*. [116] was a mono-lateral knee exoskeleton that **actuating the knee** through a linear actuator to calculate the current muscular torques based on the EMG signals. Since the controller directly depends on the **myoelectrical control** of EMG activities, TUPLEE was suited for healthy people. Experiments were performed with a single subject, performing general daily-life activities, like standing up, walking, climbing stairs, etc.

Kazerooni *et al*. [3] was the first load-carrying and augmented exoskeleton. This **multi-joint exoskeleton** adopts a **sensitivity amplification control strategy**. The user could walk at an average speed of 1.3 m/s while carrying a 34 kg payload using this control strategy by wearing BLEEX.

Yang et al. [117] was developed for helping a user carry heavy loads on different terrains with increased speed and hardiness, where vehicles can't reach. This **multi-joint exoskeleton** adopts a **sensitivity amplification control strategy**. It can serve as a rehabilitation exoskeleton and help people who partly lost their walking ability due to stroke, elderly age. It can carry a load of up to 15 Kg.

Sankai *et al*. [118] was developed to physically augment the joints power of healthy people or assist people affected by gait disorders. Different types of HAL were developed: HKAF orthosis, a whole body and a single-leg device. These all provide movement assistance on the sagittal plane using a **predefined gait trajectory control strategy**. This assistive strategy was validated with two subjects: one with lower-limb sensory paralysis, and another was healthy.

Wang *et al*. [119] was equipped with compliant series elastic actuators to regain locomotion capability for people with paraplegia. This **multi-joint exoskeleton** provides gait assistance in both lateral and sagittal planes. Its actuation capacity and structural strength can deal with subjects weighing up to 100 kg. Stable walking without crutches was achieved for healthy subjects with the assistance of MINDWALKER.

Ikehara *et al*. [120] aim to assist elderly and impaired people. Its actuation system was placed in a backpack. The use of self-contained **predefined gait trajectory control systems** in the device was allowed users to walk on the ground level. Walking experiments were carried out with both healthy subjects and paralyzed subjects [38]. EMG activities measured from healthy subjects showed decreased muscular activities for normal walking.

Alberto *et al*. [121] was a commercial bionic **multi-joint exoskeleton** walking assistance system that to enable paraplegics to stand upright, walk and climb stairs. This was powered by a backpack battery and was controlled by a simple wrist-mounted controller.

Twelve subjects with chronic motor complete cervical and thoracic SCI were trained to use ReWalk. After eight weeks of practising, all subjects could walk independently with crutches at least 50 meters continuously.

Terris *et al*. [122] addresses knee assistance for subject affected by poliomyelitis. By detecting the foot pressure of the sound leg, the knee–ankle-foot orthoses (SCKAFOs) was controlled with a **predefined torque profile**. A 54-year-old male polio subject tested the orthosis: the assisted knee pattern was close to normal, a result difficultly achievable by him with a standard passive orthosis.

Kawamoto *et al*. [123] was developed a **multi-joint exoskeleton** to aid people in moving and executing daily life activities. The motion support of HAL was activated consistently with the user's motion intention by using a **model-based control strategy**. A 60-year-old male subject with impairment on the right knee participated in this experiment. Results of repeated trials showed that HAL was effectively assisted movement and muscular activity.

Mori *et al*. [124] was a moving transfer system for subjects having impaired lower limbs. It consists of a powered **multi-joint exoskeleton**, a pair of hand crutches and a pair of foot mobile platforms to assist the wearer travelling in a standing posture, standing up from a chair, and stair ascending.

Yamamoto *et al*. [125] was a pneumatically powered **multi-joint exoskeleton** to assist nurses in lifting patients. The weight was transferred to the ground while the nurse stands up; when the nurse bends the waist or the knee, the actuators support the total weights. Assistive efficacy was proved by a subject executing a holding and up-down moving of a 60-kg-weight person.

Chen *et al*. [126] was used for human power augmentation. It decreases human inner force during certain activities, such as care workers, older adults, soldiers, and firefighters. WPAL robot represents a high integration of robotics, information technology, communication, control engineering, signal processing, etc.

Tagliamonte *et al*. [127] targets rehabilitation tasks by assisting the hip and knee joints in the sagittal plane during walking. **Adaptive oscillators** are utilized to track the fundamental frequencies of hip and knee angles and coupled with a non-linear filter to predict the values of the next angle. A healthy volunteer was walking on a treadmill with the exoskeleton for testing the stability and feasibility.

Zhang *et al*. [128] had four actuators for the hip and knee joints to move in the sagittal plane. **Adaptive oscillators** are connected to each hip joint of the robotic suit to

synchronize the suit's movement with the human user's movement. Ten subjects attended the experiments and walked back and forth in a room for one minute along a five-meter route. The experiment results showed a reduction of muscles activities and an increase in step length and speed.

Belforte *et al*. [129] was designed for gait rehabilitation and locomotion assistance for paraplegic subjects. This **multi-joint orthosis** was a pneumatic actuation system to powers the hip and knee movements based on **predefined action based control strategy**. Evaluation experiments were separately done on a bench test without user, with a healthy user and with a T3-lesion-level paraplegic subject. Both healthy and paraplegic subjects could walk with assistance, but kinematics and kinetics results were not smooth, especially the performance of the paraplegic subject.

Walsh et al. [130] was designed for load-carrying augmentation by transferring the backpack's load to the ground through a pelvic harness. The hip and knee joints were both powered. The actuation of the hip and knee joints were functions of the gait cycle. Experiments with the active hip and knee joints were shown that the exoskeleton could transfer 90 % of payload to the ground.

Kazerooni *et al*. [131] was controlled utilizing a hybrid controller in another work. This **multi-joint exoskeleton** leg was controlled by a positive feedback sensitivity amplification force controller during the swing phase. When the leg enters the stance phase, a position controller was enabled, aiming to decrease the differences between the human and BLEEX joint angles. The two legs were controlled independently, and the switch between the two controllers was decided according to the gait states. Experiments showed that a pilot could walk in BLEEX at 0.5 m/s with a payload of 18 kg, and BLEEX performances were lower than in the case of the only sensitivity controller.

Aphiratsakun *et al*. [132] was developed as a **multi-joint hybrid assistive exoskeleton**. That was used to assist patients suffering from immobility of lower limbs, mainly paraplegia. The model adopts the zero-moment point (ZMP) criteria to ensure balance, providing an estimation of the ZMP location. The differences between real-time ZMP and reference ZMP were fed to a fuzzy-logic controller to compensate for disturbances and uncertainties. This balance keeping strategy was only validated on a bench test with a simplified human body model.

Kiguchi *et al*. [133] designed multi-joint exoskeleton to assist the movements of physically weak people. The desired assistance for hip and knee movements estimated through an EMG-based **neuro-fuzzy controller**. Eight EMG signals from the lower limb of healthy males assist various movements, e.g. sitting down, standing up, climbing stairs,

and squatting with and without assistance. Results proved the effectiveness of this controller, *i.e.* reduce EMG levels while hip and knee joints being assisted smoothly.

Kong *et al*. [134] was developed a **multi-joint exoskeleton** to assist patients and older adults. The assistance desired from EXPOS was computed by a **fuzzy controller** which was based on the joint angular velocity and torque. An elderly subject was executed sitting down and standing up exercises with and without EXPOS.

Kai *et al*. [135] incorporate a progressive assist-as-needed (pAAN) controller into their custom-built lower limb exoskeleton system. This control strategy having the potential to increase subjects' active participation. The controller can dynamically estimate a subject's input without calibrations based on **electromyography (EMG)**.

The SEMG based exoskeleton has a multifactorial problem such as the variability of the SEMG over the time or define exact SEMG signal for particular human activities while designing real-time development of lower limb exoskeleton. Another difficulty also found in terms of body mass index (BMI) because every individual has a different BMI. Therefore, each has its own muscle and joint forces. Once a real time exoskeleton is developed, it become difficult to customize it according to the individual requirement. So, before going for real time Implementation, simulation-based analysis is required, to avoid any future complexity.

This chapter elaborates on the historical development of human biomechanics of the knee, sEMG signals preprocessing and estimation of muscle force, Prediction and classification of knee joint angle and sEMG signal, and control strategy of single and multi-joint exoskeletons. A soft computing study helped to fine-tune the development of a real-time sEMG based exoskeleton for every individual and eventually saves time and cost.

Chapter 3

Human Biomechanics Design Aspects using AnyBody Modelling Software

The surface electromyography (sEMG) based exoskeleton presents a new opportunity for human augmentation and rehabilitation. An exoskeleton was designed in SolidWorks CAD software and imported into AnyBody Modelling Software (AMS). Thereafter, the performance of a 3D designed exoskeleton was evaluated by placing various loads (0:5:25 kg) on both the shoulders of the human musculoskeletal. The developed model helped in understanding the load effects on different muscles and provides useful information for the construction of an individual's optimized exoskeleton.

3.1 Human Musculoskeletal and Design Exoskeleton

Globally, many people face multiple challenges while performing activities of daily living (ADL), such as walking, squatting, climbing stairs, lowering and lifting tasks (repeated tasks). These challenges may be due to ageing effects or other factors such as muscle fatigue/weakness, joint disorders and neurological diseases [136–138]. Additionally, the primary cause of disability in the workplace is associated with manual workers carrying heavy loads . Because of the repetition of heavy tasks, workers are at risk of developing various disorders such as work-related musculoskeletal disorders (WMSDs) and lower back disorders (LBD) [139]. Various assistive and rehabilitative devices for upper and lower limbs have been developed to assist a person in performing ADL and repetition exercises. These devices come under two categories, stationary (positioned in the particular area) and portable (moveable). The disadvantage of the stationary assistive device was observed, such as limiting the user's natural movement to perform ADL, while portable assistive device provides a wide range of advantages for dynamic activities such as walking, squatting, and climbing stairs, *etc* [50, 140, 141]. Researchers continue to work on the lower limb portable exoskeleton operated by sEMG [142]. This assistive system had many issues, such as a fluctuation/variation in the sEMG signal over time, which made it difficult for specific activities to predict the sEMG signal.

Experimentally evaluating muscle and joint forces during full squatting movements and optimizing the product design while developing a real-time lower limb exoskeleton is challenging. Various musculoskeletal software, such as Life Modeler, AMS (AnyBody Modelling Software), and OpenSim software, were used to conduct this type of analysis [143, 144]. This software provides the digital representation of a human body in a three-dimensional (3D) environment [145]. Among these, AMS offered a convenient tool for modelling and simulation-based analysis. In AMS, human musculoskeletal was used for various applications such as walking, squatting, interfacing, *etc.* The height, weight, and angle of the various joints (range of motion) of the human musculoskeletal can all be adjusted as per requirements.

Furthermore, SolidWorks, a well-known CAD software, was used to design 3D lower limb exoskeleton, *i.e.* portable assistive devices [146]. The simulation study of the 3D design of a lower limb exoskeleton was found cost-effective and useful in improving the efficiency of assistive devices. A simulation study carried out by Brandon et al. [147] predicts the ground reaction forces using the simulated prototyping of the ARKE exoskeleton. Similarly, Spada et al. [148] evaluated the performance of the chairless exoskeleton in the simulated environment. Several experiments were carried out in a simulated environment [146, 149–154]. The lower limb exoskeleton's 3D design performance in a simulated environment was not evaluated or studied. Therefore, there is a need to study the lower limb exoskeleton in a simulated environment before developing it in real-time.

3D design of a lower limb exoskeleton was used and evaluated in a simulated environment in this study. A simulated environment (AMS) had a human musculoskeletal and an exoskeleton along with inverse dynamics analysis. The results show variations in the knee joint and knee muscle force (vastus medialis: VM, vastus lateralis: VL, biceps femoris: BF, rectus femoris: RF, semitendinosus: STEM, Gluteus Medius: GMED) by placing the various loads on both shoulders (0:5:25 kg) of the human musculoskeletal during squatting movement in AMS. The effectiveness of the 3D design exoskeleton was examined by utilizing various loads. For validation, the force estimated from the sEMG signal of healthy male's lower limb muscles was compared to the similar muscle force of human musculoskeletal obtained from AMS. This work is intended to serve as a first step towards the modelling, validation, and real-time development of the exoskeleton. The results of the simulation will aid in the development of efficient and customised prototype exoskeletons.

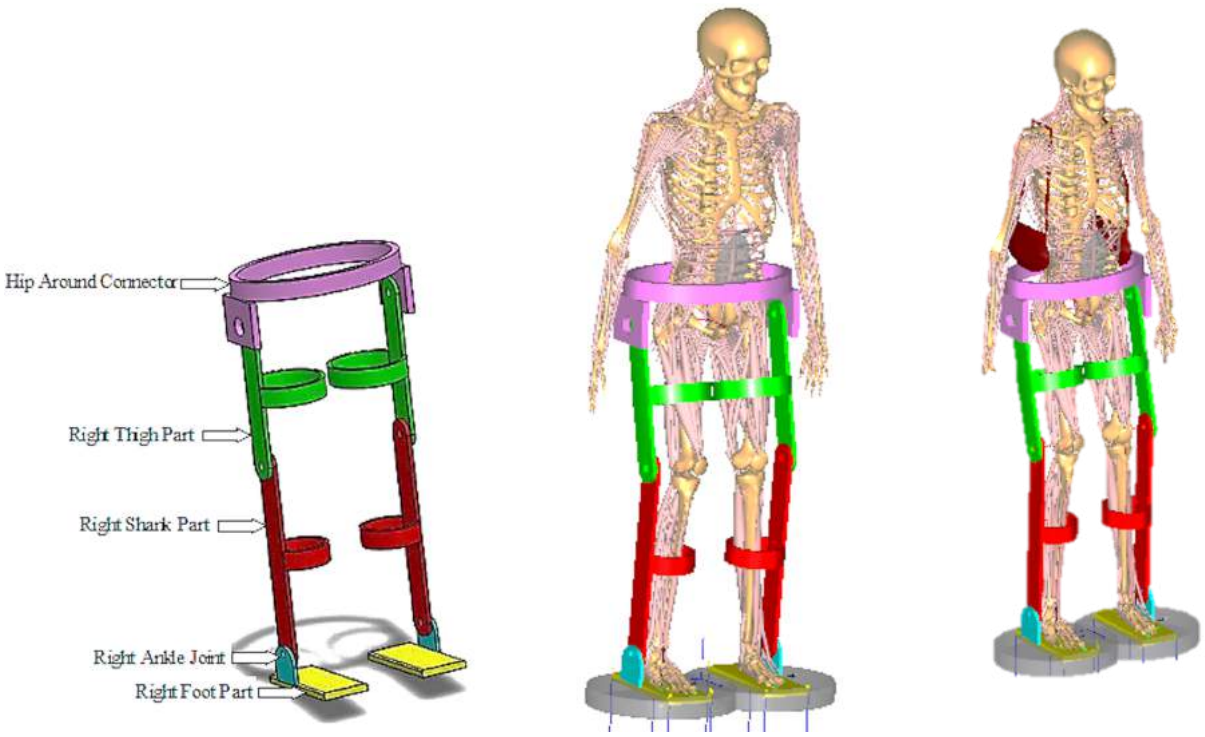

(a) (b) (c)

Figure 3.1: (a) Lower limb exoskeleton; (b) Interfacing of human–exoskeleton; (c) Carry beg on both shoulders with various load

3.2 Methodology

3.2.1 Experiment Design and Dataset

Understanding 3D lower limb exoskeleton performance in a simulated environment is the optimal way before developing a real-time exoskeleton, as shown in Figure 3.1 (a), (b). Various loads (0:5:25 kg) were placed equally on both shoulders to evaluate the performance/effectiveness of the exoskeleton during the squatting movement, as shown in Figure 3.1(c).

In AMS, the reduction of the knee joint and muscle force was the focus of the 3D design of lower limb exoskeleton performance. A standard template, namely human musculoskeletal for an average healthy European male with a height of 175 cm and a mass of 72 kg for AMS, was used [143]. An inverse dynamics analysis on a given template of human musculoskeletal for a squatting movement (without load and without exoskeleton) was performed in 61 steps through the AMS software to analyze muscles (simulation analysis). The responsible muscles for squatting movement (vastus medialis: VM, vastus lateralis: VL, biceps femoris: BF, rectus femoris: RF, semitendinosus: STEM, Gluteus Medius:

GMED) were selected [139, 155] for validation of experimental and simulation analysis. During the squatting activity of the human musculoskeletal in AMS, inverse dynamic analysis was performed for the quadriceps (VM, VL, and RF), hamstring (BF, STEM), and GMED muscles, as shown in Figure 3.2.

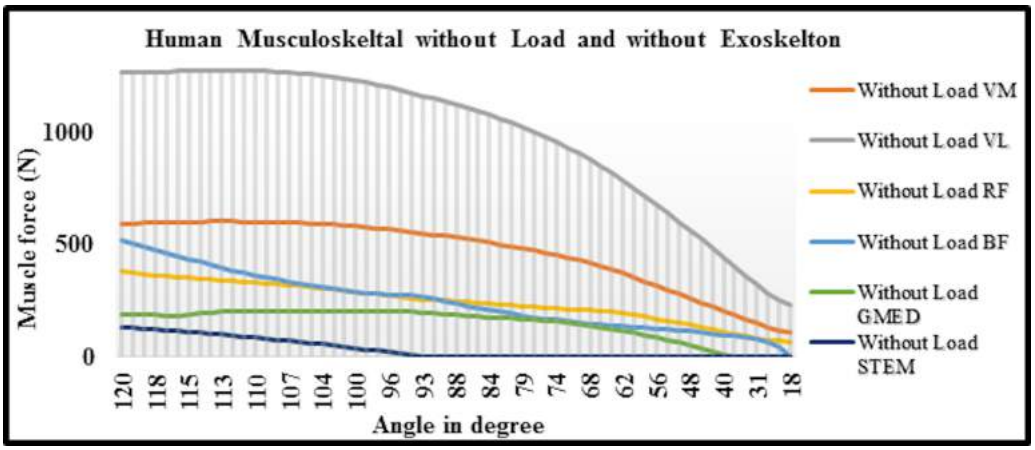

Figure 3.2: Force versus angle characteristics of six muscles

The quadriceps muscle group had higher muscle force as compared to the hamstring muscles and GMED muscle. VM and VL muscles have a higher value of force than the RF muscle between the quadriceps muscle groups. Due to the bilateral nature, the RF muscle (extensor of the knee/flexor of the hip) generates less force. The quadriceps, specifically the VL and VM muscles, play a vital role in stabilizing the knee joint and helps in the squatting activity. On the other hand, the hamstring muscles (BF, STEM) had a bilateral nature because these muscles work together for flexion of the knee and extension of the hip. The STEM muscle had the lowest force value among all the muscles due to its bilateral nature, as shown in Figure 3.2. It is one of the hamstring group muscles that are responsible for flexion of the knee movement. The GMED muscle had a higher force value than the STEM and a lower value than the other, as shown in Figure 3.2. It is mainly responsible for hip rotation and flexion/extension. It also helps to keep the pelvis stable during the squatting movement [156]. During the squatting activity, the angle between the thigh and shank was the range of 120°-18° (with and without the assistance of the exoskeleton), where an angle of 120° denotes squatting and 18° a standing position as shown in Figure 3.1 (b), (c). All muscles (VM, VL, RF, BF, GMED, STEM) were selected for exploring the effectiveness of the 3D design exoskeleton and validation purpose (simulation analysis). Also, similar knee muscles (VM, VL, RF, BF, GMED, STEM) were selected from healthy males (without muscular or bone disease) for sEMG signal recording (experimental analysis), as shown in Figure 3.3)

Nine healthy males above 70 kg mass with 170 cm height were included in the sEMG

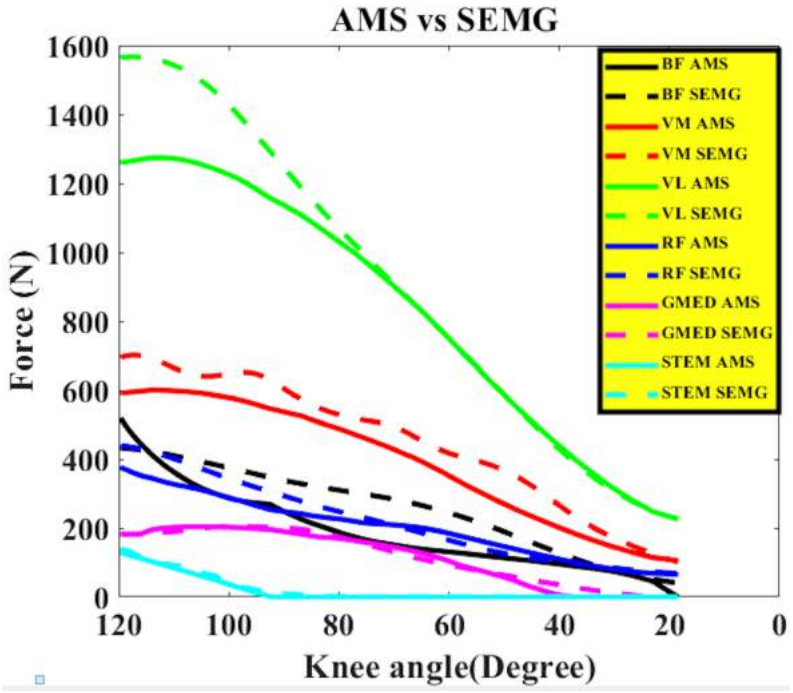

Figure 3.3: Comparison of muscle forces during the squatting movement (Bold line- simulation result. Dashed line- experimental result)

recording. The selection was based on the AMS human musculoskeletal template (mass and height). The percentage of healthy males' inclusion was $100\%(9/(9) \times 100)$. The average age of the selected males for the sEMG signal data set was 30 ± 8.2 years, with an average height of 174 ± 1.062 cm and an average mass of 72 ± 0.885 kg, respectively. The sEMG signal was recorded from nine healthy males without placing any load on both shoulders (experimental analysis). The average of nine healthy males' sEMG signals for muscles (VM, VL, RF, BF, GMED, STEM) were used for validation purposes. The sEMG signal of selected muscles from healthy males was transformed into muscle force via the Hill muscle model, as shown in Figure 3.4.

An individual average muscle force of nine healthy males was compared with the muscle force generated through AMS for a squatting movement [155]. In both cases, the healthy males were selected to compare muscle forces, either experimental or a simulation-based analysis. This study was necessary to validate the experimental results with simulation results. After validation, AMS was used to interface the lower limb exoskeleton with the human musculoskeletal. The squatting movement of both interfaces was performed in 61 steps by using inverse dynamic analysis. This interfacing helped in the reduction of knee muscle and joint force.

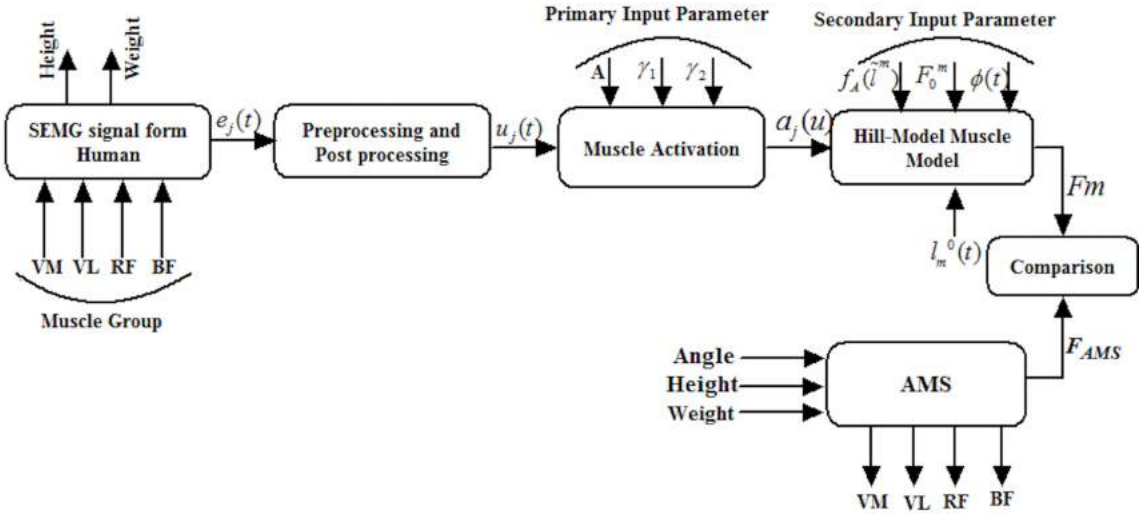

Figure 3.4: Steps for estimating the muscle forces from sEMG signal

3.2.2 sEMG Signal Acquisition to Force Estimation

The sEMG signals from selected lower limb muscles were recorded using a biopotential recording instrument (Nexus-10 MKII). The sEMG signal was recorded simultaneously at a sampling frequency of 2048 Hz. The sEMG electrode location for selected muscles was identified by SENIAM recommendations [157]. The electrodes were attached with medical tape during the experiment to fix their placement throughout the experiment (sEMG signal recording).

3.2.3 sEMG Signal Acquisition

Figure 3.4 shows the steps required to estimate muscle forces from the sEMG signal [155], [158–163]. The sEMG signal was recorded for various knee muscles, namely: VM, VL, RF, BF, GMED, STEM during squatting movement. Preprocessing was carried out to improve the quality of the sEMG signal, which included high pass filtering, rectification, normalization, followed by low pass filtering for envelope extraction. A fourth-order, zero-lag Butterworth recursive high pass filter with a cutoff frequency of 30 Hz was applied on recorded sEMG signals to eliminate the DC offset, low-frequency noises. The filtered signals were then rectified and normalized using the full-wave rectification and mini-max normalization method, respectively. A frequency between 1-5 Hz was suggested as an optimal range for envelope extraction [155]. A second-order Butterworth low-pass filter with a frequency of 1.5 Hz was used to extract the envelope.

Envelope of sEMG signals is used for the estimation of muscle force. A linear second-order critically damped differential system was used initially, as described in Equa-

tion (3.1).

$$u_j(t) = \alpha e_j(t-d) - \beta_1 u_j(t-1) - \beta_2 u_j(t-2) \tag{3.1}$$

where $e_j(t)$ is the high-pass filtered, rectified and low-pass filtered sEMG of muscle j at time t, $u_j(t)$ is the post-processed sEMG of muscle j at time t, α is gain coefficient of muscle j, β_1 and β_2 are the recursive coefficient of muscle j and d is the electromechanical delay. The transfer function of Equation (3.2) obtained by the Z-transform of the impulse response of the Equation (3.1).

$$H(z) = \frac{u(z)}{e(z)} = \frac{\alpha}{1 + \beta_1 z^{-1} + \beta_2 z^{-2}} \tag{3.2}$$

Selection of the values for β_1 and β_2 is critical to forming a stable Equation (3.2).

$$\begin{aligned} \beta_1 &= \gamma_1 + \gamma_2 \quad |\gamma_1| \leq 1 \\ \beta_2 &= \gamma_1 \gamma_2 \qquad |\gamma_2| \leq 1 \end{aligned} \tag{3.3}$$

Equation (3.2) is a recursive filter, which was used to find the unity gain. Equation (3.4) must be satisfied to ensure the following condition.

$$\alpha - \beta_1 - \beta_2 = 1 \tag{3.4}$$

Thus, if γ_1 and γ_2 are known, β_1 and β_2 can be found from Equation (3.3) and α can be found from Equation (3.4).

The muscle activation signal for jth muscle is defined as

$$a_j(u) = \frac{e^{A u_j(t) R^{-1}} - 1}{e^A - 1} \tag{3.5}$$

where $u_j(t)$ is the post-processed sEMG signal of muscle j, R is the average of the maximum value of $u_j(t)$ and A is a non-linear shape factor varying between -3 and 0, with A= -3 being highly exponential and A=0 being a linear relationship.

After the muscle activation using Equation (3.5), the next step was to determine the muscle force using Equations (3.6) and (3.7). The Hill-type muscle model was used for estimating muscle forces [164]. The model consists of two elements. One of the components is a contractile element, which produces active muscle force F_A. The other

is a parallel element with passive muscle force F_P. Thus, the total muscle force is given by

$$F_m = F_A + F_P \tag{3.6}$$

The active muscle force is obtained by

$$F_A = f_A\left(\tilde{l}^m\right) F_O^m a(u)\cos(\phi(t)) \tag{3.7}$$

where,$a(u), F_0^m, \phi$ are the muscle activation, maximum isometric force and pennation angle, respectively [22]. $f_A\left(\tilde{l}^m\right)$ is the active force-length function obtained by the cubic spline interpolation of points on the force-length curve [161] [164, 165]. $\tilde{l}^m$ is the normalized fiber length given by Equation (3.8).

$$\tilde{l}^m = \frac{l_m}{l_o} \tag{3.8}$$

l_m is the muscle fiber length, and l_0 is the optimal fiber length. The value of l_m and ϕ_0 were considered from [166]. The pennation angle $\phi(t)$ changes with the change in muscle fiber length. The following function described in Equation (3.9) was used for calculating the pennation angle at time t [159].

$$\phi(t) = \sin^{-1}\left(\frac{l_0 \sin(\phi_0)}{l_m(t)}\right) \tag{3.9}$$

$l_m^0(t)$ is the muscle fiber length at time t described as in [160]. This value obtain by using Equation (3.10) is incorporated into our muscle model using using Equation (3.8).

$$l_m^0(t) = l_m^0(\gamma(1 - a(t)) + 1) \tag{3.10}$$

where ($\gamma = 15\%$) is the percentage change in optimal fiber length, $a(t)$ the activation at time t, $l_m^0(t)$ the optimal fiber length at maximum activation, $l_m^0(t)$ the optimal fiber length at time t and activation $a(t)$.

3.2.4 Exoskeleton Modeling

Figure 3.1 (a) shows the SolidWorks CAD software used to model the lower limb exoskeleton. This model was subsequently translated into the AMS using the "AnyExp4

SOLIDWORKS" plugin. This plugin conserves the geometry, mass, inertia, and joint properties defined in the SolidWorks assembly file during the translation into AMS. The designed exoskeleton was a shank, thigh, ankle, and hip joints (connecting both legs) with a total weight of 17.39 kg. Before translating all these parts from SolidWorks software, mating (relative position of components between each other) were applied for assembling all these parts. Table 3.1 shows a complete description of the different weights, lengths, and widths of the 3D design of lower limb exoskeleton.

Table 3.1: Description of all part of the 3D design lower limb exoskeleton

Parameters	**Right thigh part**	**Right shank part**	**Right ankle part (connector + foot plate)**	**Connector (around the hip)**
Weight	1.85 kg	1.97 kg	2.09 kg	5.07 kg
Length	0.38 m	0.50 m	0.11 m, 0.30 m	0.17 m
Width	0.01 m	0.01 m	0.10 m, 0.020 m	0.019 m
	Thigh Braces	**Shank Braces**	**Ground to thigh Braces distance**	**Ground to shank Braces distance**
Length	0.05 m	0.05 m	0.69 m	0.32 m
Radius	0.09 m	0.07 m		
	Thigh upper and lower joint from ground	**Shank upper and lower joint from ground**	**Ankle joint from ground**	**Connector joint from ground**
Distance	0.09 m, 0.60 m	0.60 m, 0.09 m	0.09 m	0.60 m
	Total height from the ground		**Total weight of lower limb exoskeleton**	
	1.10 m		17.39 kg	

3.2.5 Interfacing of the Human-Exoskeleton Model

Inverse dynamic analysis of the squat movement was performed to determine the joint force and muscle forces at the knee using AMS. A CAD design of the exoskeleton shown in Figure 3.1 (a) imported into AMS using the "AnyExp4SOLIDWORKS" plugin. The imported lower limb exoskeleton does not exert a force on human musculoskeletal knee joints (Figure 3.1 (b)). Hence, an actuator driver at the knee joint of the lower limb exoskeleton was included for completing the dynamic movement in AMS [145].

3.2.6 Connectors and Braces

The exoskeleton was linked by connectors and braces to the human musculoskeletal shank and thigh for parallel movement, as shown in Figure 3.1 (b). It was designed to cover a large surface area of the shank and thigh so that the interaction forces between them could spread uniformly.

3.2.7 Mechanical and Soft Constraints

Various soft constraints available in the AMS script file were used to combine human musculoskeletal and exoskeleton. These constraints allowed the lower limb exoskeleton to move mechanically with the human musculoskeletal. The interactions between human musculoskeletal and 3D lower limbs had rotational (one degree of freedom (DOF)) and welded (zero DOF) joints in AMS. Furthermore, the centre point of the hip in the lower limb exoskeleton was created before importing it into AMS. The existing centre point of the pelvis segment of the human musculoskeletal was also highlighted in AMS. Both centre points were fixed together for interfacing. A similar process was followed for thighs and shanks. The AMS script file performed the squat movement by providing constraint values on the pelvis–thorax, hip, and knee joints. The flexion/extension of the glenohumeral joint was kept at zero constraint values in AMS. Hip abduction/adduction and external/internal rotation, ankle plantarflexion/dorsiflexion and abduction/adduction rotation, pelvis rotations were also kept at zero constraint values in the AMS script file.

3.2.8 Load Distribution

Various loads were applied on both shoulders of the human musculoskeletal, as shown in Figure 3.1 (c). Here, human musculoskeletal having carry bags on both shoulders with various loads. This load ranges from 0 kg (no load) to 25 kg with an incremental 5 kg distribution on both shoulders equally (0 : 5 : 25 kg). Various loads were used to evaluate the performance or effectiveness of the 3D design of the lower limb exoskeleton during the squatting movement.

3.2.9 Relation for Calculating Changes in Muscle Forces and Knee Joint Forces

The following relations were used to examine the changes in the selected muscle force and knee joint force for various loads, respectively.

$$\text{Change in muscle force} = \frac{\left(\begin{array}{c}\text{Average of individual muscle force}\\ i.e.\text{ with an exoskeleton}\end{array} - \begin{array}{c}\text{Average of individual muscle force}\\ i.e.\text{ without an exoskeleton}\end{array}\right)}{\begin{array}{c}\text{Average of corresponding muscle force}\\ i.e\text{ . without an exoskeleton}\end{array}} \tag{3.11}$$

Change in joint force =

$$\frac{\left(\begin{array}{c}\text{Average of individual knee joint force}\\ \textit{i.e.}\text{ with an exoskeleton}\end{array} - \begin{array}{c}\text{Average of individual muscle force}\\ \textit{i.e.}\text{ without an exoskeleton}\end{array}\right)}{\begin{array}{c}\text{Average of corresponding knee joint force}\\ \textit{i.e.}\text{ without an exoskeleton}\end{array}} \tag{3.12}$$

3.3 Results and Discussion

The sEMG signals of selected muscles (VM, VL, RF, BF, STEM, GMED) were recorded from the nine healthy males. It was observed (Figure 3.3) that the muscle forces estimated by the sEMG signal and AMS had almost similar characteristics. It was statistically verified by a two-sample t-test with a 95 % confidence interval, as shown in Table 3.2.

Table 3.2: Result of the two-sample t-test (*All pairs of muscles show the statistically no significant difference in a performance test* (t-test, p -value¿0.05))

Pair	**Mean (N)**	**P-value (two-tailed)**	
BF AMS	243.95	0.51	P>0.05*
BF EMG	255.29		
VM AMS	450.88	0.56	
VM EMG	462.71		
VL AMS	983.45	0.07	
VL EMG	904.07		
RF AMS	242.01	0.05	
RF EMG	219.49		
GMED AMS	146.23	0.05	
GMED EMG	127.07		
STEM AMS	33.35	0.57	
STEM EMG	38.16		

Before the real-time development of an exoskeleton, the muscle and joint force were considered for further analysis in the AMS. Table 3.4 shows that the human musculoskeletal in AMS could not carry more than 20 kg loads without assistance. That may be due to changes in knee joint loading and muscle fatigue. Thus, the exoskeleton assistance was required to carry the load beyond 20 kg. Equation (3.11) was used in Table 3.4 to evaluate the reduction in muscle force for the load 0 to 10 kg on both shoulders. These reduction results of muscles are shown in Table 3.3.

The average muscle force of VL, VM, and RF were reduced by 41.87-28.31 %, 42.25-28.78

%, 50.01-41.18 % as load increases from 0 kg to 10 kg load on both shoulders, respectively, as shown in (Table 3.3, Figure 3.5 (a)-(c), [167]). According to Table 3.3, the average muscle force of BF and STEM were reduced by 65.18-97.20 %, 22.54-13.13 %, as load increases from 0 kg to 10 kg load on both shoulders, respectively (Table 3.3, [167]).

Table 3.3: Muscle force reduction

Load (Kg)	Muscle Force Reduce in Newton (VL)%	Muscle Force Reduce in Newton (VM)%	Muscle Force Reduce in Newton (BF)%	Muscle Force Reduce in Newton (RF)%	Muscle Force Reduce in Newton (GMED)%	Muscle force Reduce in Newton (STEM)%
0	41.87	42.25	65.18	50.01	7.28	22.54
5	34.9	34.91	85.99	41.18	10.11	14.72
10	28.31	28.78	97.2	33.16	22.91	13.13

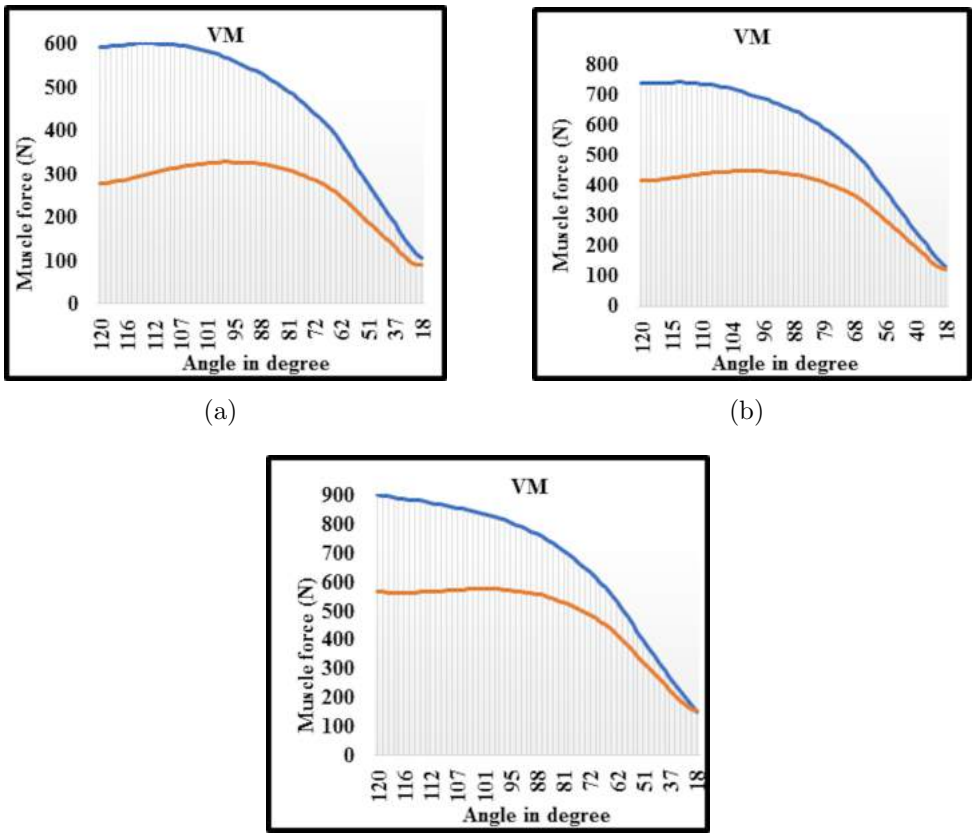

Figure 3.5: Force generated in VM muscle wrt angle (a) Without load (b) With 5kg load (c) With 10 kg load (Blue color indicates without exoskeleton, Orange color indicates with exoskeleton)

Table 3.4: Muscle force (min, max, average) for various load

Load (Kg)	VL Muscle Force (N)		VM Muscle Force (N)		BF Muscle Force (N)		RF Muscle Force (N)		GMED Muscle Force (N)		STEM Muscle Force (N)	
	Without Exoskeleton	With Exoskeleton	Without Exoskeleton	With Exoskeleton	Without Exoskeleton	With Exoskeleton	Without Exoskeleton	With Exoskeleton	Without Exoskeleton	With Exoskeleton	Without Exoskeleton	With Exoskeleton
0	226.16	192.02	105.07	88.94	27.7	13.81	65.78	52.82	0	0	0	0
	1274.58	695.98	600.68	326.48	519.27	174.25	376.98	141.82	203.5	212	129.36	81.44
	983.45	571.66	462.71	267.21	243.95	84.94	242.01	120.99	146.24	135.57	33.36	25.84
5	281.98	262.92	130.61	121.78	0	0	93.93	79.42	0	0	0	0
	1577.33	950.74	738.43	445.76	551.8	120.16	428.12	222.48	226.29	199.9	126	82
	1209.98	787.71	565.69	368.18	238.69	33.43	312	183.52	151.7	136.36	26.28	22.41
10	340.2	333.27	150.2	154.37	0	0	115.5	103.74	0	0	0	0
	1917.92	1223.18	900.37	573.32	690.01	102.29	610	315.48	274.07	129.46	141	100.53
	1419.71	1017.86	667.98	475.76	236.14	6.62	381.71	255.13	185.1	142.69	23.35	20.24
15	*	404.02	*	198.66	*	0	*	132.11	*	0	*	0
		1556.85		769.76		92.08		408.33		396.71		123.51
		1257.02		623.05		3.18		329.45		277.779		20.34
20	*	474.6	*	219.83	*	0	*	161.1	*	0	*	0
		1903.41		887.49		96.1		500.83		474.58		148.88
		1497.51		699.96		2.3		402.49		252.93		21.46
25	*	545.29	*	252.58	*	0	*	189.68	*	0	*	0
		2257.09		1052.4		122.57		593.91		556.15		176.87
		1738.88		812.78		3.04		474.82		277.86		22.84

Min, Max, Avg (Force in N), * indicate that a human is not capable of carrying more than 20 kg load on both shoulder without any assistance

Table 3.5: Pairs of muscle with a significant difference

(All pairs of muscles show the statistically significant difference in a performance test (t-test, p-value<0.05))

Pair	AMS Muscle Force in Newton	Human body without and with an exoskeleton (with no load)			Human body without and with an exoskeleton (with 5 kg equally loads on both shoulder)			Human body without and with an exoskeleton (with 10 kg equally loads on both shoulder)		
		Pair difference		p-value (two-tailed)	Pair difference		p-value (two-tailed)	Pair difference		p-value (two-tailed)
		Mean	SD		Mean	SD		Mean	SD	
Pair 1	VL-VL Exo	411.79	178.08	**p<0.05***	422.27	194.08	**p<0.05***	407.43	388.06	**p<0.05***
Pair 2	VM-VM Exo	195.49	138.16		197.51	161.83		194.68	184.88	
Pair 3	RF-RF Exo	121.03	83.66		128.48	99.92		128.47	115.66	
Pair 4	BF-BF Exo	159.47	124.44		205.27	148.23		229.52	186.99	
Pair 5	GMED-GMED Exo	10.67	32.89		15.34	33.44		42.41	20.72	
Pair 6	STEM-STEM Exo	7.51	33.72		3.87	28.67		2.48	23.08	

The average muscle force of GMED reduced by 7.28-22.91 % as load increases from 0 kg to 10 kg load on both shoulders (Table 3.3, [167]). BF muscle force 65.18-97.20 % indicates a higher reduction as load increases from 0 to 10 kg load on both shoulders (Table 3.3, [167]). However, the situation was different in STEM muscle (one of the muscles of the hamstring group), where the muscle force does not show adequate variation as the load increased from 0 to 10 kg on both shoulders. The reduced force of STEM muscle (22.54-13.13 %) was less compared to all selected muscles during the squatting movement. This muscle was not active during the squatting movement (Table 3.3, [167]). A similar condition was observed in GMED muscle (7.28-22.91 %). This muscle remains active during the squatting movement to stabilize the pelvis (Table 3.3, [167]). The average muscle force of VM (41.87-28.31 %), VL (42.25-28.78 %), and RF (50.01-33.16 %) had reduced percentage in comparison to BF (65.18-97.20 %) during the squatting movement as load increased with and without the exoskeleton (Table 3.3). These muscles (VM, VL, RF) remain active during the squatting activity and having the least reduction of average force (28.31 %, 28.78 %, 33.16 %) as load increases (with and without the exoskeleton), as shown in Table 3.3. In addition to BF, STEM GMED muscle groups, the quadriceps muscle group had a lower force value in a standing position (18°) with and without the assistance of the exoskeleton.

The quadriceps muscle (VL, VM, RF) shows significant statistically differences with a lower p-value (t-test, $p < 0.05$) with and without the exoskeleton, as shown in Table 3.5. The mean difference and standard deviation difference were enough to differentiate these muscles for all various loads. Thus, the designed exoskeleton assists an individual in the reduction of their muscle forces (VL, VM, RF).

On the other hand, the 3D design lower limb exoskeleton was significantly effective in reducing the BF muscle force as the load increased from 0 to 10 kg on both shoulders. Furthermore, hamstring muscle (BF, STEM) had a statistically significant difference with a lower p-value (t-test, $p < 0.05$) for with and without the exoskeleton, as shown in Table 3.5. The mean and standard deviation values for STEM muscle differed slightly from quadriceps and hamstring muscle. It was determined that there is insufficient variation in STEM muscle with and without exoskeleton as load increased. Furthermore, GMED muscle showed a small significant difference, but it was comparable to the mean and standard deviation value of STEM muscle. The GMED muscle showed no sufficient variation with and without an exoskeleton with increased load. STEM and GMED muscles were therefore considered to stabilise the exoskeleton lower limb. As the load increased from 0 to 10 kg on both shoulders, the average force of BF muscle with the assist of exoskeleton reduces by 65.18-97.20 %.

Thus, the developed exoskeleton reduce the risk of LBDs and WMSDs for those who perform lifting tasks regularly. Moreover, the knee joint reduction force value was calculated using Equation (3.12). Table 3.6, Figure 3.6 (a), (b), shows in reduction of knee joint force value (44.04-31.43 %) as the load increases from 0 kg to 10 kg during squatting with the assistance of the exoskeleton. A similar characteristic of the knee joint was observed as the load increased above 10 kg to 25 kg on both shoulders using the lower limb exoskeleton, as shown in Figure 3.6. Therefore, the exoskeleton assist in the reduction of knee muscle and joint forces. The 3D lower limb exoskeleton design worked effectively as the load increased beyond 10 kg to 25 kg on both shoulders in AMS, as shown in Table 3.4. Thus, the 3D design exoskeleton design showed a good response with a maximum load of 25 kg on both shoulders, *i.e.*, 50 kg.

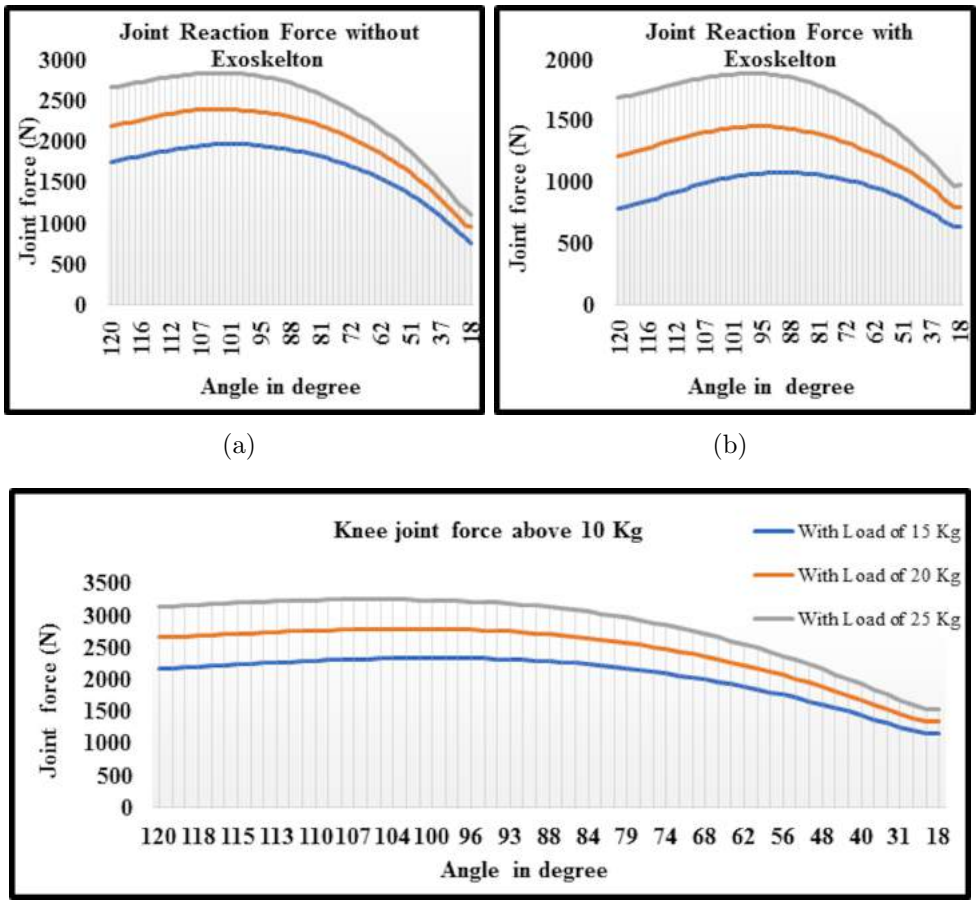

(a) (b)

(c)

Figure 3.6: (a) Knee joint force (for 0 kg, 5kg, 10kg) without exoskeleton, (b) Knee joint force (for 0 kg, 5 kg, 10 kg) with exoskeleton, (c) Knee joint force above 10 Kg (15 kg, 20 kg, 25 kg)

Table 3.6: Joint force (min, max, average) for various load

Load	**Without Exoskeleton in Newton**			**With Exoskeleton in Newton**			(**Reduce force by average in Newton**) %
	Min	Max	Average	Min	Max	Average	
0 Kg	763.48	1966.00	1679.54	636.48	1078.89	939.85	44.04
5 Kg	952.05	2395.85	2043.87	798.24	1454.80	1279.04	37.42
10 Kg	1100.50	2829.57	2413.71	973.72	1884.63	1655.16	31.43

A 3D design of a lower limb exoskeleton was evaluated in AnyBody Modelling Sottware (AMS). Selected muscles and knee joints of the human musculoskeletal were used to evaluate the exoskeleton. The results obtained with the help of the exoskeleton show a significant reduction in lower limb muscle and knee joint force. A simulation-based analysis (AMS) helped to fine-tune the development of a real-time exoskeleton for every individual and eventually saves time and cost.

Chapter 4

Develop a Simulator for Muscle Force Prediction

Different simulation tools and conventional algorithms were used in dynamic motion to determine the knee muscle forces of humans. Cost-efficient and efficient Machine Learning (ML) models were developed to predict knee muscle force for clinical interventions on certain input parameters such as height, mass, and angle. Four ML models were trained and tested to predict the force of the knee muscle: Neural Network, Generalized Linear Model and Decision Tree, random forests.

4.1 An Integration of AMS and Machine Learning Approach

The human musculoskeletal movement has an extraordinary ability to control muscle function in changing environmental conditions. The muscle force (one of the muscle functions) required to perform special tasks such as walking and squatting was unclear. There are various approaches to achieving the required muscle force during a specific task, such as conventional algorithms, simulation tools, and machine learning (ML). In the field of biomechanics, one conventional algorithm, *i.e.*, a Hill-type muscle model, was used to determine muscle forces for humans. This muscle model was based on various muscle parameters of humans, such as optimum fiber length, tendon slack length, maximum isometric muscle force, **etc**. The parameters used in this model may be generic or subject-specific. More often, generic parameters were obtained through the other associated muscle force measurements [168, 169]. The muscle forces can easily be estimated with a muscle model of type Hill. However, because of the large limits reported in clinical utilities, it is difficult to identify the best range of these parameters for human users [170–172].

Simulation-based tools were developed to overcome this problem for estimating muscle force during a particular task. This was a significant advancement in understanding ergonomic practice, shoulder implant behaviour, surgical planning, rehabilitation, and

the development of sEMG-based assistive systems. Various commercial simulation tools were available based on inverse dynamic analysis to estimate muscle forces for human musculoskeletal such as LifeMod, SIMM, Anybody Modelling (AMS, Anybody Technology), and open-source tools like OpenSim [147, 173]. These simulation tools enable the observation of internal human variables like joint, muscle forces, metabolic power consumption, *etc* [174]. The human musculoskeletal used in these tools were similar to human anatomy [173,175,176]. Using these tools, the clinician monitors the specific muscle responsible for a particular task and provides direct surgical instruction [177–181].

Existing software tools for human musculoskeletal muscle force estimation during inverse dynamic analysis had several drawbacks, including a longer computational time and a muscle recruitment problem [173,182,183]. Furthermore, performing an inverse dynamic analysis on a large number of human musculoskeletal joints at the same time is difficult. Among these, AMS offered a convenient tool for modelling and simulation-based analysis to overcome this problem using AnyPyTools. All major joints of the human musculoskeletal system, including those in the upper body, such as the trunk, arms, and head, are involved in maintaining balance and performing dynamic movements [184]. Recently, supervised learning, a type of artificial intelligence, was used to develop prediction-based models [185–188]. In computationally demanding processes, this was regarded as important, with speed and flexibility benefits. The training was extensive, but adoption was easy to understand. Therefore, artificial intelligence, together with AMS, was used for the construction of ML prediction models.

In this chapter, datasets generated from AnyPyTools via AMS were trained and tested by four different supervised ML regression-based models (neural network, random forest, generalized linear model, and decision tree) to build a prediction-based model. The models for estimating human musculoskeletal muscle forces used a variety of input parameters, including height, mass, angle, and target parameters, *i.e.*, their muscle forces. The major responsible muscles for squatting movement (*i.e.*, perform for given angle range) were Biceps Femoris (BF), Rectus Femoris (RF), Vastus Medialis (VM), and Vastus Lateralis (VL). Among all models, a random forest was the best-suited model for knee muscle force estimation. The model's performance was evaluated using mean square error (MSE), determination coefficient (R^2), and Correlation (r), which shows a good relationship between actual vs predicted muscle force. Moreover, the validation process was performed to verify the similarity of muscle force between simulation-based analysis and experimentation-based analysis.

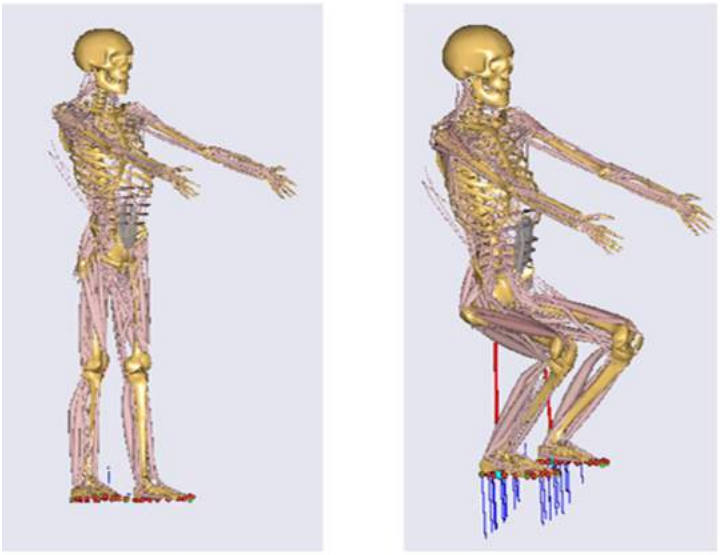

Figure 4.1: (a) Human at standing position; (b) Human movement at a specific input angle position

4.2 Methodology

4.2.1 AnyBody Modelling Software

Figure 4.1 (a) shows the standard "human musculoskeletal" template with 175 cm of height and 72 kg of mass used for generating datasets as well as for validation. The template's height and mass could be scaled up/down using the ScalingLengthMassFat function in AMS [189]. Here, scale taking mass, and fat into account and input are joint to joint distances. Fat is dependent on body mass index, *i.e.*, mass and height. Hence, the human musculoskeletal is scalable in segment mass, length, and muscle strength to fit any population. The human musculoskeletal also contains more than 400 muscles. The lower limb consists of 159 muscles and seven joint degrees of freedom (DOF). The joint degrees of freedom are:

(a) Three rotations in the hip joint (flexion/extension, abduction/adduction, external/internal rotation)

(b) One rotation in the knee joint (flexion/extension)

(c) One rotation in the ankle joint (plantar/dorsal flexion)

(d) One rotation in the subtalar joint (eversion/inversion)

(e) One rotation between the femur and the patella segment

The human template in AMS was fixed. Hence, various constraints on the pelvis–thorax, hip, and knee joints, must be applied to perform inverse dynamic analysis for squatting [190]. The flexion/extension of the glenohumeral joint was kept at zero constraint values in AMS. Abduction/adduction or external/internal rotation of the hip, plantarflexion/ dorsiflexion, or abduction/adduction of the ankle and translations or rotations of the pelvis was kept at zero constraint values.

Flexion/extension (squatting movement or repetitive movement and isokinetic) was performed by providing a constraint between the $80 - 120^{\circ}$ angle at the knee joint, as shown in Figure 4.1 (b). The angle range, *i.e.*, input parameter, was used for controlling the posture of the models for all major joints except the ankles. This movement was balanced by muscle forces, inertia, and the centre of gravity, *i.e.*, 9.8 $\mathrm{m/s^2}$.

4.2.2 Model Construction for Muscle Recruitment

AnyBody Modeling Software focuses only on inverse dynamic analysis of the Musculoskeletal models. In inverse dynamics, the squatting movement (repetitive movement or isokinetic flexion-extensions) and the external loads on the human musculoskeletal are supposed to be identified for determining internal forces (joint forces and muscle forces) [191]. However, inverse dynamics was suffered by the redundancy problem for computing individual muscle forces because it does not have sufficient equilibrium equations to estimate all the muscular forces. Here, the central nervous system (CNS) was used to the identified joint movements and determine internal forces.

The CNS modelling was based on optimal conditions to estimate each muscle's activation and force. The control of muscle forces must be based on a certain rational criterion. This was accomplished with considerable precision by repetitive movements. The criterion min/max was used to obtain a unique solution for human musculoskeletal as the basis of the inverse dynamic analysis in the AMS [143, 192].

The solution of the muscle recruitment problem is expressed as an optimization problem as

$$\text{Minimize: } f \quad G\left(f^{(M)}\right) \tag{4.1}$$

$$\text{Subject to } C^{*} f = d \tag{4.2}$$

$$0 \leq f_i^{(M)} \leq N_i, \quad i \in \left\{1, \ldots\ldots\ldots, n^{(M)}\right\} \tag{4.3}$$

where G is the objective function, *i.e.*, the assumed criterion of the recruitment strategy of the CNS stated in terms of the muscle forces, $f^{(M)} \cdot G$ is minimized with respect to all unknown forces in the problem, $f = \left[f^{(M)^T} f^{(R)^T}\right]^T$, *i.e.*, muscle force, $f^{(M)}$, and joint reactions, $f^{(R)}$ as described in Equation (4.1) . C is the coefficient-matrix for the unknown forces and the right-hand side, d, contains all known applied loads and inertia forces. Equation (4.2) is the dynamic equilibrium equations, which enter as constraints into the optimization. The non-negativity constraints on the muscle forces,Equation (4.4), state that muscles can only pull, not push, and the upper bounds limit their capability, *i.e.*, N_i is the strength of the muscle.

The objective function G is the min / max criterion that can be considered as minimization of the maximal muscle activity as described in Equation (4.4).

$$G\left(f^{(M)}\right) = \max\left(\frac{f_i^M}{N_i}\right) \tag{4.4}$$

Here, G is stated with a normalizing function for each muscle, N_i. The normalized muscle force is often referred to as muscle activity. Where N_i represents the strength of muscles.

4.2.3 Dataset Arrangement using AnyPyTools in AMS

This could be time-consuming for inverse dynamic analysis in AMS to simultaneously process a large population of human musculoskeletal and scale individuals (template). A python library, AnyPyTools, developed by the Aalborg University researchers and incorporated with AMS, can handle the large populations of musculoskeletal models at the same time [192]. Using AnyPyTools through AMS, a dataset of 500 different musculoskeletal models were constructed from the template by varying range of height, mass, and angle, as shown in Table 4.1. The locus of the squatting movement for a given angle range was divided into 11 steps for inverse dynamic analysis

Table 4.1: Description of the input parameters

Input Parameters	**Range**
Height	(1.2-1.9) m
Mass	(60-110) kg
Angle	(80-120) degree

Table 4.2: Description of muscles

Muscle	**Muscle Symbol**
M_1	VL
M_2	VM
M_3	BF
M_4	RF

Every step corresponds to 11 different muscle force value for all four different knee muscles (M_1, M_2, M_3, M_4). The knee flexion/extension responsible muscles (also, squatting movement) were considered, as shown in Table 4.2. Therefore, three different input parameters, namely angle, mass, height, were given to the human musculoskeletal for finding knee muscle forces (F_1 to F_{11}) using inverse dynamics analysis in AnyPyTools. Dataset of each human musculoskeletal comprises four different knee muscle (M_1, M_2, M_3, M_4) and input parameters (height, mass, angle). These datasets have a mean angle, mean mass, mean height of $99.79 \pm 19.79°$ degrees, 84.81 ± 24.81 kg, and 1.55 ± 0.35 m. Demo of M_1 (*i.e.* BF) for the four randomly selected human musculoskeletal that generated muscle forces while performing the squatting movement in 11 steps, shown in Table 4.3.

Preparation of datasets was done in the following order with the help of AnyPyTools through AMS before fed into ML models. All muscles of every human musculoskeletal initially combine in column order and then concatenated to musculoskeletal in row order. Figure 4.2 shows how to extract each muscle from individual human musculoskeletal datasets at the same time. Expend each muscle of every human musculoskeletal sequentially into 11 different muscle forces. To realize the target parameter for ML models, extract each value of muscle force step by step from datasets. In total, 44 different knee muscle forces of given datasets were trained and tested as a target on four different ML models for four different muscles (M_1, M_2, M_3, M_4, as shown in Equation (4.5)).

$$\begin{aligned} &M_1(\text{BF}), F_{1-\ldots}F_{11} \sim \text{f (Height, Mass, Angle)} \\ &M_2(\text{VM}), F_{1-\ldots}F_{11} \sim \text{f (Height, Mass, Angle)} \\ &M_3(\text{RF}), F_{1-\ldots}F_{11} \sim \text{f (Height, Mass, Angle)} \\ &M_4(\text{VL}), F_{1-\ldots}F_{11} \sim \text{f (Height, Mass, Angle)} \end{aligned} \tag{4.5}$$

Table 4.3: Sample dataset for M_1 (BF)

Subject	**Input Parameter**			**M_1 Muscle force value (Newton) correspond to 11 steps for inverse Dynamic Analysis**										
	Angle (degree)	Mass (Kg)	Height (Meter)	F_1	F_2	F_3	F_4	F_5	F_6	F_7	F_8	F_9	F_{10}	F_{11}
1	104.04	83.45	1.4	0	72.57	168.14	276.74	400.99	542.96	703.8	874.5	1023.56	1147.82	1248.71
2	97.84	80.96	1.87	0	64.44	153.42	251.46	363.05	489.98	633.86	790.26	942.83	1067.67	1168.7
3	89.42	91.4	1.33	0	59.21	149.15	239.66	344.13	462.54	596.47	742.69	891.48	1019.14	1127.17
4	102.24	63.49	1.62	0	60.42	142.27	233.15	336	452.54	583.95	730.2	884.8	1013.73	1104.95

Table 4.4: Machine learning and their tuning parameters

Models	**Package**	**Tuning Parameter and Value**
Decision Tree	rpart	MinSplit=20, MaxDepth=30, MinBucket=7
Random Forest	randomForest	ntree=500, mtry=3
Generalized Liner Model	glm	None
Neural Network	neuralnet	Hlayers=10, MaxNwts=10000, maxi=100

Table 4.5: Performance comparison of machine learning models in the prediction of individual muscle force

Models	**M_1 Muscle**			**M_2 Muscle**			**M_3 Muscle**			M_4 Muscle		
	r	R^2	MSE	r	R^2	MSE	r	R^2	MSE	r	R^2	MSE
Random Forest	**0.94**	**0.88**	**19.92**	**0.92**	**0.84**	**9.06**	**0.92**	**0.84**	**5.97**	**0.94**	**0.89**	**5.46**
Decision Tree	0.83	0.69	45.07	0.69	0.48	23.11	0.77	0.59	13.18	0.84	0.70	13.17
Linear Model	0.69	0.47	55.77	0.68	0.46	15.20	0.62	0.39	17.38	0.80	0.64	8.80
Neural Network	0.69	0.47	55.71	0.68	0.46	15.89	0.65	0.43	15.91	0.81	0.65	8.98

4.2.4 Machine Learning Models

Table 4.4 shows the ML models and their tuning parameters used to predict muscle forces for the given value of input parameters. Four models viz. Neural Network, Generalized Linear Model, Decision Tree, Random Forest were considered, as these models had strong utility in sEMG signal analysis [185]. These models were trained and tested in open-source R studio software. A brief detail of the trained model is elaborated below;

4.2.4.1 Neural Network (nn)

This works in the same way as the human brain work in carries out regression and classification tasks. Neural networks, in this sense, refer to neuron systems, either organic or of an artificial nature. This adapts changing input easily to produce the best possible result without the need to redesign the output criteria.

4.2.4.2 Decision Trees (rpart)

This method is an up-gradation of C4.5 classification algorithms as referred by Quinlan. This builds regression or classification models in the form of a tree structure. The dataset is divided into smaller chunks and results in the incremental development of a decision tree. The decision nodes and leaf nodes are the essential components of the resultant tree.

4.2.4.3 Generalized Linear Models (glm)

This usually refers to conventional linear regression models to perform regression and classification task.

4.2.4.4 Random Forest (randomForest)

This is an ensemble supervised machine learning technique that combine multiple classifiers in order to solve a complex problem and improve the model's performance. Rather than using a classifier, the random forest takes the prediction from each tree and predicts the final output based on the majority vote of the predictions. So, multiple decision trees utilized to perform regression and classification tasks.

4.2.5 Methodology

ML models were trained and tested for the given datasets having input parameters (*i.e.*, input feature vector) and target parameter (*i.e.*, knee muscle forces). Figure 4.2 shows the dataset of given ML models. The distribution of the dataset for ML models was

set to 80% as training data and 20% as testing data. All comparative models were run based on this training-testing dataset separation. The output from the ML models had 11 steps prediction muscle force value of every knee muscle (M_1, M_2, M_3, M_4). After that, 11 value of forces for four different muscle sums up in row order to take a single value of each muscle force (F_1, F_2, F_3, F_4). It predicts four different muscle forces of 500 different human musculoskeletal. Based on actual muscle force of 4 different muscles for given datasets was compared with predicted muscle force. Finally, model performance was evaluated on different parameters described in Section 4.2.6.

4.2.6 Performance Assessment

1. **Mean Squared Error (MSE)** MSE is a popular formula for measuring a regression model's error rate. It can only be compared, however, between models whose errors are measured in the same units. It is calculated as follows:

$$\text{MSE} = \frac{\sum_{i=1}^{n} (y_i - x_i)^2}{n} \tag{4.6}$$

   where x is an actual target, y is the predicted target and n is the total number of instances.

2. **Correlation (r)** Correlation describes the statistical relationship between actual and predicted values. It is defined as follows:

$$r = \frac{\sum_{i=1}^{n} (x_i - \bar{x})(y_i - \bar{y})}{\sqrt{\sum_{i=1}^{n} (x_i - \bar{x})^2 \sum_{i=1}^{n} (y_i - \bar{y})^2}} \tag{4.7}$$

   where x is the actual value, y is the predicted value, $\bar{x}$ is the mean of all actual values, $\bar{y}$ is the mean of all predicted values, and n is the number of instances. Correlation lies in $[-1, 1]$ and is considered to be good if its value tends towards 1 for a positive value.

3. **The coefficient of determination(R^2)**

   The (R^2) describes the proportion of variance of the dependent variable explained. If the compression between actual vs predicted is perfect, then R^2 is 1 and zero in the failure case, *i.e.* no variance is explained by the regression. It is defined as follows:

$$R^2 = r * r \tag{4.8}$$

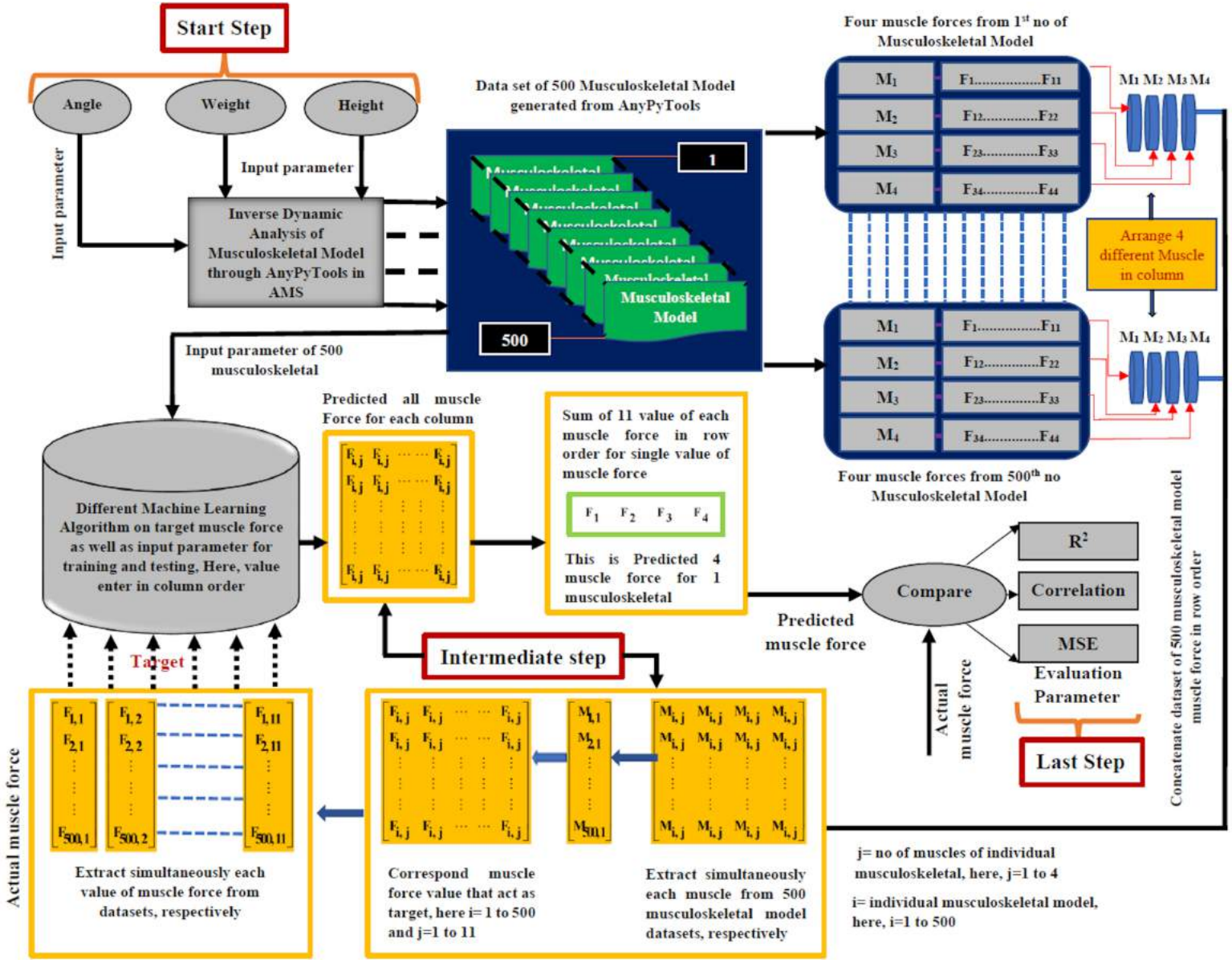

Figure 4.2: Steps for methodology

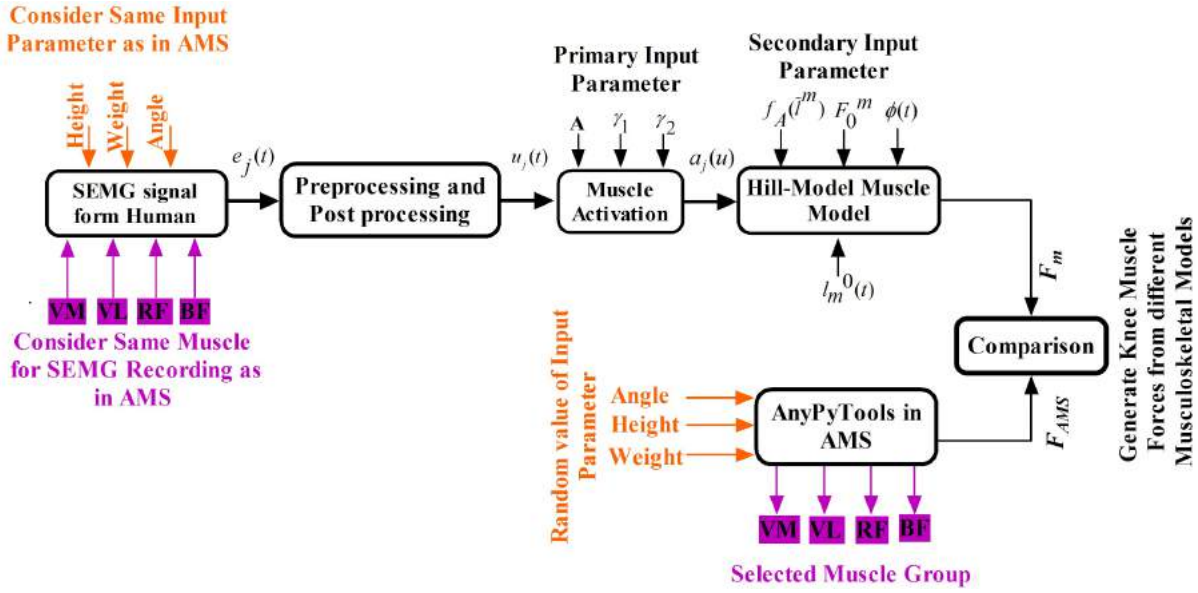

Figure 4.3: Step of hill muscle model

4.2.7 sEMG to force estimation using Hill-type muscle model

The average age of the selected males for the sEMG signal dataset is 30 ± 8.2 years, with an average height of 159 ± 21 cm and an average mass of 65 ± 8.70 kg, respectively. Using NeXus-10 BioTrace with a sampling frequency of 2048 Hz, sEMG signals from selected humans were transformed into the muscle force (Figure 4.3). The muscle force was compared between selected human and human musculoskeletal to validate simulation and experimental results [155].

Skin preparation and sensor locations have been recommended by SENIAM [157]. The muscle force was calculated using the Hill type muscle model [159] and Equations (3.1) to (3.10). Preprocessing was done to improve the sEMG signal quality, which included high pass filtering, rectification, normalization, followed by low pass filtering. A 4^{th} order, zero-lag Butterworth filter with a cutoff frequency of 30 Hz was applied for high pass filtering. The high-pass filtering removes the DC offset, low-frequency noises, and artifacts from the recorded sEMG signal. The fullwave rectification of the filtered sEMG signal has been completed. After that, normalization (max-normalization) was completed.

4.3 Results and Discussion

This section analyzes the prediction results of all four different ML models on visual with scatter plot, and performance assessment for a given training and testing datasets and validated results of both simulation and experiment. All comparative ML models for

regression analysis had human musculoskeletal input and target parameters.

4.3.1 Training-Testing Experiment

Figure 4.4 shows the visual results of actual vs predicted muscle force on the testing datasets by the scatter plot. A scatter plot shows a good correlation between the actual vs predicted with a positive sign. It was done in a regression analysis. There after, ML models' performance was evaluated as MSE, Correlation, and R^2, respectively, as shown in Table 4.5. The performance assessment result shows that the random forest model was superior in comparison to other ML models. The MSE (Eq. 6) was used to quantify the difference between actual and predicted values. The random forest had the lowest MSE of BF, VM, VL, and RF, *i.e.*, 19.92, 9.06, 5.97, and 5.46, respectively, in the prediction of muscle force on the testing dataset. The lower the MSE represents, the predicted value closer to the actual value.

The Correlation (Eq.7) presents the statistical relation between actual and predicted values. The random forest has the highest correlation value of BF, VM, VL, and RF, *i.e.*, 0.94, 0.92, 0.92 and 0.94 respectively, in predicting muscle force on the testing dataset. A higher correlation represents a good statistical relation between actual and predicted value. The R^2 (Eq. 8) presents the proportion of variance between actual and predicted values. For predicting the muscle force on the testing data set, the random forest shows the maximum R^2 of BF, RF, VM and VL, *i.e.*, 0.88, 0.84, 0.84 and 0.89, respectively. The high value of R^2 presents the least variability between actual and predicted muscle forces. These are the main evaluation parameter of the regression-based ML model for comparing actual and predicted performance. It was also shown in Figure 4.5-4.6 that the actual muscle force characteristics of four different human musculoskeletal [Table 4.3] and its predicted muscle force characteristics from the developed ML model (Figure 4.7) were very close to each other.

4.3.2 Validation of Experiment

sEMG signal of selected muscles (BF, RF, VM, VL) was recorded from the lower limb selected human. The conventional hill muscle model then transformed sEMG signals into muscle force (experiment results). Similar muscle was used to quantify muscle force from subject-specific human musculoskeletal in AMS (simulation results).

A two-sample t-test with a 95 % confidence interval was used to validate simulation and experiment results. Table 4.6 shows that the confidence interval with 95 %, both estimated muscle forces via sEMG and AMS, was a comparable mean value. This was

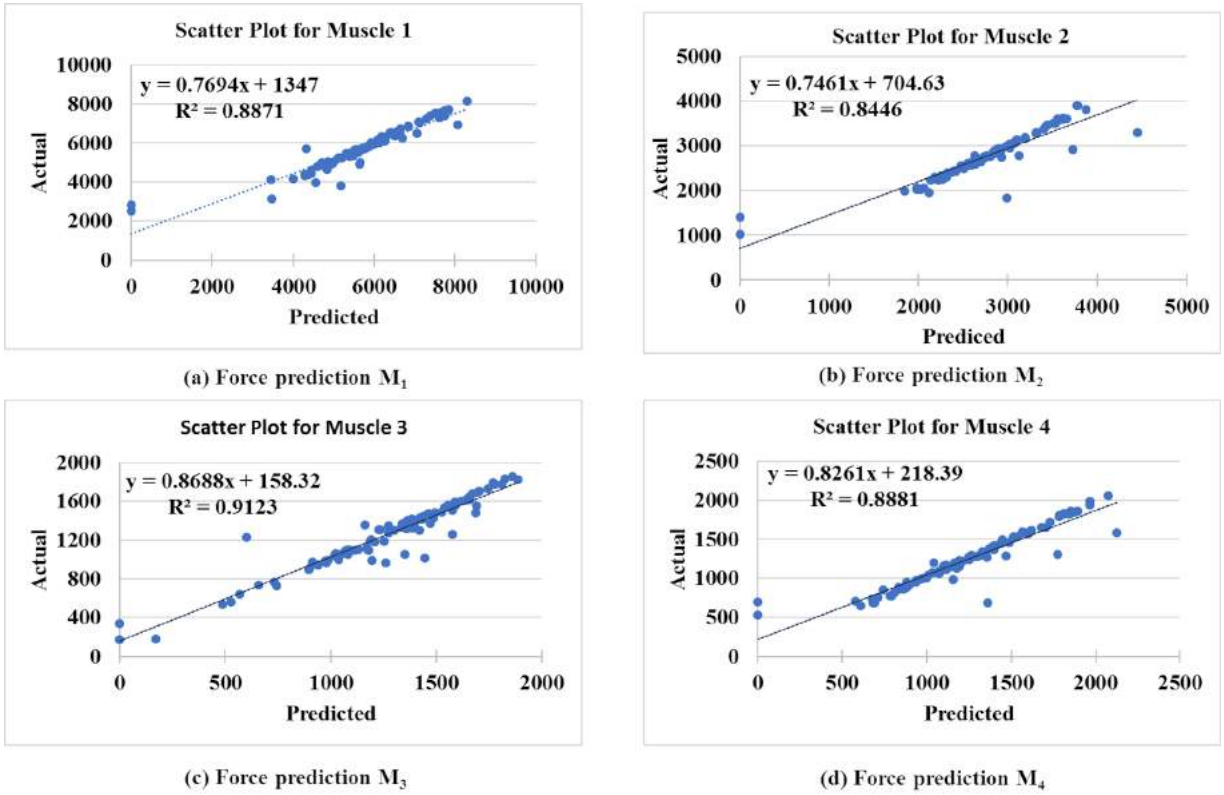

Figure 4.4: Scatter plot between actual and predicted of muscle force

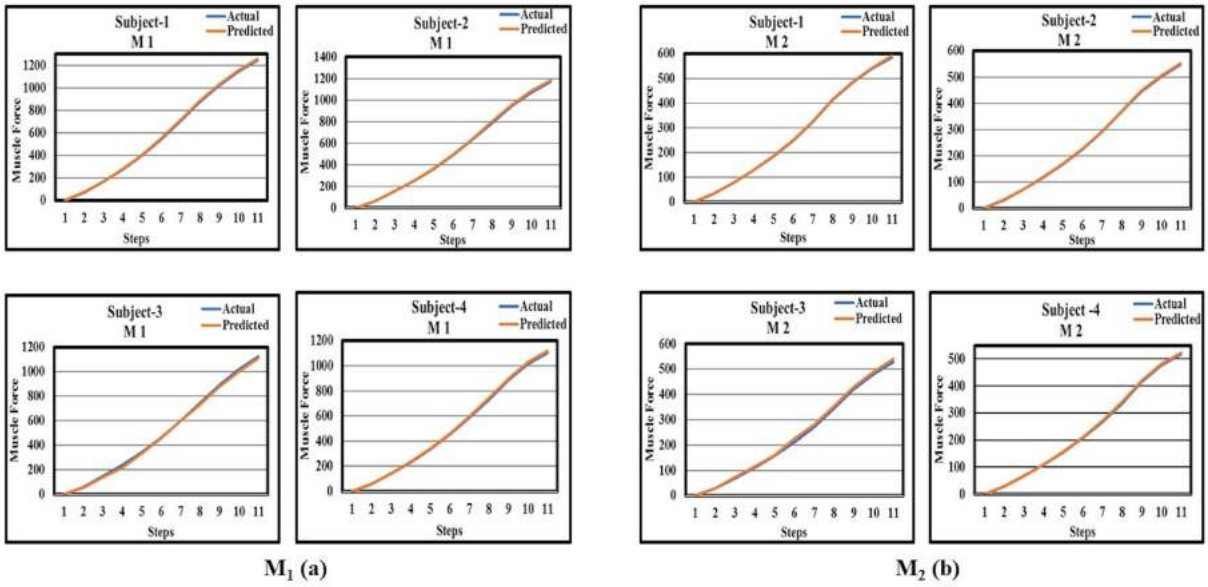

Figure 4.5: (a) and (b) represents VL, VM muscle force characteristics of the actual and predicted from the developed models for 4 different subjects, respectively

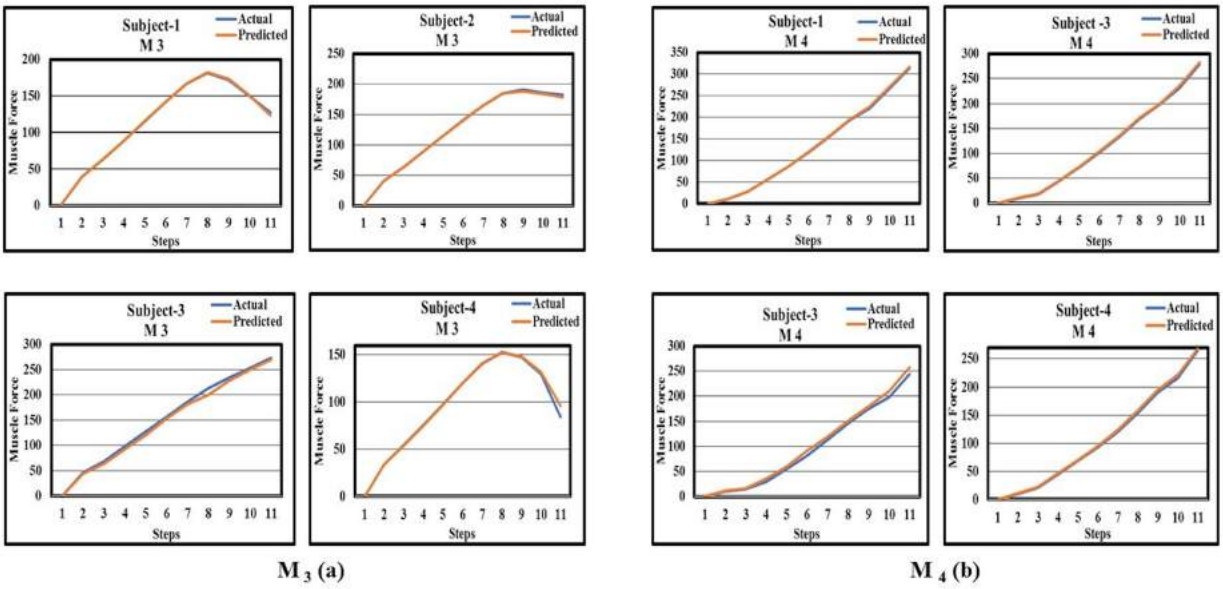

Figure 4.6: (a) and (b) represents BF, RF muscle force characteristics of the actual and predicted from the developed for 4 different subjects, respectively

Table 4.6: Result of the two-sample t-test

Pair	Mean (N)	P value(two-tailed)
VL AMS	530.45	0.07
VL EMG	550.07	
VM AMS	248.88	0.56
VM EMG	256.71	
BF AMS	120.95	0.51
BF EMG	130.29	
RF AMS	112.01	0.05
RF EMG	116.49	

also verified by the p-value of all 4-muscle pairs, which is greater than 0.05. It shows that there was no significant difference between simulation and experiment results. Therefore, AMS could be used for further research work.

To estimate muscle force from the conventional Hill muscle-based model was a cumbersome process. It needs too many input parameters, and missing any parameter leads to incorrect knee muscle force estimation for subject-specific musculoskeletal. It was also challenging to understand the muscle-based model since it is very complex as many steps are involved in estimating the muscle forces. In available tools such as AMS, the time required for inverse dynamic analysis of individual human musculoskeletal is between 120-160 seconds to estimate knee muscle force. The time becomes prohibitively long, especially when a large number of human musculoskeletal analyses based on input parameters are required in clinical applications. The developed ML model took 2-3 seconds

to predict muscle forces for a given value of input parameter. The results show that the model (4.7) was both cost-effective and efficient in terms of processing speed. Further, the Hill-based model is used for validations of muscle forces value with musculoskeletal models in AMS.

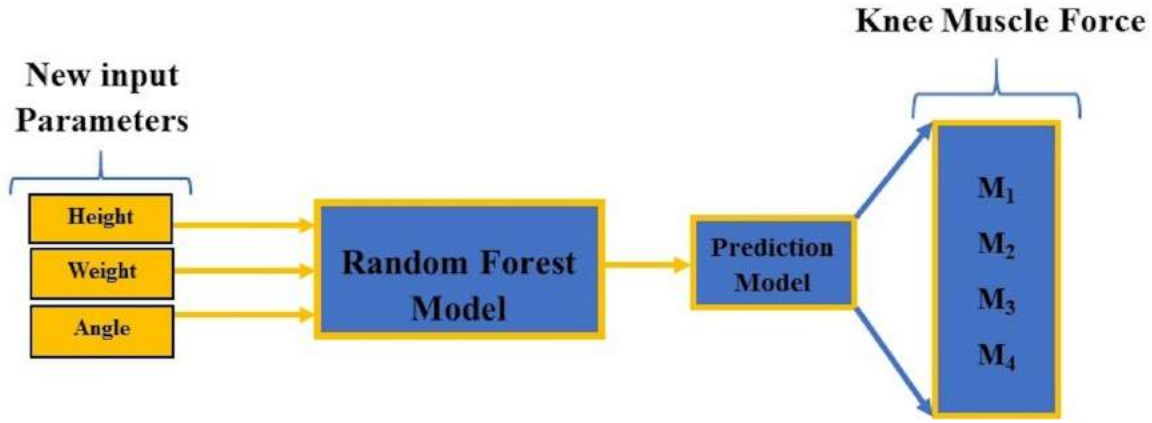

Figure 4.7: Random Forest based prediction model

Four ML models were explored with specified input and target parameters for estimating the muscle forces. The entire model's performance was evaluated on MSE, Correlation, and R^2. The random forest model outperforms other ML models. It provides an effective and efficient solution over existing software for estimating muscle forces. In addition, the t-test found that the difference between experimental and AMS datasets was not significant. This model will be helpful in many applications, like developing and optimizing the lower limb exoskeleton, rehabilitation, clinical, *etc.*

Chapter 5

Hybrid Bioinspired and Deep Neural Network Algorithm and Prototype Development

This chapter deals with predicting of sEMG signal and knee joint angle, and movement classification using PSO-LSTM on a single platform. Particle Swarm Optimization - Long Short Term Memory (PSO-LSTM) model was used to classify and predict movements and compared with random LSTM model to validate the performance. Both model performances were evaluated on RMSE, r, and R^2 and the results indicate that PSO-LSTM performs better. In the subsequent part of the chapter, details of the developed lower limb knee exoskeleton prototype and its control sequence have been presented.

5.1 Prediction and Classification using PSO-LSTM and Random LSTM

Clinicians use different disability diagnostic techniques to rehabilitate the movement for various daily activities [193]. Traditional clinical rehabilitation techniques require extensive laboratory settings that are inconvenient, expensive, and sometimes unavailable in remote areas. Remote rehabilitation monitoring with soft computing is needed. Assistive technology has considerable potential to improve the quality of life of individuals. The various soft computing techniques are applicable in the exoskeleton's real-time development by predicting the sEMG signal and knee joint angle. The inertial sensor was used to estimate the knee joint angle [194]. An autoregressive integrated (ARI) model predicts time series knee joint angle for rehabilitation [195]. An artificial neural network to estimate knee joint angles using EMG signals was proposed [196]. Time-domain features of SEMG were used to predict knee joint angle by generalized regression neural network [197]. Recently, a recurrent neural network was used to predict the knee joint angle from a combination of sEMG and inertial data [9, 198, 199] and movement classification [25, 199–202].

The section focuses on predicting sEMG signal and knee joint angle and movement classi-

fication using PSO-LSTM on the single platform without promising the results [203,204]. While dealing with nonlinear time-series data, LSTM has several advantages [195, 205]. Also, PSO is a widely used optimization algorithm with the most straightforward implementation. LSTM and PSO have separately achieved impressive results in many applications such as rehabilitation and clinical utilities [9,25], wind power forecasting [206], metal price forecasting, load forecasting [204, 206, 207], and stock market forecasting [208–210]. Using the PSO algorithm to optimize the LSTM model was a feasible strategy to improve the classification and prediction results. Three lower limb movements (Flexion, Extension, Ramp Walking) were classified using PSO-LSTM based on sEMG signals in the present study. Also, sEMG signal and knee angle for three movements were predicted using the PSO-LSTM model. After that, PSO-LSTM model performance for predicted results of sEMG signals and knee angle validated with a random LSTM model using Root Mean Square Error (RMSE), Coefficient of Determination (R^2), and Correlation Coefficient (r).

5.2 Methodology

5.2.1 Data Acquisition

Five healthy male volunteers (age 27±5, weight 75±5 kg, height 172±8 cm) participated in this research work. Texas Instrument microcontroller (Tiva C Series-TM4C123GH6PM, ARM Cortex-M-based architecture) was used for data acquisition. Lower limb muscles of volunteers generate sEMG signals and knee angles in time series arrangement. The generation of massive data depends on the placement of the sEMG electrode and ADXL 335 sensor. Eleven measuring sensors (nine sEMG and two accelerometers) were utilized, as shown in Figure 5.1. Each participant was trained for the data acquisition protocol before the acquisition. PUTTY software was used to record the data using a universal asynchronous receiver and transmitter (UART) communication.

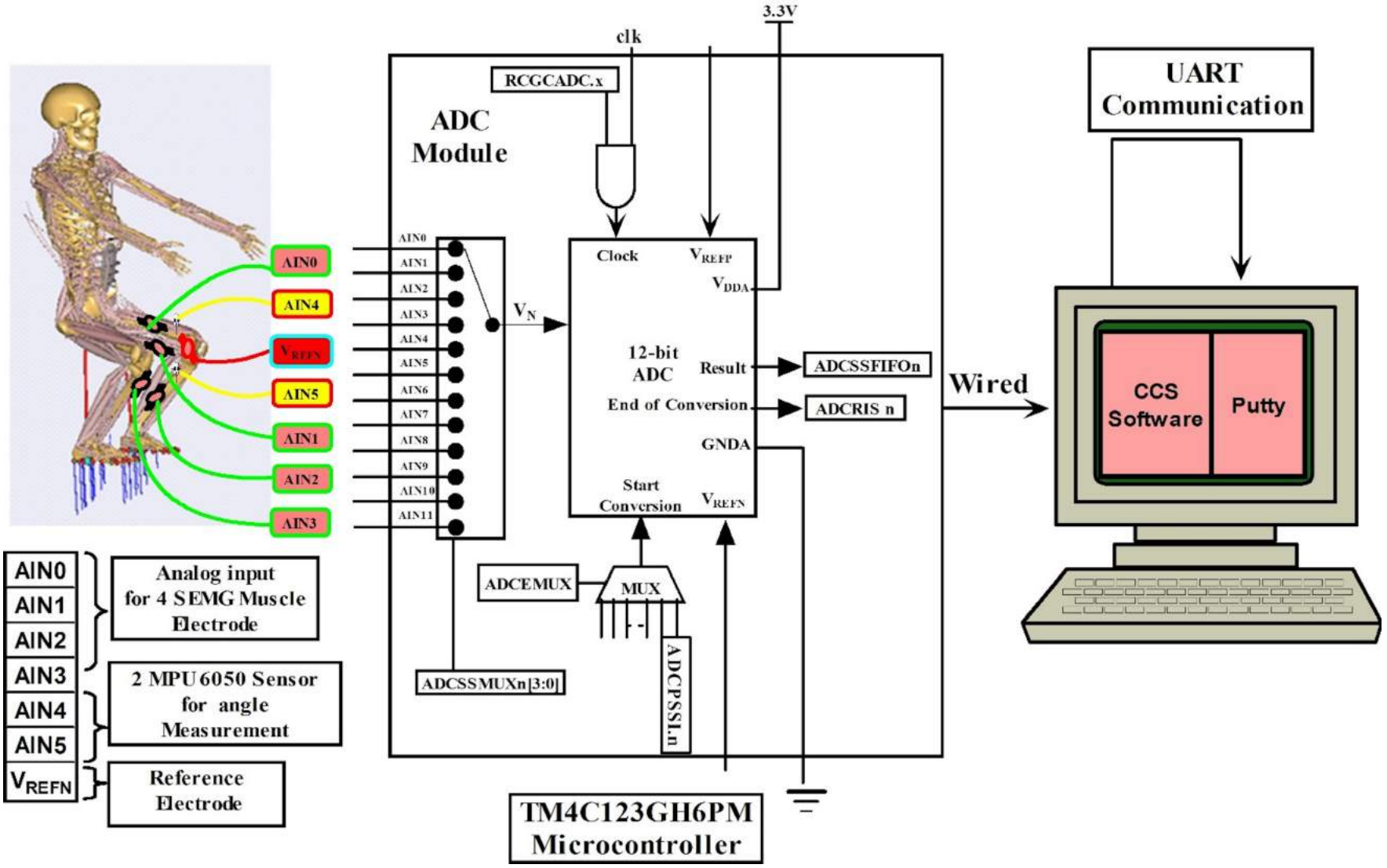

Figure 5.1: sEMG signal and knee angle acquisition architecture

5.2.2 sEMG Signals Processing

The sEMG electrodes were placed on knee muscles with the help of conducting gel as per SENIAM recommendation [157]. sEMG signal from biceps femoris (BF), vastus medialis (VM), rectus femoris (RF), and semitendinosus (ST) was recorded at 1000 Hz sampling frequency [211]. The sEMG signals recorded for three different movements: Ramp Walk ($15 - 20^{\circ}$ incline), Flexion and Extension, as shown in Figure 5.1. Knee joint angles and SEMG signals are recorded simultaneously during three movements without any load. There is no transition phase like walking to sitting, sitting to standing, *etc.* Volunteers were instructed to stand in a relaxed condition (without any limb movement) before starting the walking session. A total of four sessions of the procedure were completed for recording for each volunteer. The acquisition frequency of the real-time knee joint angle is 100 Hz [212]. Initially, a 50 Hz notch filter was used to remove power line interference from the raw sEMG signal. Subsequently, bandpass filters with a 20-250 Hz frequency range use to filter raw sEMG signals. Then full-wave rectification was used to make the signal amplitude greater than 0. Finally, each muscle's sEMG signal normalized for its maximum voluntary isometric contraction value (MVC). Equations (3.1) to (3.3) shows the complete extraction process of muscle activity (MA) from raw sEMG signals.

5.2.3 Joint Angle Measurement

The human body can be considered as a link of rigid segments. The connection between the two rigid segments (shank and thigh) can be defined as a knee joint. Range of motion (ROM) is a movement examination parameter for joint angle measurement. For normal functional activities, the knee joint Flexion/Extension angle plays a significant role by the American Academy of Orthopedic Surgeons (AAOS). Two accelerometers, ADXL 335, as shown in Figure 5.2, were placed on the individual knee segments for measuring the ROM of the knee [85, 193]. It is computed by subtracting the thigh and shank segments' angles, as shown in Equation (5.1).

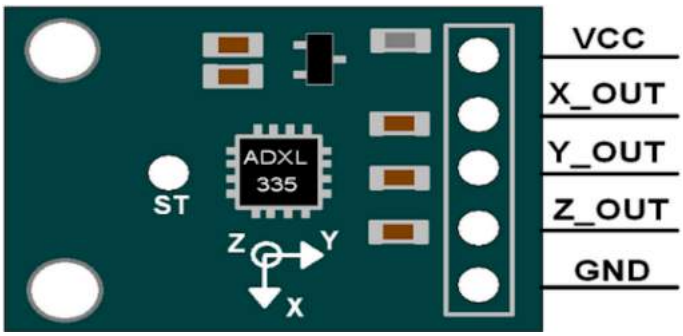

Figure 5.2: Accelerometer ADXL335

$$\theta_{\text{knee}} = |\theta_{\text{thigh}} - \theta_{\text{shank}}| \tag{5.1}$$

An accelerometer (ADXL335) is an electromechanical device to measure 3-axis acceleration in the x, y, and z-axis. The output signals are analog voltages proportional to the acceleration, which was a sampled at 100 Hz sample rate. TM4C123GH6PM microcontroller was used for data acquisition of knee angle and sEMG signals. The data obtained from the microcontroller was stored by wired (UART-based communication) through PUTTY software, as shown in Figure 5.1. The stored data was used for offline analysis in MATLAB software.

5.2.4 Long Short-Term Memory (LSTM)

LSTM has overcome several Recurrent Neural Network (RNN) restrictions, such as long time-dependence learning. Information from past events disappears exponentially as the number of time steps in the RNN increases. LSTM store past details of more than 1000-timesteps. The LSTM deep neural model's input layer includes three parameters: hidden layer, dropout rate, learning rate. These parameters assisted in setting the LSTM neural model to improve the prediction and classification results. LSTM works with feedback connections and remembers previous information inside the model, as shown in Figure 5.3. LSTM model has mainly three types of gates inside: input gate, output gate, and forget gate for remembering previous information and has three activation functions such as tanh, sigmoid, and Relu. Hyperbolic tangent function (tanh) was used as an activation function for input nodes and hidden nodes. Tanh returns an output value between 0 and 1. The output node's activation function was defined as a linear function to predict the sEMG signal of four muscles and knee joint angle. This model sets initial weights as random values, and the network's weights adjust by using a gradient-based "Adam" optimizer, famous for its simplicity and computational efficiency. Therefore, LSTM was found appropriate for the large dataset and had strength in dealing with a non-stationary problem [204].

In the LSTM process following steps were carried out.

(a) The first step was to decide which information to select from the cell state. This decision was taken by the forget gate layer, a sigmoid layer, whereas 0 or 1 were the output number for each cell state. Therefore, for value 1, it indicates the information is selected and if 0, it shows that the information is discarded.

(b) In the second step, the LSTM model predicts the information based on all the previous ones. Here, the cell state might include the new information if it is correct,

and after getting it, the old information is discarded.

(c) In the third step, stored new information was placed in the cell state. The complete operation of the LSTM is shown in Figure 5.4.

Table 5.1 shows the components of the LSTM cell. The process within an LSTM follows

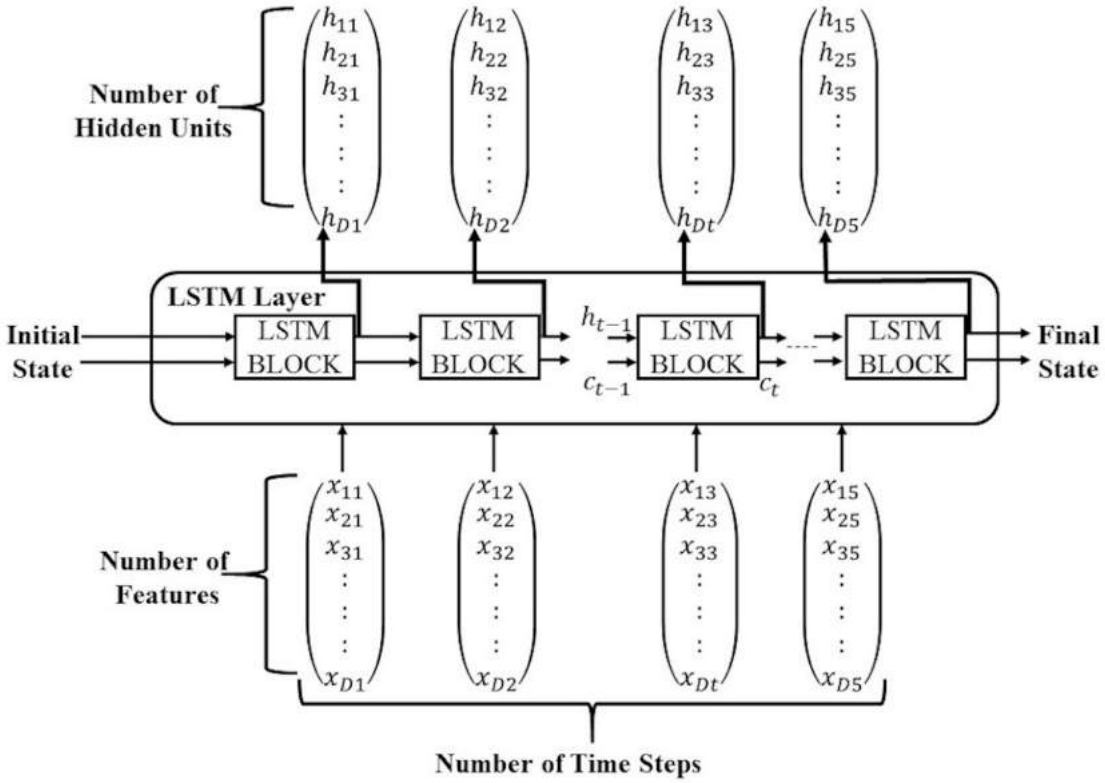

Figure 5.3: LSTM architecture

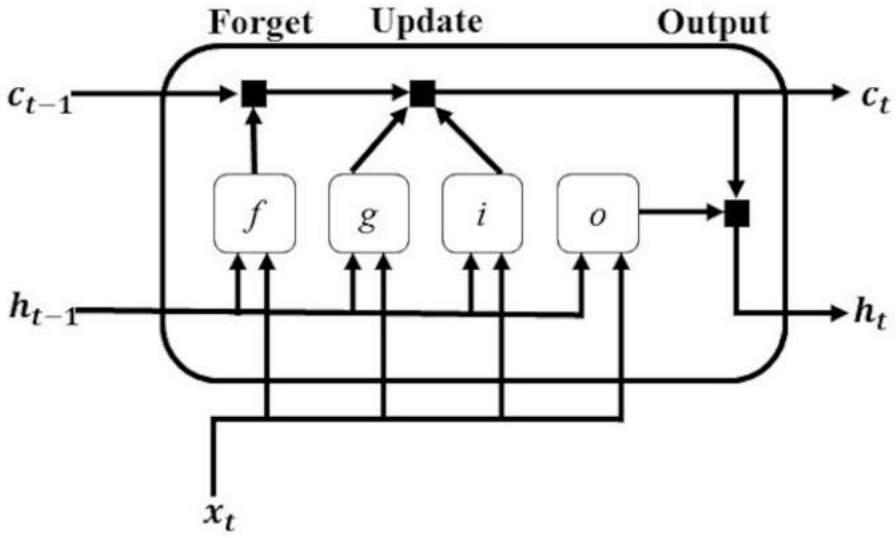

Figure 5.4: LSTM block

Equations (5.2) to (5.6). The input value can be stored in the cell state if it is allowed by the input gate.

Table 5.1: LSTM Components

SN	Component	Formula
1	Input gate (i)	$i_t = \sigma_g\left(W_i x_t + R_i h_{t-1} + b_i\right)$
2	Forget gate (f)	$f_t = \sigma_g\left(W_f x_t + R_f h_{t-1} + b_f\right)$
3	Cell candidate (g)	$g_t = \sigma_c\left(W_g x_t + R_g h_{t-1} + b_g\right)$
4	Output gate (o)	$o_t = \sigma_g\left(W_o x_t + R_o h_{t-1} + b_o\right)$

The value of i_t, g_t at time step t is calculated as follows:

$$\begin{aligned} i_t &= \sigma_g\left(W_i x_t + R_i h_{t-1} + b_i\right) \\ g_t &= \sigma_c\left(W_g x_t + R_g h_{t-1} + b_g\right) \end{aligned} \tag{5.2}$$

R = $[R_{\mathrm{i}}, R_f, R_g, R_o]$, W = $[W_i, W_f, W_g, W_o]$ and and b = $[b_i, b_f, b_g, b_o]$ matrices represent recurrent weights, the input weights, and the bias of each component, respectively. The forget gate manages the weight of the state unit, and the value of forget gate is computed as follows:

$$f_t = \sigma_g\left(W_f x_t + R_f h_{t-1} + b_f\right) \tag{5.3}$$

The new state of a memory cell updated as

$$g_t = f_t^{\circ} g_{t-1} + i_t^{\circ} g_t \tag{5.4}$$

where $^{\circ}$ denotes the Hadamard product, *i.e.*, element-wise multiplication of vectors and the output value of the gate is calculated with the new state of a memory cell as follows:

$$o_t = \sigma_g\left(W_o x_t + R_o h_{t-1} + g_t + b_o\right) \tag{5.5}$$

The final output value of the cell at time step t is given by

$$h_t = o_t^{\circ} \sigma_c\left(c_t\right) \tag{5.6}$$

where σ_{C} denotes the state activation function, *i.e.*, the hyperbolic tangent function

(tanh). In these calculations, σ_g denotes the gate activation function. To compute the gate activation function, LSTM layer function uses the sigmoid function, *i.e.*, $\sigma(x) = (1 + e^{-x})^{-1}$. The output gate controls the cell's output, and all gates use sigmoidal nonlinearity. The state unit performs as an extra input to other gating units.

5.2.5 Particle Swarm Optimization (PSO)

The PSO algorithm is inspired by the Birds' Social Behavior Group as they move step by step across the region in search of food. PSO is an artificial intelligence (AI) technique used to find approximate solutions using an objective function [15]. Depending on the fitness score, PSO provides a better solution. Inertia Weight Damping Ratio (wdamp), Inertia Weight (w), Global Learning Coefficient (k_2) and Personal Learning Coefficient (c_1) play an essential role in this algorithm. PSO is initialized with a group of random particles for searching optima. Each particle updates every iteration by following best values: $p_{best,}$ g_{best} and l_{best} (local best). The particle updates its velocity and positions after finding the two best values using Equations (5.7) and (5.8).

$$v_{n+1} = v_n + c_1 \text{ rand1}(\ ) * (p_{\text{ best, } n} - \text{ CurrentPosition}_n + c_2 \text{ rand2 } () * (g_{\text{best },n} - \text{CurrentPosition }_n\ ) \tag{5.7}$$

where, v_{n+1} = particle velocity at $n+l^{\text{th}}$ iteration, v_n = particle velocity at n^{th} iteration, c_1 = acceleration factor linked with gbest, c_2 = acceleration factor linked with 1_{best}, rand ()1 = random number between 0 and 1, rand()2 = random number between 0 and 1, g_{best} = global best position of the swarm, p_{best} = personal best position of a particle.

$$CurrentPosition[n+1] = CurrentPosition[n] + v[n+1] \tag{5.8}$$

where, Current Position $[n+1]$ = particle position at $n+1^{\text{th}}$ iteration, Current Position $[n]$ = particle position at n^{th} iteration, $v[n+1]$ = particle velocity at $n+l^{\text{th}}$ iteration. The parameter value of PSO is shown in Table 5.2.

5.2.6 Hybrid Optimization Approach PSO-LSTM

The dataset generated from healthy males' lower limb muscles is time-series and non-stationary. Before applying the data to the PSO-LSTM model, it was first converted

Table 5.2: PSO parameters

SN	PSO Parameters	Values
1	Inertia Weight Damping Ratio	0.99
2	Personal Learning Coefficient	1.5
3	Global Learning Coefficient	2.0
4	Population Size	200

into static data using MATLAB. The classification and prediction were carried out with a hybrid approach of the PSO-LSTM model.

Complete data divided into two training and testing data sets for each activity (five signals for each movement). Here, 70% of the data was used for the training, and 30% used for testing before applying it into the PSO-LSTM model. The activation of sEMG signals was very complicated for the LSTM model. The window method's enveloping technique makes the sEMG signal (Figure 5.5) compatible with this model.

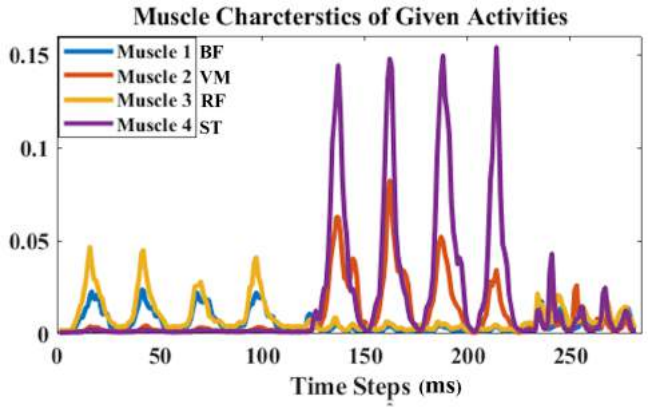

Figure 5.5: Muscle characteristics (BF, VM, RF, ST) of three given activities

PSO was used to tune the LSTM model's parameters, such as hidden layers, dropout rate, learning rate. The model performance is evaluated by Root Mean Square Error (RMSE), Correlation Coefficient (r), Coefficient of Determination (R^2). In the PSO-LSTM model, PSO explores each parameter's optimal value in LSTM (Table 5.3) based on the fitness function of PSO. The fitness function was calculated from RMSE at each step and returns to its lowest value for the optimal solution. The optimal or near-optimal solution was applied to the prediction model if it meets the termination criteria. Otherwise, the entire selection process would be repeated.

To acquire an outstanding solution for the model, PSO uses a population size, c_1, c_2 and w input parameter value, as shown in Table 5.2. PSO-LSTM shows its applicability for predicting knee joint angle and the sEMG signal of selected muscles [54][46][48]. The

Table 5.3: LSTM parameters

SN	Parameter	Range
1	Hidden Units	Range $(100, 450)$
2	Dropout rate	Range $(0.2, 0.3)$
3	Learning Rate	Range $(0.01, 0.000001)$

fitness function (F) is described using Equation (5.9).

$$\mathrm{F} = \min(\mathrm{RMSE}(\mathrm{LSTM}(\mathrm{x}))) \tag{5.9}$$

where x = [Learning Rate, Hidden Units, Dropout Rate] was shown in Table 5.3 and RMSE was root mean square.

The PSO optimizes the value of the LSTM parameters as in the following steps:

(a) The acquired sEMG signal and knee joint angle data are preprocessed, as shown in Figure 5.9 & 5.10. The values of knee joint angle and four sEMG signals were used as the input feature vector. Therefore, the input layer of the LSTM was five neurons.

(b) PSO parameters were initialized using the population size, the number of iterations, learning factors, and bounded intervals for particle position and velocity values.

(c) Table 5.4 shows the learning rate, hidden units and the dropout rate parameter with a searching range to establish the LSTM model.

(d) The optimal parameter value of the LSTM model was finally determined by the fitness function (F).

(e) Various updated particle values evaluate the particle's global best optimum position g_{best} and the local best optimum position pbest. Then it records its best position and updates the particle's optimum common and local position.

(f) When the maximum number of iterations was achieved, the parameter optimal random values were set to train the LSTM model (Table 5.3). Otherwise, it will return to the previous step and continued executing iterations until the termination condition is met.

PSO-LSTM model was used to find optimum random values of hidden layer, dropout rate and learning rate from Table 5.3. All random optimum value for muscles (VM, VL, RF, BF) and the knee angle of five subject for PSO-LSTM was described in Table 5.5. After that, a random LSTM value for all muscles and knee angle (Table 5.6) was obtained with

Table 5.4: Algorithm steps

Algorithm PSO with LSTM Steps		
SN	**Initialize the PSO parameters**	**Initialize LSTM parameters**
1.	w=1; Inertia Weight	Dropout Rate = [0.2, 0.3]
2.	wdamp=0.99; Inertia Weight Damping Ratio	Hidden Units = [100, 450]
3.	c1=1.5; Personal Learning Coefficient	Learning Rate = [0.01, 0.0001]
4.	c2=2.0; Global Learning Coefficient	Dropout Rate = [0.2, 0.3]
5.	Iterations = 200	
6.	pop Size = 50	
7.	Evaluate RMSE = LSTM (Learning Rate, Hidden Units, Dropout Rate)	
8.	Return the individual with the best fitness as the solution	

the help of Table 5.5 by taking the average of optimum random values of five subjects. Different parameters such as the RMSE, r, R^2 were evaluated on random LSTM model performance.

PSO-LSTM and random LSTM relationship: To analyse incremental and reduction value of RMSE, r, R^2 for PSO-LSTM % in comparison to random LSTM,Equation (5.10) was used.

$$\frac{\text{PSO-LSTM (RMSE, r, } R^2) - \text{ Random-LSTM (RMSE, r, } R^2 \text{)}}{\text{PSO-LSTM (RMSE, r, } R^2 \text{)}} \tag{5.10}$$

5.3 Result and Discussion

The results were analyzed from the random LSTM (Table 5.6) and PSO-LSTM model (Figure 5.6, Figure 5.7, Table 5.5) based on five healthy subjects. The model performance was measured by computing RMSE, r, R^2 between actual and predicted values.

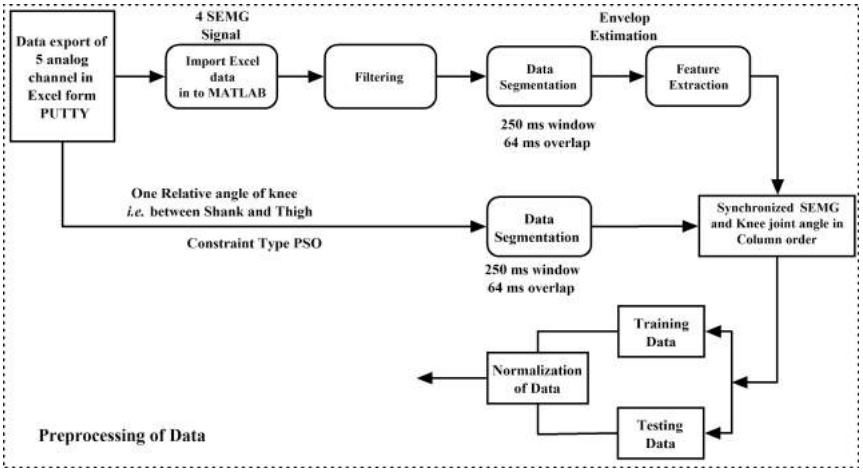

Figure 5.6: Workflow of the pre-processing of data

Table 5.5: Obtained parameter value of given LSTM for different Muscles by using PSO: extension activity

Extension Activity						
Muscle No	**LSTM Parameter**	**Subject-1**	**Subject-2**	**Subject-3**	**Subject-4**	**Subject-5**
Muscle_1	Hidden Layer	250	200	250	200	230
	Dropout Rate	0.4	0.2	0.2	0.2	0.2
	Learning Rate	0.005	0.08	0.008	0.001	0.03
Muscle_2	Hidden Layer	250	250	250	220	150
	Dropout Rate	0.2	0.2	0.2	0.2	0.2
	Learning Rate	0.0008	0.00013	0.0007	0.005	0.0002
Muscle_3	Hidden Layer	450	200	250	220	250
	Dropout Rate	0.2	0.2	0.2	0.2	0.2
	Learning Rate	0.0008	0.0008	0.007	0.05	0.01
Muscle_4	Hidden Layer	250	400	200	300	260
	Dropout Rate	0.2	0.2	0.2	0.2	0.2
	Learning Rate	0.005	0.000035	0.007	0.009	0.02
Knee Angle	Hidden Layer	250	200	200	280	260
	Dropout Rate	0.2	0.3	0.2	0.2	0.2
	Learning Rate	0.006	0.0005	0.003	0.009	0.02

5.3.1 Lower Limb Movement Analysis

PSO-LSTM model was developed to classify three individual lower limb movements (Flexion, Extension, Ramp Walking) with 98.58 % accuracy, as shown in Figure 5.8. To improve the model's classification, PSO was implemented to find the best classification accuracy. The developed PSO-LSTM model successfully classifies sEMG signals. This model could implement in sEMG based exoskeleton for controlling movement.

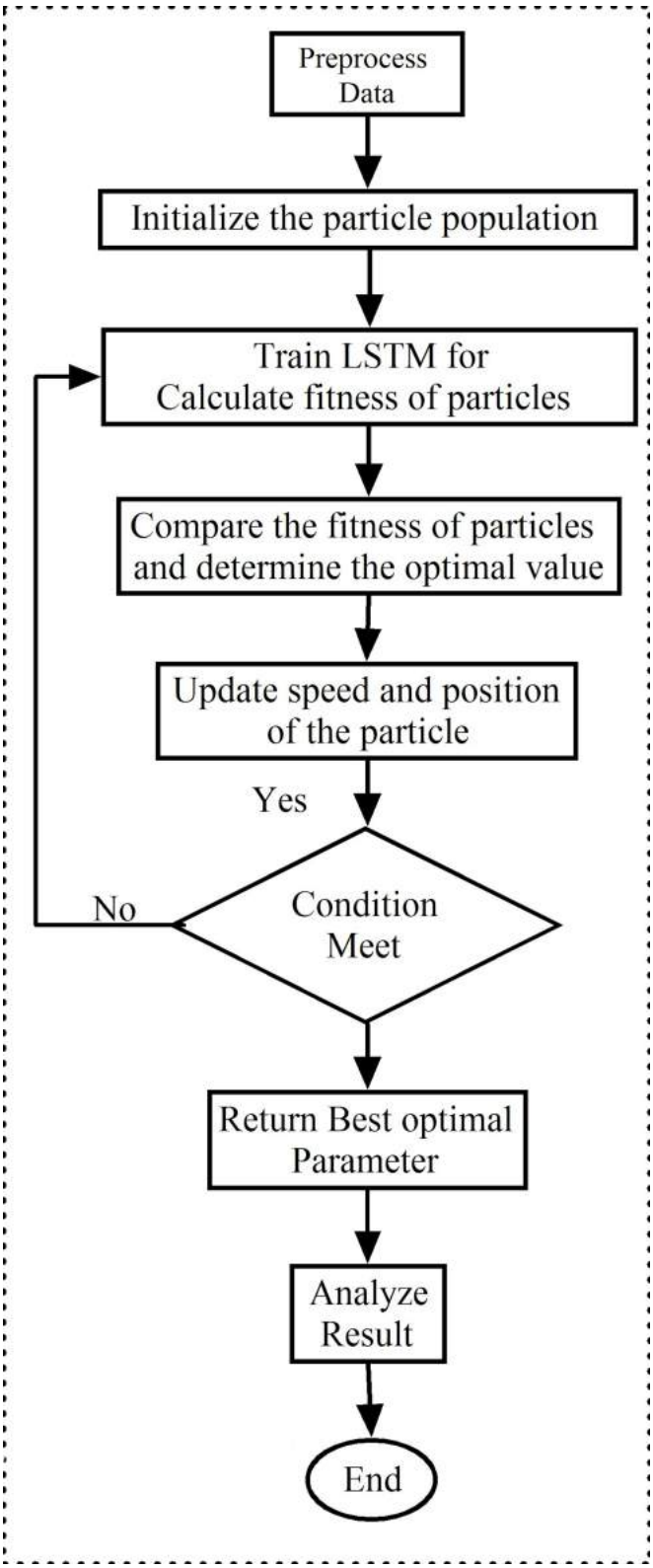

Figure 5.7: Flowchart of PSO-LSTM model

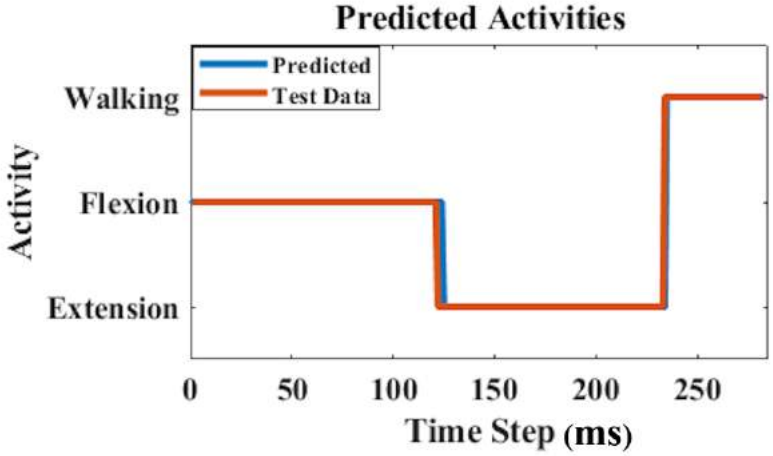

Figure 5.8: Classification of activities based on sEMG signal

5.3.2 Models Evaluation Parameter for Prediction of sEMG Signal and Knee angle

Here, root mean square error, correlation coefficient, and coefficient of determination were calculated.

1. **Root Mean Square Error (RMSE)** indicates the concentration of data around the most suitable line. Using fundamental principles, the best value of RMSE would be close to zero. Both model RMSE for sEMG signals and knee angle were (0.005, 4.72), (0.003, 2.39), (0.003, 2.72) for an extension, flexion and ramp walking movement, respectively.

2. **Correlation Coefficient (r)** is a statistical measure of the strength between the actual and the predicted values from -1 to 1. A '-1' correlation shows a perfect negative correlation, and a perfect positive correlation is shown by '1'. A '0' correlation shows no relationship between actual and predicted values. Both model correlation for sEMG signals and knee angle were (0.86, 0.99), (0.87, 0.99), (0.84, 0.99) for an extension, flexion, and ramp walking movement, respectively. Therefore, all muscles were selected for three movements.

3. **Coefficient of Determination** (R^2) is used to explore the variability of actual and predicted values. It is referred to as the goodness of fit. This model represents a value between 0 and 1, where a value of '1' shows a perfect fit and a highly reliable prediction model. In contrast, a value of '0' shows that the model fails. Both model (R^2) for sEMG signals and knee angle were (0.85, 0.98), (0.89, 0.99), (0.75, 0.98) for an extension, flexion and ramp walking movement, respectively.

5.3.3 Comparisons of the Results of PSO-LSTM with Random LSTM model

Table 5.5 shows the average of five subjects for the concerned muscles and knee angle, obtained from the parameters' values shown in Table 5.6 for developing a random LSTM model. The PSO-LSTM and random LSTM model performance was evaluated by different parameters such as RMSE, r, R^2. After that, a comparison of the results of PSO-LSTM with random LSTM for the prediction of sEMG signal and knee angle was carried out. These parameters have their advantage/disadvantage for evaluating the model's performance. RMSE was alone insufficient to evaluate the models' performance because of having high sensitivity to outlier values (highly dependent on the absolute measure of fit). Hence, the outliers from the data sets must remove before calculating the RMSE. Otherwise, RSME shows larger uncertainty variation during statistics analysis, as shown in Figure 5.11 (A), making it very difficult to identify outliers in some datasets. The other parameters (R^2, r) were used along with RMSE due to the relative measure between actual and predicted values. Table 5.7 and Table 5.8 shows optimum parameter value of given LSTM-PSO for flexion and ramp walking activity. Table 5.9

Table 5.6: The parameter value of random LSTM for different muscles

Extension Activity		
Muscle No	**LSTM Parameter**	**Average of all Subject**
Muscle_1	Hidden Layer	226
	Dropout Rate	0.24
	Learning Rate	0.0248
Muscle_2	Hidden Layer	224
	Dropout Rate	0.2
	Learning Rate	0.0013
Muscle_3	Hidden Layer	274
	Dropout Rate	0.2
	Learning Rate	0.013
Muscle_4	Hidden Layer	260
	Dropout Rate	0.2
	Learning Rate	0.0082
Knee Joint Angle	Hidden Layer	282
	Dropout Rate	0.22
	Learning Rate	0.0077

and Table 5.10 , along with Figure 5.9 and Figure 5.10, shows the results of the RMSE, r, R^2 between the actual and predicted value of both inputs for the random LSTM model and the PSO-LSTM model.

Table 5.7: The obtained parameter value of given LSTM for different muscles by using PSO: flexion activity

Flexion Activity						
Muscle No	**LSTM Parameter**	**Subject-1**	**Subject-2**	**Subject-3**	**Subject-4**	**Subject-5**
Muscle_1	Hidden Layer	200	200	250	200	250
	Dropout Rate	0.2	0.2	0.2	0.4	0.2
	Learning Rate	0.0005	0.0009	0.0004	0.0003	0.005
Muscle_2	Hidden Layer	200	200	220	400	250
	Dropout Rate	0.2	0.2	0.2	0.4	0.2
	Learning Rate	0.004	0.0009	0.009	0.003	0.005
Muscle_3	Hidden Layer	200	200	250	200	250
	Dropout Rate	0.2	0.3	0.2	0.2	0.2
	Learning Rate	0.00412	0.00009	0.006	0.0005	0.006
Muscle_4	Hidden Layer	250	200	250	200	200
	Dropout Rate	0.2	0.2	0.2	0.2	0.2
	Learning Rate	0.0008	0.0009	0.008	0.0005	0.05
Knee Angle	Hidden Layer	200	200	250	200	250
	Dropout Rate	0.2	0.2	0.2	0.2	0.2
	Learning Rate	0.005	0.009	0.008	0.005	0.008

Figure 5.11 (A) and Figure 5.12 (A) shows the RMSE of the PSO-LSTM model was a lower value than that of the random LSTM model for the sEMG signals and knee joint angle model's input. The average RMSE value for an extension, flexion and ramp walking for both PSO-LSTM and random LSTM model was $(80\%, 10.16\%)$, $(133.33\%, 30.96\%)$ and $(116.66\%, 19.48\%)$, respectively. Figure 5.11 (B,C) and Figure 5.12 (B, C) shows that R^2, r value of random LSTM was lower than that of the PSO-LSTM model for sEMG signals and knee joint angle model's input. The average 'r' value for an extension, flexion, ramp walking for both PSO-LSTM and random LSTM model was more by $(4.65\%, 4.04\%)$, $(6.60\%, 3.03\%)$ and $(3.57\%, 7.07\%)$, respectively. The average R^2 value of sEMG for an extension, flexion, ramp walking for both PSO-LSTM and random LSTM model was higher by $(5.88\%, 4.08\%), (5.05\%, 4.04\%)$ and $(5.33\ \%, 8.16\%\ )$, respectively. It was observed that the proposed PSO-LSTM model shows better capability than the random LSTM model for both inputs (sEMG signals, knee joint angle).

Table 5.8: Obtained parameter value of given LSTM for different muscles by using PSO: Ramp Walking Activity

Ramp Walking Activity						
Muscle No	LSTM Parameter	Subject-1	Subject-2	Subject-3	Subject-4	**Subject-5**
Muscle_1	Hidden Layer	202	200	200	200	300
	Dropout Rate	0.2	0.2	0.2	0.2	0.2
	Learning Rate	0.08	0.005	0.006	0.005	0.01
Muscle_2	Hidden Layer	200	200	200	200	200
	Dropout Rate	0.2	0.4	0.2	0.2	0.4
	Learning Rate	0.06	0.001	0.008	0.01	0.02
Muscle_3	Hidden Layer	200	200	200	200	200
	Dropout Rate	0.2	0.2	0.4	0.2	0.2
	Learning Rate	0.05	0.03	0.09	0.01	0.05
Muscle_4	Hidden Layer	200	200	200	200	200
	Dropout Rate	0.2	0.2	0.4	0.2	0.2
	Learning Rate	0.02	0.04	0.0085	0.009	0.07
Knee Angle	Hidden Layer	200	200	200	200	200
	Dropout Rate	0.2	0.2	0.2	0.2	0.2
	Learning Rate	0.015	0.04	0.008	0.003	0.07

Table 5.9: Evaluation parameter value for given activities using Random LSTM

		Muscle_1*	**Muscle_2***	**Muscle_3***	**Muscle_4***	**Average Muscle**	**Knee Joint Angle**
Extension	RMSE	0.0087	0.009	0.0089	0.01	0.009	5.2
	r	0.80	0.87	0.81	0.83	0.82	0.95
	R^2	0.81	0.83	0.80	0.78	0.80	0.94
Flexion	RMSE	0.008	0.005	0.0085	0.0065	0.007	3.13
	r	0.90	0.78	0.92	0.65	0.8125	0.96
	R^2	0.87	0.80	0.87	0.84	0.845	0.95
Ramp Walking	RMSE	0.005	0.0062	0.007	0.008	0.0065	3.25
	r	0.72	0.82	0.80	0.92	0.81	0.92
	R^2	0.60	0.70	0.68	0.85	0.71	0.90
(*) Represent average of five healthy males							

Table 5.10: Evaluation parameter value for given activities using PSO-LSTM

		Muscle_1*	**Muscle_2***	**Muscle_3***	**Muscle_4***	**Average Muscle**	**Knee Joint Angle**
Extension	RMSE	0.0007	0.0085	0.0007	0.0096	0.005	4.72
	r	0.83	0.92	0.85	0.86	0.86	0.99
	R^2	0.85	0.85	0.82	0.87	0.85	0.98
Flexion	RMSE	0.004	0.001	0.006	0.001	0.003	2.39
	r	0.95	0.80	0.95	0.67	0.87	0.99
	R^2	0.90	0.82	0.90	0.86	0.89	0.99
Ramp Walking	RMSE	0.003	0.003	0.003	0.004	0.003	2.72
	r	0.77	0.84	0.83	0.94	0.84	0.99
	R^2	0.64	0.75	0.71	0.89	0.75	0.98
(*) Represent average of five healthy males							

Table 5.11: Comparison of evaluation parameter values for given activities using Random LSTM and PSO-LSTM

		Random LSTM		**LSTM-PSO**		**Reduction/Incremental % w.r.t. PSO-LSTM**	
		Average Muscle	Knee Joint Angle	Average Muscle	Knee Joint Angle	Average Muscle	Knee Joint Angle
Extension	RMSE	0.009	5.2	0.005	4.72	-80	-10.16
	r	0.82	0.95	0.86	0.99	4.65	4.04
	R^2	0.80	0.94	0.85	0.98	5.88	4.08
Flexion	RMSE	0.007	3.13	0.003	2.39	-133.33	-30.96
	r	0.8125	0.96	0.87	0.99	6.60	3.03
	R^2	0.845	0.95	0.89	0.99	5.05	4.04
Ramp Walking	RMSE	0.0065	3.25	0.003	2.72	-116.66	-19.48
	r	0.81	0.92	0.84	0.99	3.57	7.07
	R^2	0.71	0.90	0.75	0.98	5.33	8.16

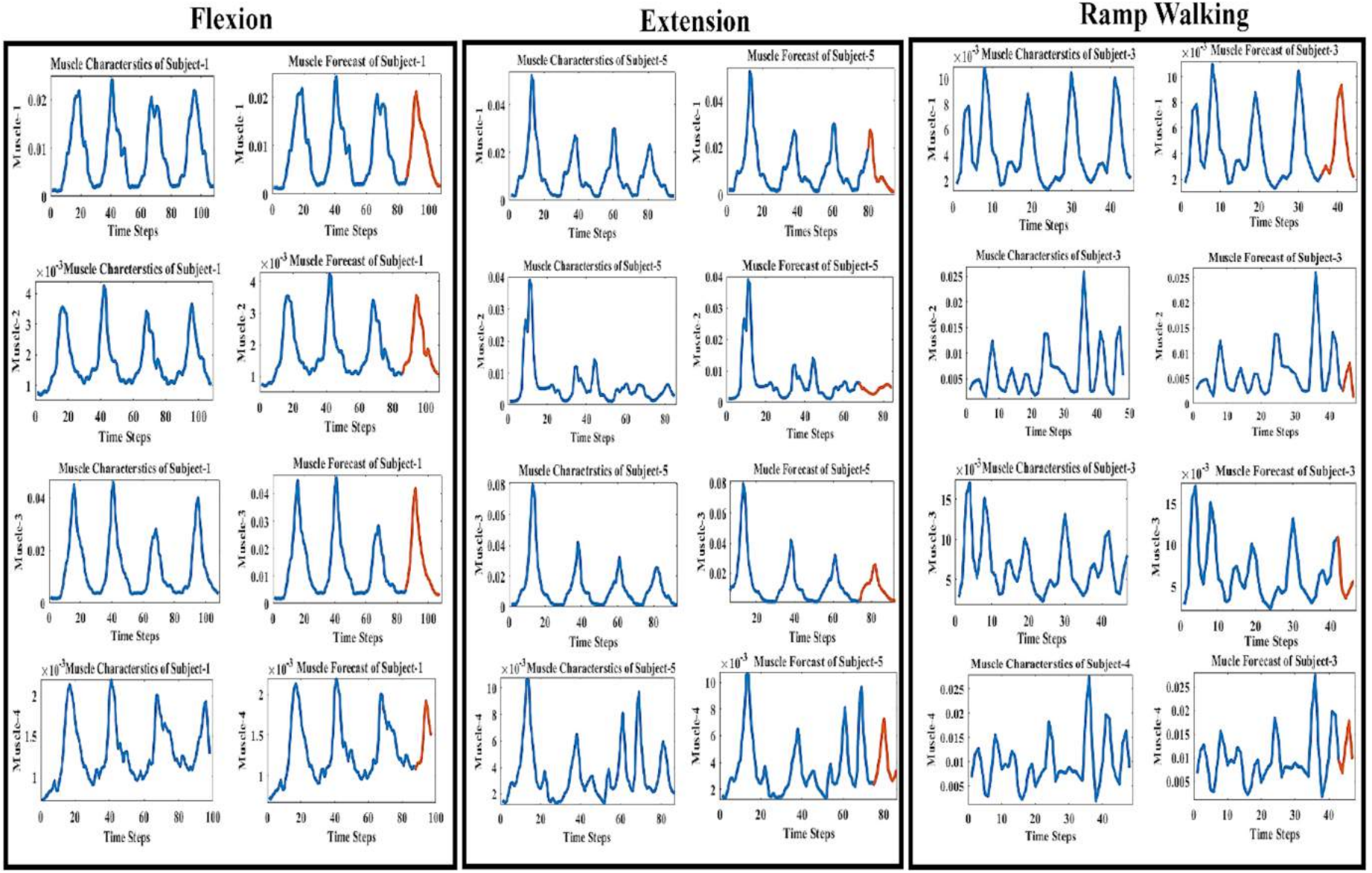

Figure 5.9: Knee muscle characteristics and prediction of subject-1,5,3 for three movements

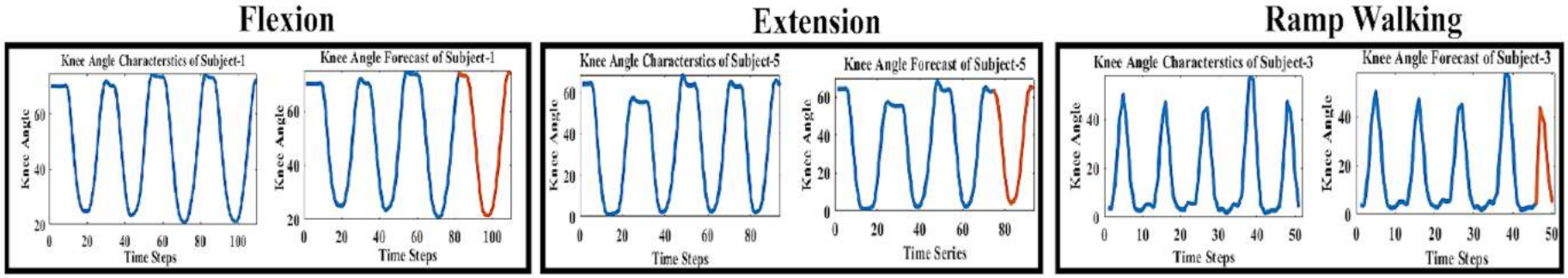

Figure 5.10: Knee angle characteristics and prediction of subject-1,5,3 for three movements

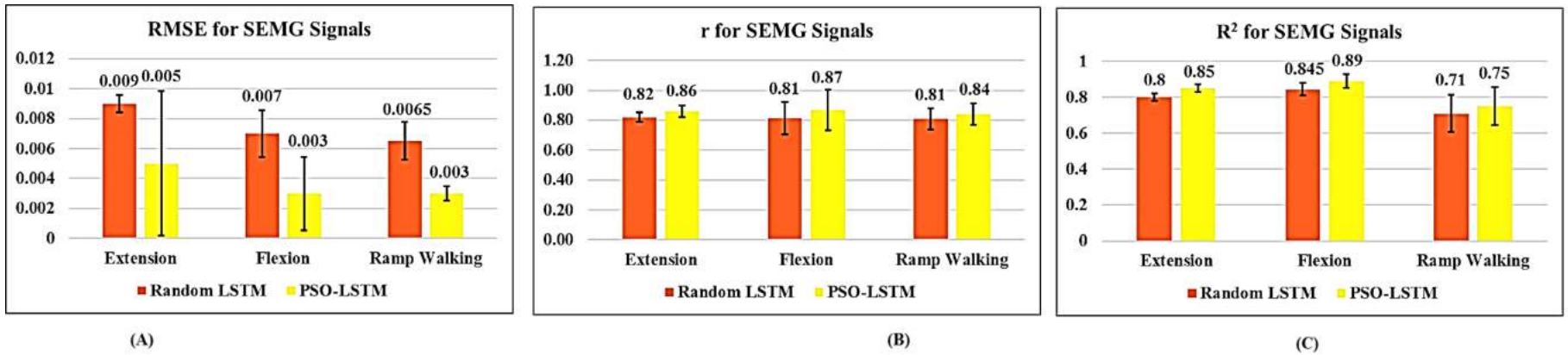

Figure 5.11: Uncertainty measure and comparison of models for RMSE, r R^2, of sEMG signals

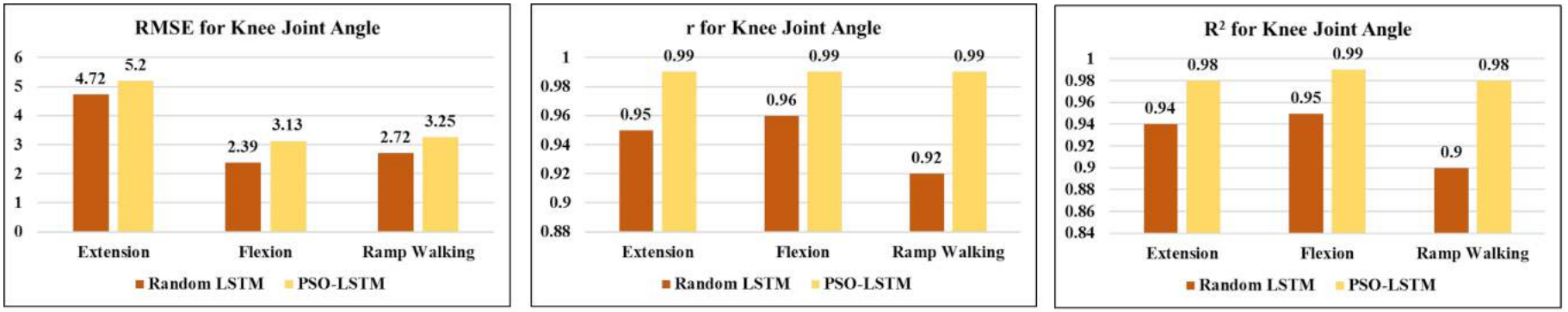

Figure 5.12: Comparison of models for RMSE, r, R^2 of knee angle

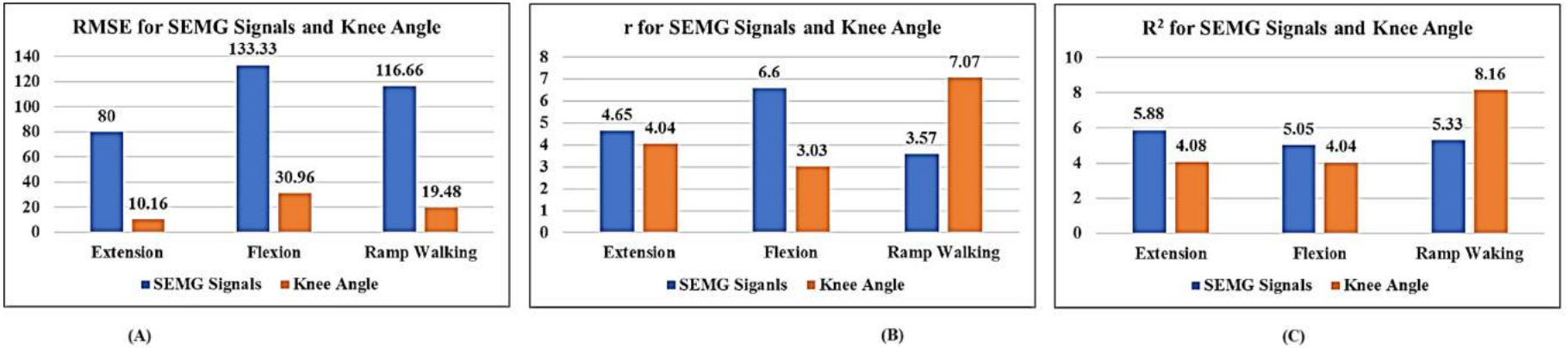

Figure 5.13: Reduction/incremental value of RMSE, r, R^2 for PSO-LSTM with respect to random LSTM

To calculate the reduction/incremental value of RMSE, r, R^2 for PSO-LSTM with respect to random LSTM, the absolute of Equation (5.10) was used. Table 5.11 a shows the incremental decremental value of the average RMSE, r, R^2 of sEMG signal and knee angle for PSO-LSTM versus random LSTM. The average RMSE value of sEMG signals and knee angle for PSO-LSTM was reduced compared to random LSTM, as shown in Figure 5.13 (A). The negative sign of RMSE was compensated in this case by using the absolute value of Equation (5.10). Figure 5.13 (B, C) show that the average r, R^2 value of sEMG signal and knee joint angle for PSO-LSTM was increased compared to random LSTM. These results clearly show that LSTM with PSO was better for predicting the knee joint angle. The maximum increased percentage of 'r' value of PSO-LSTM was 0.58 % compared to random LSTM. The correlation coefficient obtained by PSO-LSTM gradually increased during each movement. The 'r' value of LSTM using PSO was suitable for each activity. This model also improved accuracy for three movements. The PSO-LSTM could be the best application prospect in continuous predictions. The training time for the PSO-LSTM was shorter than the random LSTM. Reducing training time helps to improve the system's response speed. sEMG signals and knee joint angles' active training can be better implemented on the lower limb rehabilitation for stroke patients to restore muscles' strength.

5.3.4 Prototype Development

The control circuit is consists of a microcontroller (ATmega328p), motor driver (L298D), SEMG electrode, linear actuator, instrumentation amplifier (INA118P), two accelerometer (ADXL335), RMS to DC converter, and (AD536AJD), as shown in Figure 5.14. The microcontroller generates the control signal that transmits to the motor driver to operate the linear actuator through a sEMG signal recorded from an electrode. The linear actuator provides high torque to prototype for performing 80° range of motion at the knee joint. The actuator is able to generate a holding torque of 1500 N with operating 12 V and having 330 mm stroke length to operate the prototype. An accelerometer was used to measure the angle of range of motion as briefly described in subsection (5.2.3). Figure 5.19 shows the design prototype of the knee exoskeleton. The prototype structure consists of thigh segment, shank segment, and connecting braces. Connecting braces support the design prototype for wear on the lower limb. This support at the shank and thigh provides two fold function: space for sEMG electrode, sensor, and strength for the muscles. The prototype has one DOF (Flexion/ Extension) with an active knee joint movement. A linear electric actuator and control circuit (INA118P, AD536AJD, sEMG electrode) was used to control knee movement. The prototype was developed in the laboratory and operated through sEMG signal for three activities (Flexion, Extension, Ramp Walking).

The prototype was developed in the laboratory and operated through a single-channel sEMG signal for three activities (Flexion, Extension, Ramp Walking). Thus, a single muscle (VL) is responsible for operating this prototype [213].

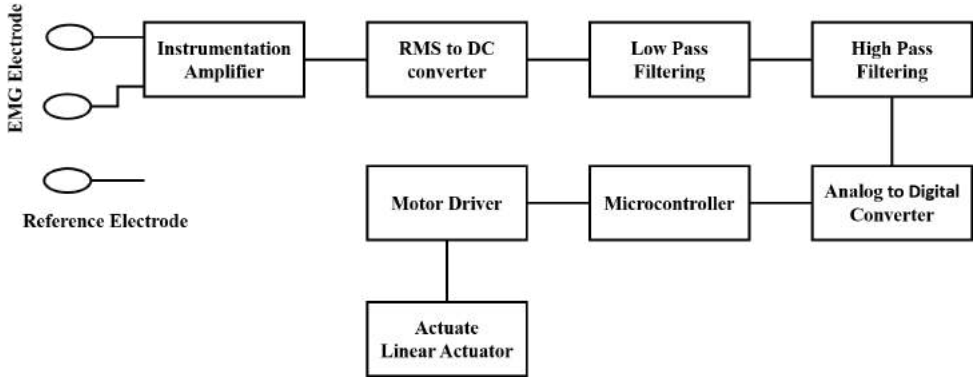

Figure 5.14: Single channel sEMG signal acquisition

The **INA118** is a low-power, high-accuracy general-purpose instrumentation amplifier, as shown in Figure 5.15. Gain between 1 and 10000 can be set with a single external resistor, as shown in Figure 5.16. Internal input protection can withstand a voltage of up to ±40 volts without causing damage. The common-mode rejection of the INA118 is high (110 dB at G = 1000). It can run on as little as 1.35 V and has a quiescent current of only 350 A, making it an excellent choice for battery-powered systems.

The **AD536A** determines the root-mean-square level of a complex ac (or ac plus dc) input signal and outputs a dc equivalent, as shown in Figure 5.17. The true RMS value of a waveform was more useful than the average rectified value because it corresponds

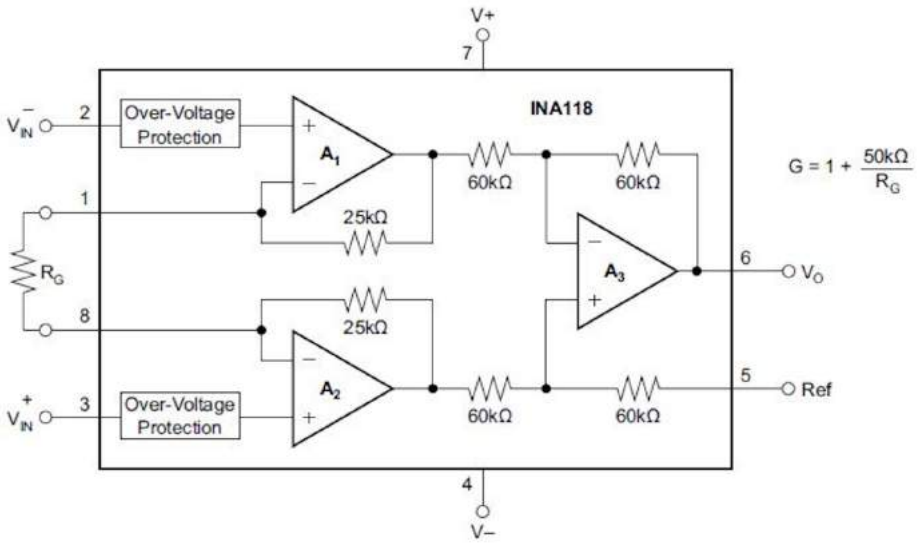

Figure 5.15: INA118 Shematic

DESIRED GAIN	R_G (Ω)	NEAREST 1% R_G (Ω)
1	NC	NC
2	50.00k	49.9k
5	12.50k	12.4k
10	5.556k	5.62k
20	2.632k	2.61k
50	1.02k	1.02k
100	505.1	511
200	251.3	249
500	100.2	100
1000	50.05	49.9
2000	25.01	24.9
5000	10.00	10
10000	5.001	4.99

NC: No Connection.

Figure 5.16: Register Table

to the signal's power. To achieve the full specified accuracy, an external capacitor was required. The settling time, ripple amplitude, and low-frequency ac accuracy were all determined by the value of this capacitor. With total supply levels ranging from 5 V to 36 V, the AD536A works equally well with split or single supplies. The device worked well suited for a wide range of remote controllers and battery-powered instruments, with a quiescent supply current of 1 mA. A multisim software was used for making circuits on the breadboard. Amplification of low-level signal was done by using these ic's combine together, as shown in Figure 5.18.

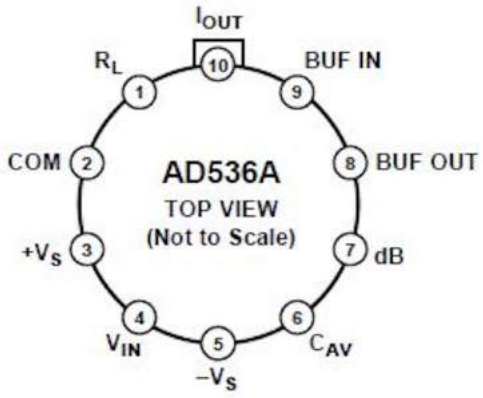

Figure 5.17: Pin Diagram of AD536A

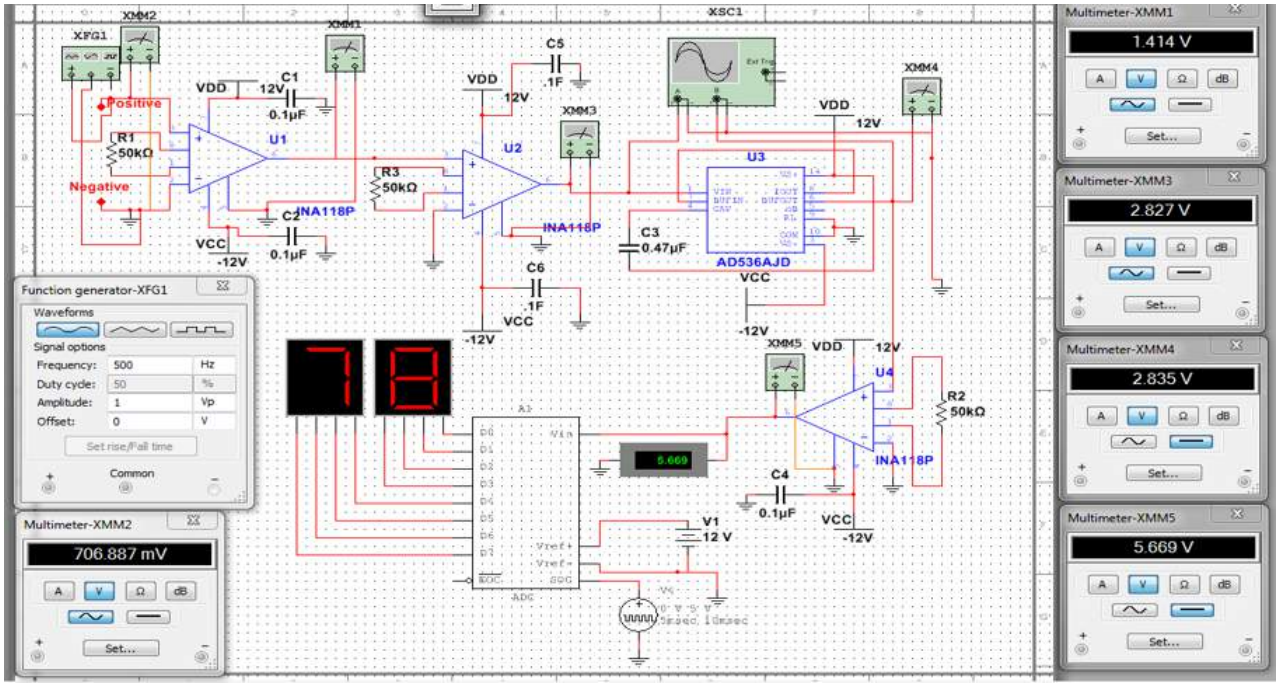

Figure 5.18: Signal conversion from RMS to hexadecimal using ADC

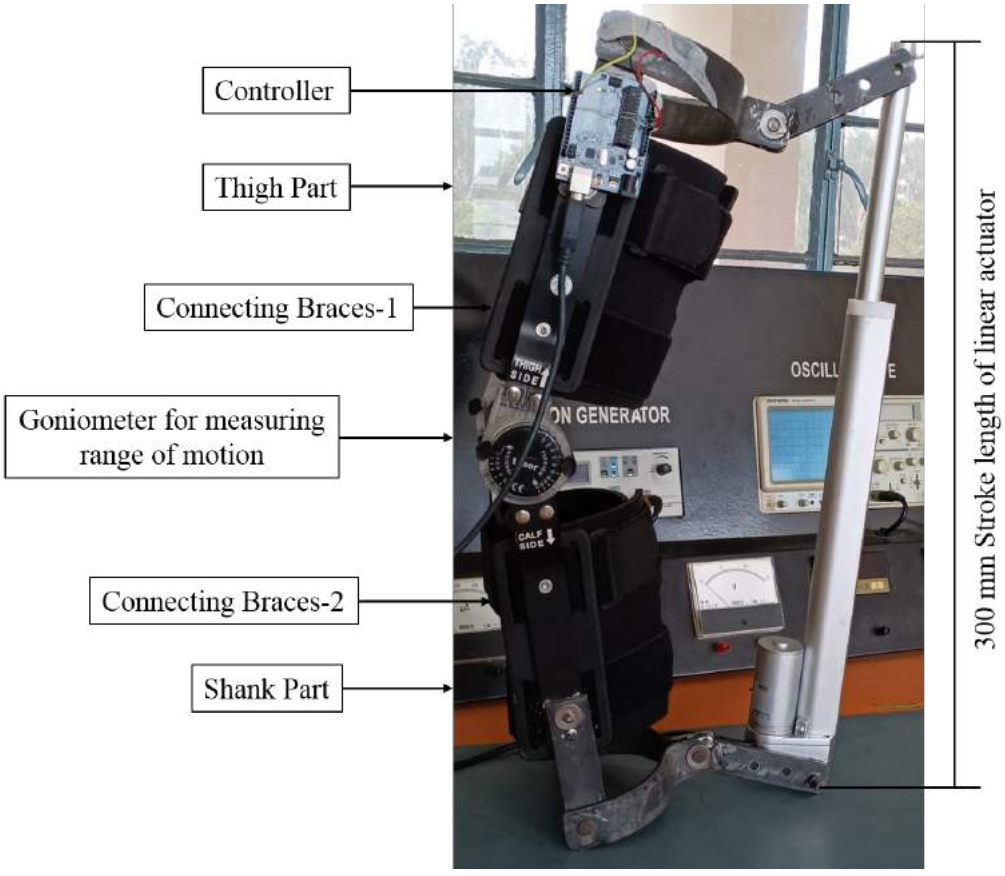

Figure 5.19: Prototype of sEMG based exoskeleton

PSO-LSTM models were explored for prediction and classification with specified input and compared to random LSTM. Selected muscles (VM, VL, RF, BF) and knee joint angles of healthy humans were used as input for both models. Both model performances were evaluated on RMSE, r, and R^2. The PSO-LSTM model outperforms other models in terms of prediction and classification accuracy.

Chapter 6

Conclusions and Future Scope

6.1 Conclusions

This thesis was intended to improve the performance and stability of a sEMG-based real-time exoskeleton. The main contributions of the thesis work can be divided into four categories: human biomechanics, sEMG signal preprocessing and force estimation, prediction and classification of knee joint angle and sEMG signal, and control strategy for single and multi-joint exoskeletons. The research primarily focused on simulation tools for understanding human musculoskeletal biomechanics. Various studies of human musculoskeletal postures (ROM, DoF), joints and their movements, and lower limb muscles were conducted. Simulation tools were useful for analyzing various joint muscle parameters such as muscle forces, joint forces and moments, metabolism, elastic energy in tendons, antagonistic muscle actions, and many others.

A simulation-based study of a 3D design exoskeleton using inverse dynamic analysis for squatting movement in AMS was carried out, and its effects on human musculoskeletal systems were investigated. Furthermore, simulation-based muscle force results were validated against experimentally obtained muscle force results. To remove noise from sEMG signals obtained from a healthy individual, preprocessing was performed (experimentally). The hill muscle model was then used to convert this sEMG signal into muscle force for validation using simulation results. The results with the assistance of the exoskeleton for the knee muscles were reduced significantly in biceps femoris, rectus femoris, vastus lateralis, vastus medialis, gluteus medius, and semitendinosus as the load increases. With the help of the exoskeleton, the force in the knee joint was also reduced as the load increased. The AMS muscle force results were statistically validated against experimental muscle force results. Validation of muscle results with and without an exoskeleton was also done using ANOVA t-tests. The developed 3D model aided in understanding the effects of load on various muscles and provided useful information for designing an individual's optimal exoskeleton.

Furthermore, Developed a machine learning-based simulator for estimating muscle forces. Four different machine learning (ML) models were trained and tested on 500 human

musculoskeletal data sets for predicting knee muscle force. The result based on the datasets predicts the random forest ML model to outperforms the other models: Neural Network, Generalized Linear Model, Decision Tree in terms of mean square error (MSE), coefficient of determination (R^2), and Correlation (r). The developed ML model-based took only $2-3$ seconds to predict muscle forces for a given input parameter value. Thus, the proposed model will be helpful in many applications, like developing and optimizing the lower limb exoskeleton, rehabilitation, clinical, selecting actuators etc.

Moreover, Developed a PSO-LSTM model for classification and prediction to control sEMG based exoskeleton for three activities: flexion, extension, and ramp climbing. Particle Swarm Optimization-Long Short Term Memory (PSO-LSTM) was used to classify three movements (Flexion, Extension, Ramp Walking) with an accuracy of 98.58% and predict the results. After that, random LSTM was used to validate the results to explore the effectiveness of PSO-LSTM. Four knee muscles sEMG signals, namely biceps femoris (BF), vastus medialis (VM), rectus femoris (RF) and semitendinosus (ST), and knee angle, were used as model inputs. RMSE, r, and R^2 were taken as evaluation parameters to identify the model's robustness for predicting SEMS signal and knee angle. The average RMSE value for an extension, flexion and ramp walking for PSO-LSTM than random LSTM model was lower. The average 'r' value for an extension, flexion, ramp walking for both PSO-LSTM compare to the random LSTM model was more. The average R^2 value of sEMG for an extension, flexion, ramp walking for PSO-LSTM compare to the random LSTM model was higher. It was observed that the proposed PSO-LSTM model shows better capability than the random LSTM model for both inputs (sEMG signals, knee joint angle). The signals estimation model's predicted results would assist in selecting operating a prototype with the help of sEMG signals control strategy. A simulation-based analysis helped to fine-tune the development of a real-time exoskeleton for every individual and eventually save time and cost.

6.2 Future Scope

There are the following suggestions for the future development of sEMG based knee exoskeleton.

(a) Work is needed on muscle properties for parametric studies to improve the efficiency of the designed exoskeleton.

(b) The footplate would include to measuring ground reaction forces in developing a prototype. It will provide valuable data required for users.

(c) This simulation-based study could be extended in the analysis of the human's joint and muscle forces for various activities, such as stair climbing, ramp walk, and so forth.

(d) Wireless sEMG acquisition systems would likely incorporate to produce better results than wired electrode systems to remove motion artefacts.

References

[1] United Nations. World Population Ageing. Technical report, 2017.

[2] Andrew M Briggs and Jeremy Shiffman. Global health policy in the 21st century: challenges and opportunities to arrest the global disability burden from musculoskeletal health conditions. *Best Practice & Research Clinical Rheumatology*, page 101549, 2020.

[3] Adam B Zoss and Hami Kazerooni. Biomechanical design of the berkeley lower extremity exoskeleton (bleex). *IEEE/ASME Transactions on mechatronics*, 11(2):128–138, 2006.

[4] Aaron M. Dollar and Hugh Herr. Lower extremity exoskeletons and active orthoses: Challenges and state-of-the-art. *IEEE Trans. Robot.*, 24(1):144–158, 2008.

[5] Di Ao, Rong Song, and JinWu Gao. Movement performance of human–robot cooperation control based on emg-driven hill-type and proportional models for an ankle power-assist exoskeleton robot. *IEEE Transactions on Neural Systems and Rehabilitation Engineering*, 25(8):1125–1134, 2016.

[6] Yuyang Chen and Chenyun Dai. Cross-Comparison of EMG-to-Force Methods for Multi-DoF Finger Force Prediction Using One-DoF Training. *IEEE Access*, 8:13958–13968, 2020.

[7] Kai Gui and Honghai Liu. A Practical and Adaptive Method to Achieve EMG-Based Torque Estimation for a Robotic Exoskeleton. *IEEE/ASME Trans. Mechatronics*, 24:483–494, 2019.

[8] Jiangcheng Chen and Xiaodong Zhang. Surface EMG based continuous estimation of human lower limb joint angles by using deep belief networks, 2018.

[9] Chenfei Ma and Lin Chuang. Continuous estimation of upper limb joint angle from sEMG signals based on SCA-LSTM deep learning approach. *Biomed. Signal Process. Control*, 61:13, 2020.

[10] Marzieh Mostafavizadeh Ardestani and Xuan Zhang. Human lower extremity joint moment prediction: A wavelet neural network approach. *Expert Syst. Appl.*, 41(9):4422–4433, 2014.

[11] Gabriel Aguirre-ollinger and Haoyong Yu. Lower-Limb Exoskeleton With Variable-Structure Series Elastic Actuators : Phase-Synchronized Force Control for Gait Asymmetry Correction. *IEEE Trans. Robot.*, 37:763–779, 2021.

[12] Z. H. Michalopoulou and D. Alexandrou. Performance Evaluation of Multilayer Perceptrons in Signal Detection and Classification. 6(2):2–7, 1995.

[13] Harikumar Rajaguru and Sunil Kumar Prabhakar. Hilbert Transform with Elman Backpropagation and Multilayer Perceptrons for Epilepsy Classification. pages 571–576, 2017.

[14] Jiyuan Song and Aibin Zhu. Effects of Different Feature Parameters of sEMG on Human Motion Pattern Recognition Using Multilayer Perceptrons and LSTM Neural Networks. pages 1–19, 2020.

[15] Jianda Han and Qichuan Ding. A state-space EMG model for the estimation of continuous joint movements. *IEEE Trans. Ind. Electron.*, 62(7):4267–4275, 2015.

[16] Qichuan Ding and Jianda Han. Continuous Estimation of Human Multi-Joint Angles from sEMG Using a State-Space Model. *IEEE Trans. Neural Syst. Rehabil. Eng.*, 25:1518–1528, 2017.

[17] Feiyun Xiao and Yong Wang. Continuous estimation of joint angle from electromyography using multiple time-delayed features and random forests. *Biomed. Signal Process. Control*, 39:303–311, 2018.

[18] Damian De Arruda and Gerhard P Hancke. Wearable Device Localisation Using Machine Learning Techniques. In *2016 IEEE 25th Int. Symp. Ind. Electron.*, pages 1110–1115, Santa Clara, CA, USA, 2016. IEEE.

[19] Feng Zhang and Pengfeng Li. SEMG-based continuous estimation of joint angles of human legs by using BP neural network. *Neurocomputing*, 78:139–148, 2012.

[20] Yan Chen and Song Yu. A Continuous Estimation Model of Upper Limb Joint Angles by Using Surface Electromyography and Deep Learning Method. *IEEE Access*, 7:174940–174950, 2019.

[21] Arvind Gautam and Madhuri Panwar. MyoNet: A Transfer-Learning-Based LRCN for Lower Limb Movement Recognition and Knee Joint Angle Prediction for Remote Monitoring of Rehabilitation Progress from sEMG. *IEEE J. Transl. Eng. Heal. Med.*, 8:1–10, 2020.

[22] Teodor Adrian Teban and Radu Emil Precup. Recurrent neural network models for myoelectricbased control of a prosthetic hand. In *2018 22nd Int. Conf. Syst. Theory, Control Comput. ICSTCC 2018 - Proc.*, pages 603–608. IEEE, 2018.

[23] Jia Liang Ren and Ya Hui Chien. Deep learning based motion prediction for exoskeleton robot control in upper limb rehabilitation. *Proc. - IEEE Int. Conf. Robot. Autom.*, 2019-May:5076–5082, 2019.

[24] Tianzhe Bao and Ali Zaidi. Surface-EMG based wrist kinematics estimation using convolutional neural network. In *2019 IEEE 16th Int. Conf. Wearable Implant. Body Sens. Networks, BSN 2019 - Proc.*, pages 1–4. IEEE, 2019.

[25] Peng Xia and Hu Jie. EMG-based estimation of limb movement using deep learning with recurrent convolutional neural networks. *Artif. Organs*, 42:11, 2017.

[26] Yongchuang Huang, Zexia He, Yuxuan Liu, Ruiyuan Yang, Xiufeng Zhang, Guang Cheng, Jingang Yi, Joao Paulo Ferreira, and Tao Liu. Real-Time Intended Knee Joint Motion Prediction by Deep-Recurrent Neural Networks. *IEEE Sens. J.*, 19(23):11503–11509, 2019.

[27] Yifan Cai and Simon X Yang. An improved PSO-based approach with dynamic parameter tuning for cooperative multi- robot target searching in complex unknown environments. *Int. J. Control*, 86(10):1720–1732, 2013.

[28] Anupam Shukla and Bhattacharya Mahua. Structure stability analysis of Ni n (n = 2 – 22) using nature inspired algorithms : a performance study. *Int. J. Adv. Intell. Paradig.*, 5:16–30, 2013.

[29] Neha Hooda, Ratan Das, and Neelesh Kumar. Biomedical Signal Processing and Control Fusion of EEG and EMG signals for classification of unilateral foot movements. *Biomed. Signal Process. Control*, 60:101990, 2020.

[30] Gaurav Varshney, Manoj Misra, and Pradeep K Atrey. A survey and classification of web phishing detection schemes. *Secur. Commun. Netw.*, page 1674, 2016.

[31] Orly Yadid-Pecht. Machine - Learning based Medical Analysis System and Method Therefor, 2020.

[32] Shu Shen and Kang Gu. Movements Classification of Multi-Channel sEMG Based on CNN and Stacking Ensemble Learning. *IEEE Access*, 7:137489–137500, 2019.

[33] Alexander E. Olsson and Paulina Sager. Extraction of Multi-Labelled Movement Information from the Raw HD-sEMG Image with Time-Domain Depth. *Sci. Rep.*, 9(1):1–10, 2019.

[34] Zhen Ding and Chifu Yang. sEMG-based gesture recognition with convolution neural networks. *Sustain.*, 10(6):1–12, 2018.

[35] Yuheng Wu and Bin Zheng. Dynamic Gesture Recognition Based on LSTM-CNN. In *Proc. 2018 Chinese Autom. Congr. CAC 2018*, pages 2446–2450. IEEE, IEEE, 2019.

[36] Manfredo Atzori and Matteo Cognolato. Deep learning with convolutional neural networks applied to electromyography data: A resource for the classification of movements for prosthetic hands. *Front. Neurorobot.*, 10:1–10, 2016.

[37] Muhammad Zia ur Rehman and Syed Omer Gilani. Stacked sparse autoencoders for EMG-based classification of hand motions: A comparative multi day analyses between surface and intramuscular EMG. *Appl. Sci.*, 8(7):1126–1140, 2018.

[38] Hyeon Min Shim and Hongsub An. EMG pattern classification by split and merge deep belief network. *Symmetry (Basel).*, 8:148–159, 2016.

[39] Domenico Buongiorno and Giacomo Donato Cascarano. A survey on deep learning in electromyographic signal analysis. In *International Conference on Intelligent Computing*, pages 751–761. Springer, 2019.

[40] Wentao Wei and Yongkang Wong. A multi-stream convolutional neural network for sEMG-based gesture recognition in muscle-computer interface. *Pattern Recognit. Lett.*, 119:131–138, 2019.

[41] Wentao Sun and Huaxin Liu. sEMG-based hand-gesture classification using a generative flow model. *Sensors (Switzerland)*, 19:1–16, 2019.

[42] Marcello Zanghieri and Simone Benatti. Robust Real-Time Embedded EMG Recognition Framework Using Temporal Convolutional Networks on a Multicore IoT Processor. *IEEE Trans. Biomed. Circuits Syst.*, 14:244–256, 2020.

[43] General Electric Co. Hardiman i prototype project, special interim study, 1968.

[44] Thomas Sugar and Yasuhisa J Hasegawa. Wearable robotics for motion assistance and rehabilitation [tc spotlight]. *IEEE Robotics and Automation Magazine*, 25(1):19–28, 2018.

[45] Brian D Lowe and William G Billotte. Astm f48 formation and standards for industrial exoskeletons and exosuits. *IISE transactions on occupational ergonomics and human factors*, 7(3-4):230–236, 2019.

[46] Michiel de Looze and Tim Bosch. Assessment of an active industrial exoskeleton to aid dynamic lifting and lowering manual handling tasks. *Appl. Ergon.*, 68(November 2017):125–131, 2018.

[47] Di Wang and Fei Dai. Risk Assessment of Work-Related Musculoskeletal Disorders in Construction: State-of-the-Art Review. 141(6):04015008, 2015.

[48] Yongtian He and David Eguren. Risk management and regulations for lower limb medical exoskeletons: a review. *Medical devices (Auckland, NZ)*, 10:89, 2017.

[49] Erin M Sadler and Ryan B Graham. The personal lift-assist device and lifting technique: a principal component analysis. *Ergonomics*, 54(4):392–402, 2011.

[50] Slavka Viteckova and Patrik Kutilek. Wearable lower limb robotics A review. *Biocybern. Biomed. Eng.*, 33(2):96–105, 2013.

[51] Leslie Mertz. The next generation of exoskeletons: lighter, cheaper devices are in the works. *IEEE pulse*, 3(4):56–61, 2012.

[52] Ümit Önen and Fatih M Botsalı. Design and actuator selection of a lower extremity exoskeleton. *IEEE/ASME Transactions on Mechatronics*, 19(2):623–632, 2013.

[53] Aaron J Young and Daniel P Ferris. State of the art and future directions for lower limb robotic exoskeletons. *IEEE Transactions on Neural Systems and Rehabilitation Engineering*, 25(2):171–182, 2016.

[54] Sai K Banala and Sunil K Agrawal. Gravity-balancing leg orthosis and its performance evaluation. *IEEE Transactions on robotics*, 22(6):1228–1239, 2006.

[55] Emily Rogers and Panagiotis Polygerinos. A quasi-passive knee exoskeleton to assist during descent. In *Wearable Robotics: Challenges and Trends*, pages 63–67. Springer, 2017.

[56] Michael Wehner and Brendan Quinlivan. A lightweight soft exosuit for gait assistance. In *2013 IEEE international conference on robotics and automation*, pages 3362–3369. IEEE, 2013.

[57] Alan T Asbeck and Kai Schmidt. Multi-joint soft exosuit for gait assistance. In *2015 IEEE International Conference on Robotics and Automation (ICRA)*, pages 6197–6204. IEEE, 2015.

[58] Shengquan Shane Xie, Quan Liu, and Zhou. Recent development of mechanisms and control strategies for robot-assisted lower limb rehabilitation. *Mechatronics*, 31:132–145, 2015.

[59] Susan Karlin. Raiding iron man's closet [geek life]. *IEEE Spectrum*, 48(8):25–25, 2011.

[60] Tomohiro Hayashi and Yoshiyuki Sankai. Control method of robot suit hal working as operator's muscle using biological and dynamical information. In *2005 IEEE/RSJ International Conference on Intelligent Robots and Systems*, pages 3063–3068. IEEE, 2005.

[61] Atsushi Tsukahara and Ryota Kawanishi. Sit-to-stand and stand-to-sit transfer support for complete paraplegic patients with robot suit hal. *Advanced robotics*, 24(11):1615–1638, 2010.

[62] Mukul Talaty and Alberto Esquenazi. Differentiating ability in users of the rewalk tm powered exoskeleton: An analysis of walking kinematics. In *2013 IEEE 13th international conference on rehabilitation robotics (ICORR)*, pages 1–5. IEEE, 2013.

[63] Saso Jezernik and Gery Colombo. Robotic orthosis lokomat: A rehabilitation and research tool. *Neuromodulation: Technology at the neural interface*, 6(2):108–115, 2003.

[64] David A Winter. Overall principle of lower limb support during stance phase of gait. *Journal of biomechanics*, 13(11):923–927, 1980.

[65] Mariem Abid and Neila Mezghani. Knee joint biomechanical gait data classification for knee pathology assessment: a literature review. *Applied bionics and biomechanics*, 2019, 2019.

[66] Robert Riener, Marco Rabuffetti, and Carlo Frigo. Stair ascent and descent at different inclinations. *Gait & posture*, 15(1):32–44, 2002.

[67] Nok-Hin Law. *Kinematics & kinetics analysis of the lower extremity of normal weight, overweight, and obese individuals during stair ascent & descent.* University of Ottawa (Canada), 2013.

[68] Tung-Wu Lu and Chu-Fen Chang. Biomechanics of human movement and its clinical applications. *The Kaohsiung journal of medical sciences*, 28(2):S13–S25, 2012.

[69] Roberto Merletti and Loredana R Lo Conte. Surface emg signal processing during isometric contractions. *Journal of Electromyography and Kinesiology*, 7(4):241–250, 1997.

[70] Angkoon Phinyomark and Evan Campbell. Surface electromyography (emg) signal processing, classification, and practical considerations. In *Biomedical signal processing*, pages 3–29. Springer, 2020.

[71] Bernabe Rodríguez-Tapia and Israel Soto. Myoelectric interfaces and related applications: current state of emg signal processing–a systematic review. *IEEE Access*, 8:7792–7805, 2020.

[72] Kurt Manal and Thomas S Buchanan. An emg-driven model to estimate muscle forces and joint moments in stroke patients. *Computers in biology and medicine*, 39(12):1083–1088, 2009.

[73] Di Ao and Rong Song. Movement performance of human–robot cooperation control based on emg-driven hill-type and proportional models for an ankle power-assist exoskeleton robot. *IEEE Transactions on Neural Systems and Rehabilitation Engineering*, 25(8):1125–1134, 2016.

[74] Masayuki Yokoyama and Ryohei Koyama. An evaluation of hand-force prediction using artificial neural-network regression models of surface emg signals for handwear devices. *Journal of Sensors*, 2017, 2017.

[75] Wei Yang, Dapeng Yang, Yu Liu, and Hong Liu. Decoding Simultaneous Multi-DOF Wrist Movements from Raw EMG Signals Using a Convolutional Neural Network. *IEEE Trans. Human-Machine Syst.*, 49(5):411–420, 2019.

[76] Yang Yu and Chen Chen. Surface electromyography image driven torque estimation of multi-dof wrist movements. *IEEE Transactions on Industrial Electronics*, 2021.

[77] Jian Zhang and Jun Yu. Local deep-feature alignment for unsupervised dimension reduction. *IEEE transactions on image processing*, 27(5):2420–2432, 2018.

[78] Jie Liu and Yupeng Ren. Emg-based real-time linear-nonlinear cascade regression decoding of shoulder, elbow, and wrist movements in able-bodied persons and stroke survivors. *IEEE Transactions on Biomedical Engineering*, 67(5):1272–1281, 2019.

[79] Zhichuan Tang and Hongnian Yu. Impact of Load Variation on Joint Angle Estimation from Surface EMG Signals. *IEEE Trans. Neural Syst. Rehabil. Eng.*, 24(12):1342–1350, 2016.

[80] Toshihiro Kawase and Takeshi Sakurada. Estimating joint angles from biological signals for multi-joint exoskeletons. In *2014 IEEE International Conference on Systems, Man, and Cybernetics (SMC)*, pages 1470–1474. IEEE, 2014.

[81] Tianzhe Bao and Syed Ali Raza Zaidi. A cnn-lstm hybrid model for wrist kinematics estimation using surface electromyography. *IEEE Transactions on Instrumentation and Measurement*, 70:1–9, 2020.

[82] Jia-Liang Ren and Ya-Hui Chien. Deep learning based motion prediction for exoskeleton robot control in upper limb rehabilitation. In *2019 International Conference on Robotics and Automation (ICRA)*, pages 5076–5082. IEEE, 2019.

[83] Ali Ameri and Mohammad Ali Akhaee. Regression convolutional neural network for improved simultaneous emg control. *Journal of neural engineering*, 16(3):036015, 2019.

[84] Shengquan Xie and Pengfei Yang. A deep kalman filter network for hand kinematics estimation using semg. *Pattern Recognition Letters*, 143:88–94, 2021.

[85] Xunju Ma and Yali Liu. Continuous estimation of knee joint angle based on surface electromyography using a long short-term memory neural network and time-advanced feature. *Sensors*, 20(17):4966, 2020.

[86] Chenfei Ma, Chuang Lin, Oluwarotimi Williams Samuel, Lisheng Xu, and Guanglin Li. Continuous estimation of upper limb joint angle from semg signals based on sca-lstm deep learning approach. *Biomedical Signal Processing and Control*, 61:102024, 2020.

[87] Lina Tong and Feng Zhang. Bp-ar-based human joint angle estimation using multi-channel semg. *International Journal of Robotics and Automation*, 30(3):227–237, 2015.

[88] Yikang Yang and Feng Duan. Performance comparison of gesture recognition system based on different classifiers. *IEEE Transactions on Cognitive and Developmental Systems*, 13(1):141–150, 2020.

[89] Ganesh R Naik and Al-Timemy. Transradial amputee gesture classification using an optimal number of semg sensors: an approach using ica clustering. *IEEE Transactions on Neural Systems and Rehabilitation Engineering*, 24(8):837–846, 2015.

[90] Ghulam Rasool and Bouaynaya. Surface myoelectric signal classification using the ar-garch model. *Biomedical Signal Processing and Control*, 13:327–336, 2014.

[91] Weidong Geng and Yu Du. Gesture recognition by instantaneous surface emg images. *Scientific reports*, 6(1):1–8, 2016.

[92] Md Rabiul Islam and Daniel Massicotte. Hog and pairwise svms for neuromuscular activity recognition using instantaneous hd-semg images. In *2018 16th IEEE International New Circuits and Systems Conference (NEWCAS)*, pages 335–339. IEEE, 2018.

[93] Manfredo Atzori and Matteo Cognolato. Deep learning with convolutional neural networks applied to electromyography data: A resource for the classification of movements for prosthetic hands. *Frontiers in neurorobotics*, 10:9, 2016.

[94] Nadia Nasri and Orts-Escolano. Inferring static hand poses from a low-cost non-intrusive semg sensor. *Sensors*, 19(2):371, 2019.

[95] Miguel Simão and P. Neto. EMG-based online classification of gestures with recurrent neural networks. *Pattern Recognit. Lett.*, 128:45–51, 2019.

[96] Ali Samadani. Gated recurrent neural networks for emg-based hand gesture classification. a comparative study. In *2018 40th annual international conference of the IEEE Engineering in Medicine and Biology Society (EMBC)*, pages 1–4. IEEE, 2018.

[97] Mariel Alfaro-Ponce and Isaac Chairez. Continuous and recurrent pattern dynamic neural networks recognition of electrophysiological signals. *Biomedical Signal Processing and Control*, 57:101783, 2020.

[98] Muhammad Zia ur Rehman and Syed Omer Gilani. Stacked sparse autoencoders for emg-based classification of hand motions: A comparative multi day analyses between surface and intramuscular emg. *Applied Sciences*, 8(7):1126, 2018.

[99] Hyeon-min Shim and Hongsub An. Emg pattern classification by split and merge deep belief network. *Symmetry*, 8(12):148, 2016.

[100] Jianhua Zhang and Chen Ling. Emg signals based human action recognition via deep belief networks. *IFAC-PapersOnLine*, 52(19):271–276, 2019.

[101] Wentao Sun and Huaxin Liu. semg-based hand-gesture classification using a generative flow model. *Sensors*, 19(8):1952, 2019.

[102] Zhen Ding and Chifu Yang. semg-based gesture recognition with convolution neural networks. *Sustainability*, 10(6):1865, 2018.

[103] Xin Cao and Masami Iwase. Gesture recognition based on convlstm-attention implementation of small data semg signals. In *Adjunct Proceedings of the 2019 ACM International Joint Conference on Pervasive and Ubiquitous Computing and Proceedings of the 2019 ACM International Symposium on Wearable Computers*, pages 21–24, 2019.

[104] Baao Xie and Baihua Li. Movement and gesture recognition using deep learning and wearable-sensor technology. In *Proceedings of the 2018 International Conference on Artificial Intelligence and Pattern Recognition*, pages 26–31, 2018.

[105] Runze Tong and Yue Zhang. Learn the temporal-spatial feature of semg via dual-flow network. *International Journal of Humanoid Robotics*, 16(04):1941004, 2019.

[106] Panagiotis Tsinganos and Bruno Cornelis. Improved Gesture Recognition Based on sEMG Signals and TCN. In *ICASSP, IEEE Int. Conf. Acoust. Speech Signal Process. - Proc.*, pages 1169–1173. IEEE, 2019.

[107] Marcello Zanghieri and Simone Benatti. Robust real-time embedded emg recognition framework using temporal convolutional networks on a multicore iot processor. *IEEE transactions on biomedical circuits and systems*, 14(2):244–256, 2019.

[108] Hongfeng Chen and Yue Zhang. Surface electromyography feature extraction via convolutional neural network. *International Journal of Machine Learning and Cybernetics*, 11(1):185–196, 2020.

[109] Junkai Shao and Yafeng Niu. Single-channel SEMG using wavelet deep belief networks for upper limb motion recognition. *Int. J. Ind. Ergon.*, 76:102905, 2020.

[110] Jerry E Pratt, Benjamin T Krupp, Christopher J Morse, and Steven H Collins. The roboknee: an exoskeleton for enhancing strength and endurance during walking. In *IEEE International Conference on Robotics and Automation, 2004. Proceedings. ICRA'04. 2004*, volume 3, pages 2430–2435. IEEE, 2004.

[111] Andrej Gams and Tadej Petrič. Effects of robotic knee exoskeleton on human energy expenditure. *IEEE Transactions on Biomedical Engineering*, 60(6):1636–1644, 2013.

[112] Wai-Yin Lai and Hao Ma. Hip-knee control for gait assistance with powered knee orthosis. In *2013 IEEE international conference on robotics and biomimetics (ROBIO)*, pages 762–767. IEEE, 2013.

[113] Kyung Kim and Chang-Ho Yu. Analysis of the assistance characteristics for the knee extension motion of knee orthosis using muscular stiffness force feedback. *Journal of Mechanical Science and Technology*, 27(10):3161–3169, 2013.

[114] Nikos Karavas and Arash Ajoudani. Tele-impedance based stiffness and motion augmentation for a knee exoskeleton device. In *2013 IEEE international conference on robotics and automation*, pages 2194–2200. IEEE, 2013.

[115] Alexander N Spring and Jonathan Kofman. Design and evaluation of an orthotic knee-extension assist. *IEEE Transactions on Neural Systems and Rehabilitation Engineering*, 20(5):678–687, 2012.

[116] Christian Fleischer and Günter Hommel. A human–exoskeleton interface utilizing electromyography. *IEEE Transactions on Robotics*, 24(4):872–882, 2008.

[117] Zhiyong Yang and Yuguang Zhu. Impedance control of exoskeleton suit based on adaptive rbf neural network. In *2009 International conference on intelligent human-machine systems and cybernetics*, volume 1, pages 182–187. IEEE, 2009.

[118] Yoshiyuki Sankai. Hal: Hybrid assistive limb based on cybernics. In *Robotics research*, pages 25–34. Springer, 2010.

[119] Shiqian Wang, Letian Wang, and Meijneke. Design and control of the mindwalker exoskeleton. *IEEE transactions on neural systems and rehabilitation engineering*, 23(2):277–286, 2014.

[120] Tadaaki Ikehara and Kazuteru Nagamura. Development of closed-fitting-type walking assistance device for legs and evaluation of muscle activity. In *2011 IEEE international conference on rehabilitation robotics*, pages 1–7. IEEE, 2011.

[121] Alberto Esquenazi and Mukul Talaty. The rewalk powered exoskeleton to restore ambulatory function to individuals with thoracic-level motor-complete spinal cord injury. *American journal of physical medicine & rehabilitation*, 91(11):911–921, 2012.

[122] Terris Yakimovich and Edward D Lemaire. Engineering design review of stance-control knee-ankle-foot orthoses. *Journal of Rehabilitation Research & Development*, 46(2), 2009.

[123] Hiroaki Kawamoto and Stefan Taal. Voluntary motion support control of robot suit hal triggered by bioelectrical signal for hemiplegia. In *2010 Annual international conference of the IEEE engineering in medicine and biology*, pages 462–466. IEEE, 2010.

[124] Yoshikazu Mori and Jun Okada. Development of a standing style transfer system" able" for disabled lower limbs. *IEEE/ASME Transactions on Mechatronics*, 11(4):372–380, 2006.

[125] Keijiro Yamamoto and Kazuhito Hyodo. Development of power assisting suit for assisting nurse labor. *JSME International Journal Series C Mechanical Systems, Machine Elements and Manufacturing*, 45(3):703–711, 2002.

[126] Feng Chen and Yong Yu. Wpal for human power assist during walking using dynamic equation. In *2009 International conference on mechatronics and automation*, pages 1039–1043. IEEE, 2009.

[127] Nevio Luigi Tagliamonte and Fabrizio Sergi. Human-robot interaction tests on a novel robot for gait assistance. In *2013 IEEE 13th international conference on rehabilitation robotics (ICORR)*, pages 1–6. IEEE, 2013.

[128] Xia Zhang and Minoru Hashimoto. Synchronization based control for walking assist suit-evaluation on synchronization and assist effect. In *Key engineering materials*, volume 464, pages 115–118. Trans Tech Publ, 2011.

[129] Guido Belforte and Laura Gastaldi. Pneumatic active gait orthosis. *Mechatronics*, 11(3):301–323, 2001.

[130] Conor James Walsh and Kenneth Pasch. An autonomous, underactuated exoskeleton for load-carrying augmentation. In *2006 IEEE/RSJ International Conference on Intelligent Robots and Systems*, pages 1410–1415. IEEE, 2006.

[131] Hami Kazerooni and Ryan Steger. Hybrid control of the berkeley lower extremity exoskeleton (bleex). *The International Journal of Robotics Research*, 25(5-6):561–573, 2006.

[132] Narong Aphiratsakun and Manukid Parnichkun. Balancing control of ait leg exoskeleton using zmp based flc. *International Journal of Advanced Robotic Systems*, 6(4):34, 2009.

[133] H He and Kazuo Kiguchi. A study on emg-based control of exoskeleton robots for human lower-limb motion assist. In *2007 6th International special topic conference on information technology applications in biomedicine*, pages 292–295. IEEE, 2007.

[134] Kyoungchul Kong and Doyoung Jeon. Design and control of an exoskeleton for the elderly and patients. *IEEE/ASME Transactions on mechatronics*, 11(4):428–432, 2006.

[135] Kai Gui and U-Xuan Tan. Electromyography-driven progressive assist-as-needed control for lower limb exoskeleton. *IEEE Transactions on Medical Robotics and Bionics*, 2(1):50–58, 2020.

[136] Simon Field. World Report on Disability. Technical report, 2011.

[137] S. Jeyalakshmi and S. Chakrabarti. Situation Analysis Of The Elderly in India, 2011.

[138] Banurekha Velayutham and Boopathi Kangusamy. The prevalence of disability in elderly in India–Analysis of 2011 census data. *Disabil. Health J.*, 9(4):584–592, 2016.

[139] MF Antwi-Afari and Heng Li. Biomechanical analysis of risk factors for work-related musculoskeletal disorders during repetitive lifting task in construction workers. *Automation in Construction*, 83:41–47, 2017.

[140] Nathanaël Jarrassé and Guillaume Morel. Connecting a human limb to an exoskeleton. *IEEE Trans. Robot.*, 28:697–709, 2012.

[141] Wei Meng and Quan Liu. Recent development of mechanisms and control strategies for robot-assisted lower limb rehabilitation. *Mechatronics*, 31:132–145, 2015.

[142] Kexiang Li and Zhang. A review of the key technologies for semg-based human-robot interaction systems. *Biomedical Signal Processing and Control*, 62:102074, 2020.

[143] Michael Damsgaard, John Rasmussen, Søren Tørholm Christensen, Egidijus Surma, and Mark De Zee. Analysis of musculoskeletal systems in the anybody modeling system. *Simulation Modelling Practice and Theory*, 14(8):1100–1111, 2006.

[144] Apoorva Rajagopal and Christopher L. Dembia. Full-Body Musculoskeletal Model for Muscle-Driven Simulation of Human Gait. *IEEE Trans. Biomed. Eng.*, 63:2068–2079, 2016.

[145] Haerin Lee and Moonki Jung. A 3D human-machine integrated design and analysis framework for squat exercises with a smith machine, 2017.

[146] Shuo Ding and Xiaoping Ouyang. Dynamic simulation of a hydraulic exoskeleton robot based on virtual prototyping. In *2016 IEEE Int. Conf. Adv. Intell. Mechatronics*, pages 1479–1484, 2016.

[147] Brandon N. Fournier and Edward D. Lemaire. Modeling and Simulation of a Lower Extremity Powered Exoskeleton. *IEEE Trans. Neural Syst. Rehabil. Eng.*, 26:1596–1603, 2018.

[148] Stefania Spada. Physical and Virtual Assessment of a Passive Exoskeleton. In *Proc. 20th Congr. Int. Ergon. Assoc.*, volume 827, pages 247–257, 2018.

[149] Tim Bosch and Jennifer van Eck. The effects of a passive exoskeleton on muscle activity, discomfort and endurance time in forward bending work. *Appl. Ergon.*, 54:212–217, 2016.

[150] Jing Deng and Pengfei Wang. Structure design of active power-assist lower limb exoskeleton APAL robot. *Adv. Mech. Eng.*, 9(11):1–11, 2017.

[151] Brandon Fournier and J J Sm. Modelling and simulation of lower extremity powered exoskeleton. In *Conf. Pap. 2017 New Orleans, LA*, pages 1–4, 2017.

[152] Nazim Mir-Nasiri and Hudyjaya Siwoyo Jo. Autonomous low limb exoskeleton to suppress the body weight. In *3rd Int. Conf. Control. Autom. Robot.*, pages 47–51, 2017.

[153] Max K. Shepherd and Elliott J. Rouse. Design and Validation of a Torque-Controllable Knee Exoskeleton for Sit-to-Stand Assistance. *IEEE/ASME Trans. Mechatronics*, 22:1695–1704, 2017.

[154] Guoan Zhang and Gangfeng Liu. Biomechanical design of escalading lower limb exoskeleton with novel linkage joints. *Technology and Health Care*, 25(S1):267–273, 2017.

[155] I. S. Dhindsa and R. Agarwal. Principal component analysis-based muscle identification for myoelectric-controlled exoskeleton knee. *J. Appl. Stat.*, 44:1707–1720, 2017.

[156] Su Kyoung Lee. The effect of a vertical load on gluteus medius activity and gait characteristics during walking. *J. Phys. Ther. Sci.*, 25(11):1397–1399, 2013.

[157] SENIAM, 2013.

[158] T. S. Buchanan and L. Wang. Prediction of joint moments using a neural network model of muscle activations from EMG signals. *IEEE Trans. neural Syst. Rehabil. Eng.*, 10(1):30–7, 2002.

[159] Thomas S. Buchanan and David G. Lloyd. Neuromusculoskeletal modeling: Estimation of muscle forces and joint moments and movements from measurements of neural command. *J. Appl. Biomech.*, 20:367–395, 2004.

[160] David G. Lloyd. An EMG-driven musculoskeletal model to estimate muscle force and knee joint moment in vivo. *J. Biomech.*, 36:765–776, 2003.

[161] A M Gordon and A F Huxtey. The variation in isometric tension with sarcomere length in vertebrete muscle fibres. *jouranal Physiol.*, 184:170–192, 1966.

[162] Young Nam Jo and Moon Jeong Kang. Estimation of muscle and joint forces in the human lower extremity during rising motion from a seated position, 2014.

[163] Sandra J. OLNEY. Predictions of knee and ankle moments of force in walking from EMG. *J. Biomech.*, 18:9–20, 1985.

[164] Zajac FE. Muscle and tendon: properties, models, scaling, and application to biomechanics and motor control. *Crit Rev Biomed Eng*, 17:359–411, 1989.

[165] G.T. Yamaguchi and J.M. Winters. A survey of human musculotendon actuator parameters. *Mult. Org*, 84:717–773, 1990.

[166] Scott L. Delp and J. Peter Loan. A graphics-based software system to develop and analyze models of musculoskeletal structures. *Comput. Biol. Med.*, 25:21–34, 1995.

[167] Anurag Sohane and Ravinder Agarwal. Evaluation of 3d design lower limb exoskeleton on human musculoskeletal with various loads. *Expert Systems*, page e12738, 2021.

[168] Darryl G. Thelen. Adjustment of muscle mechanics model parameters to simulate dynamic contractions in older adults. *J. Biomech. Eng.*, 125:70–77, 2003.

[169] Stephen J. Piazza. Muscle-driven forward dynamic simulations for the study of normal and pathological gait. *J. Neuroeng. Rehabil.*, 3:1–7, 2006.

[170] Wen Wu and Peter V.S. Lee. Subject-specific musculoskeletal modeling in the evaluation of shoulder muscle and joint function. *J. Biomech.*, 49:3626–3634, 2016.

[171] Cláudio Bastos Heine and Luciano Luporini Menegaldo. Numerical validation of a subject-specific parameter identification approach of a quadriceps femoris EMG-driven model. *Med. Eng. Phys.*, 53:66–74, 2018.

[172] Lance Rane and Ziyun Ding. Deep Learning for Musculoskeletal Force Prediction. *Ann. Biomed. Eng.*, 47:778–789, 2019.

[173] Ursula Trinler and Hermann Schwameder. Muscle force estimation in clinical gait analysis using AnyBody and OpenSim. *J. Biomech.*, 86:55–63, 2019.

[174] Edith M. Arnold and Samuel R. Ward. A model of the lower limb for analysis of human movement. *Ann. Biomed. Eng.*, 38:269–279, 2010.

[175] Marcus G Pandy. Computer Modelling and Simulation of Human Movement. *Kinesiology*, 3:245–273, 2001.

[176] Carlos Quental and João Folgado. Critical analysis of musculoskeletal modelling complexity in multibody biomechanical models of the upper limb. *Comput. Methods Biomech. Biomed. Engin.*, 18:749–759, 2015.

[177] David Fone and Sandra Hollinghurst. Systematic review of the use and value of computer simulation modelling in population health and health care delivery. *J. Public Health Med.*, 25:325–335, 2003.

[178] T. S. Buchanan and K. Manal. An EMG-driven model to estimate muscle forces and joint moments in stroke patients. *Comput. Biol. Med.*, 39:1083–8, 2009.

[179] Danilo S. Catelli and Mariska Wesseling. A musculoskeletal model customized for squatting task. *Comput. Methods Biomech. Biomed. Engin.*, 22:21–24, 2018.

[180] Daniel Nolte and Mary E. Finnegan. Anthropometric Scaling of Anatomical Datasets for Subject-Specific Musculoskeletal Modelling of the Shoulder. *Ann. Biomed. Eng.*, 47:924–936, 2019.

[181] Joshua T. Weinhandl and Hunter J. Bennett. Musculoskeletal model choice influences hip joint load estimations during gait. *J. Biomech.*, 91:124–132, 2019.

[182] Frank Mendel. Case studies of musculoskeletal-simulation-based rehabilitation program evaluation. *IEEE Trans. Robot.*, 25:634–638, 2009.

[183] Morten Enemark Lund and Michael Skipper Andersen. Scaling of musculoskeletal models from static and dynamic trials. *Int. Biomech.*, 2:1–11, 2015.

[184] Kim J. Boström and Tim Dirksen. The contribution of upper body movements to dynamic balance regulation during challenged locomotion. *Front. Hum. Neurosci.*, 12:1–10, 2018.

[185] Prashant Singh Rana and Harish Sharma. Quality assessment of modelled protein structure using physicochemical properties. *J. Bioinform. Comput. Biol.*, 13:1–16, 2015.

[186] Eni Halilaj and Apoorva Rajagopal. Machine learning in human movement biomechanics: Best practices, common pitfalls, and new opportunities. *J. Biomech.*, 81:1–11, 2018.

[187] Yu Chen Lo and Stefano E. Rensi. Machine learning in chemoinformatics and drug discovery. *Drug Discov. Today*, 23:1538–1546, 2018.

[188] Marinka Zitnik and Francis Nguyen. Machine learning for integrating data in biology and medicine: Principles, practice, and opportunities. *Inf. Fusion*, 50:71–91, 2019.

[189] Pieter Oomen and Janneke Annegarn. Development and validation of a rule based strength scaling method for musculoskeletal modelling. *Int. J. Hum. Factors Model. Simul.*, 5:19, 2015.

[190] Ning Guo and Xingyu Fan. Effect of constraint loading on the lower limb muscle forces in weightless treadmill exercise. *J. Healthc. Eng.*, 2018:1–9, 2018.

[191] Nicola Petrone and Daniele Tregnaghi. Musculoskeletal simulation of isokinetic exercises: A biomechanical and electromyographical pilot study. In *7th Asia-Pacific Congr. Sport. Technol.*, volume 112, pages 250–255. Elsevier, 2015.

[192] Zhongqiu Ji and Huihui Wang. Analysis of muscle activity utilizing bench presses in the AnyBody simulation modelling system. *Model. Simul. Eng.*, 2016:1–7, 2016.

[193] Chenlei Xie and Daqing Wang. A long short-term memory neural network model for knee joint acceleration estimation using mechanomyography signals. *Int. J. Adv. Robot. Syst.*, 17(6), 2020.

[194] Rezvan Kianifar and Lee Alexander. Automated assessment of dynamic knee valgus and risk of knee injury during the single leg squat. *IEEE J. Transl. Eng. Heal. Med.*, 5:13, 2017.

[195] Zhang G.Peter. Time series forecasting using a hybrid ARIMA and neural network model. *Neurocomputing*, 50:159–175, 2003.

[196] Jiangcheng Chen and Xiaodong Zhang. Surface EMG based continuous estimation of human lower limb joint angles by using deep belief networks. *Biomed. Signal Process. Control*, 40:335–342, 2018.

[197] Quan Liu and Ma Liangyun. Knee joint angle prediction based on muscle synergy theory and generalized regression neural network. In *IEEE/ASME Int. Conf. Adv. Intell. Mechatronics*, page 5, Auckland, New Zealand, 2018. IEEE.

[198] Yongchuang Huang and Zexia He. Real-time intended knee joint motion prediction by deep-recurrent neural networks. *IEEE Sens. J.*, 19(23):11503–11509, 2019.

[199] Wang Chao and Guo Weiyu. sEMG-based continuous estimation of grasp movements by long-short term memory network. *Biomed. Signal Process. Control*, 59:14, 2020.

[200] Wang Ying and Wu Qun. Deep back propagation-long short-term memory network based upper-limb sEMG signal classification for automated rehabilitation. *Biocybern. Biomed. Eng.*, 40:987–1001, 2020.

[201] Bao Tianzhe and Xie Shengquan. A CNN-LSTM hybrid model for wrist kinematics estimation using surface electromyography. *IEEE Trans. Instrum. Meas.*, 70:9, 2021.

[202] Christopher Millar and Nazmul Siddique. LSTM classification of sEMG signals for individual finger movements using low cost wearable sensor. In *2020 Int. Symp. Community-centric Syst.*, page 8, Tokyo, Japan, 2020. IEEE.

[203] Yushan Zhang and Sitong Yang. Prediction on the highest price of the stock based on PSO-LSTM neural network. In *3rd Int. Conf. Electron. Inf. Technol. Comput. Eng.*, page 4, Xiamen, China, 2019.

[204] Venkateswarlu Gundu and Sishaj P. Simon. PSO–LSTM for short term forecast of heterogeneous time series electricity price signals. *J. Ambient Intell. Humaniz. Comput.*, page 11, 2020.

[205] Sepp Hochreiter and J Urgen Schmidhuber. Long Short-Term Memory. *Neural Comput.*, 9(8), 1997.

[206] Xiaohui Yuan and Chen Chen. Prediction interval of wind power using parameter optimized Beta distribution based LSTM model. *Appl. Soft Comput. J.*, 82:10, 2019.

[207] Arpita Samanta Santra and Jun Lin Lin. Integrating long short-term memory and genetic algorithm for short-term load forecasting, 2019.

[208] Hyejung Chung and Kyung Shik Shin. Genetic algorithm-optimized long short-term memory network for stock market prediction. *Sustain.*, 10(1):3765, 2018.

[209] Thitimanan Damrongsakmethee and VictEmil Neagoe. Stock market prediction using a deep learning approach. In *12th Int. Conf. Electron. Comput. Artif. Intell.*, page 6, Bucharest, Romania, 2020. IEEE.

[210] Huang Yusheng and Yelin Gao. A new financial data forecasting model using genetic algorithm and long short-term memory network. *Neurocomputing*, 425:207–218, 2021.

[211] Anurag Sohane and Ravinder Agarwal. Knee muscle force estimating model using machine learning approach. *Comput. J.*, 00, 2020.

[212] Kumar Neelesh and Vidhya S. System for measurement of joint range of motion using inertial sensors. *Biomed. Res.*, 28:3699–3703, 2017.

[213] Yi Zhang and Peiyang Li. Extracting time-frequency feature of single-channel vastus medialis emg signals for knee exercise pattern recognition. *PloS one*, 12(7):e0180526, 2017.

List of Publications

Journal Publications

1. Anurag Sohane, Ravinder Agarwal *"Knee Muscle Force Estimating Model Using Machine Learning Approach"*, **The Computer Journal**, Oxford University Press, 2020. [**DOI**: https//doi: 10.1093/comjnl/bxaa160, SCI, IF 1.494]

2. Anurag Sohane, Ravinder Agarwal *"Evaluation of 3D design lower limb exoskeleton on human musculoskeletal with various loads"*, **Expert System**, Wiley, 2021. [**DOI**: https//doi.org/10.1111/exsy.12738, SCI, IF 2.587]

3. Anurag Sohane, Ravinder Agarwal *"A Single Platform for Classification and Prediction using a Hybrid Bioinspired and Deep Neural Network (PSO-LSTM) "*, **MAPAN**, Springer, 2021. [**DOI** : 10.1007/s12647-021-00478-6SCI, IF 1.009]

Conference Publications

1. Sohane Anurag, Agarwal Ravinder, *Machine Learning Approach for Prediction of the Knee Muscle Force*, 7th National Conference on Advances in Metrology (AdMet-2021) on 5th-6th March 2021, Maharaja Surajmal Institute of Technology (MSIT) C-4, Janakpuri, New Delhi

2. Sohane Anurag, Ryait, S Hardeep, Agarwal Ravinder, *A comparative Study of Time Domain Features for SEMG Signal for Hand Movement Classification*, 9th International Conference on "Advances in Metrology-2016", February 23-26, 2016, National Physical Laboratory, New Delhi